Summer 7-7-2017

Stratigraphic Architecture and Lithofacies of High-Frequency Deltaic Sequences: Virtual Outcrop Analysis of the Upper Cretaceous (Turonian) Ferron Sandstone Member of the Mancos Shale, South-Central Utah, USA

Conor J. Horton
University of Nebraska-Lincoln, conorjhorton@gmail.com

STRATIGRAPHIC ARCHITECTURE AND LITHOFACIES OF HIGH-FREQUENCY DELTAIC SEQUENCES: VIRTUAL OUTCROP ANALYSIS OF THE UPPER CRETACEOUS (TURONIAN) FERRON SANDSTONE MEMBER OF THE MANCOS SHALE, SOUTH-CENTRAL UTAH, USA

by

Conor J. Horton

A THESIS

Presented to the Faculty of

The Graduate College at the University of Nebraska

In Partial Fulfillment of Requirements

For the Degree of Master of Science

Major: Earth and Atmospheric Sciences

Under the Supervision of Professor Christopher R. Fielding

Lincoln, Nebraska

June, 2017

STRATIGRAPHIC ARCHITECTURE AND LITHOFACIES OF HIGH-FREQUENCY DELTAIC SEQUENCES: VIRTUAL OUTCROP ANALYSIS OF THE UPPER CRETACEOUS (TURONIAN) FERRON SANDSTONE MEMBER OF THE MANCOS SHALE, SOUTH-CENTRAL UTAH, USA

Conor J. Horton, M.S.

University of Nebraska, 2017

Adviser: Christopher R. Fielding

Sequence stratigraphic models for low-accommodation settings are not well-formulated and lack documented examples illustrating lithofacies stratal stacking pattern complexities. Presented herein is a detailed stratigraphic analysis of the Upper Cretaceous (Turonian) Ferron Sandstone Member of the Mancos Shale Formation; a fluvial-deltaic succession that primarily accumulated under forced-regressive, falling stage systems tracts during decreasing accommodation. The small (4 km^2) study area is located at the connecting point of a 67 km long, depositional strike-oriented and a 30 km long, depositional-dip transect within the western-limb of the Henry Mountains Syncline. Detailed outcrop sections and digital Light Detection and Ranging (LiDAR) derived Virtual Outcrop Models (VOM) analysis are used to define and characterize the stratigraphic architecture. Correlation of all bodies within the stratigraphic interval display the anatomy of a prograding deltaic system composed of crudely coarsening-upward cycles. This paper focuses on the 'Critical Interval', a <8 m thick, cyclic succession of entrenched distributary channels, reworked delta plain, and transgressive shoreface sandstones that lies above a regionally extensive sequence boundary and

separates the lower and upper Ferron members. The moderately incised (<5 m), relatively small (150-300 m wide) channel bodies and locally preserved delta plain deposits are interpreted to record two individual sea-level cycles. The incomplete sequences and the facies were influenced by marine-processes and the low-amplitude and high-frequency nature of sea-level fluctuations that characterize Ferron Sandstone Member accumulation. This study provides detailed facies characterization and illustrations of the stratigraphic architecture with implications for deltaic sequences deposited in a low accommodation setting.

ACKNOWLEDGEMENTS

The successful completion of this thesis project would not have achievable if not for the following individuals. I am grateful for the overwhelming support and encouragement from my family, including; my parents, Jeff and Theresa and my brother, Kaylor. I would like to recognize my girlfriend Dana, for her unrelenting support and patience during my studies and research. I thank my closest friends from Lincoln and those within the department for the comradery and experiences we shared that made this process so enjoyable.

I would like to express my full gratitude and sincere thanks to my advisor Dr. Christopher Fielding for his immense assistance and advice during the completion of this project. I appreciate his wisdom and encouragement and greatly appreciate the thought-provoking discussions held during meetings. The success of this research would have not been possible if not for his professional guidance and support. I would like to extend my gratitude to my committee members; Dr. Cara Burberry and Dr. David Loope. I would also like to thank the University of Nebraska-Lincoln Department of Earth and Atmospheric Sciences for offering me the opportunity to conduct graduate level research.

TABLE OF CONTENTS

INTRODUCTION 1

GEOLOGICAL BACKGROUND 11

STUDY AREA AND METHODS 14

FACIES ANALYSIS 19

- Facies 1 19
  - Variant 1 19
  - Variant 2 20
- Facies 2 26
- Facies 3 28
- Facies 4 33
- Facies 5 36
- Facies 6 39
- Facies 7 42
- Facies 8 43

KEY SURFACES 44

FACIES ARCHITECTURE AND STACKING PATTERNS 47

- Virtual Outcrop Model Descriptions 50
  - The Post VOM 50
  - The Labyrinth VOM 53
- Stratigraphic Intervals 55
  - Lower Ferron Member 55
  - Critical Interval 56

Incised Distributary Channel Bodies 56

Channel 1 56

Channel 2 66

DISCUSSION 62

Compound Incised Distributary Channel Fill 62

Critical Interval Sequence Stratigraphy 62

Channel Incision Response to Base-Level Fall 65

CONCLUSIONS 77

REFERENCES 76

APPENDICES 87

INTRODUCTION

Sequence stratigraphy is a methodology allowing for identification of cyclic, genetically related stratal sequences bounded by unconformities or correlative conformities providing a time-stratigraphic framework for any given stratigraphic succession (Posamentier et al., 1992; Van Wagoner et al., 1988). Stratal stacking patterns of genetically related sequences reflect the interplay between subsidence and sea-level (accommodation), and sediment supply, resulting in depositional trends (e.g. progradation, retrogradation, aggradation and downcutting; Catuneanu et al., 2009). A depositional sequence records one complete cycle of sea-level and can subdivided into smaller-scale genetically related systems tracts by the identification of well-defined surfaces (Fig. 1; Van Wagoner, 1988). The four systems tract division of Plint and Nummedal (2000) contains the following systems tracts in this order; lowstand systems tract (LST), transgressive systems tract (TST), highstand systems tract (HST), and forced regressive systems tract (FRST), each of which correspond to individual phases of sea-level (Fig. 1; Posamentier and Allen, 1999; Plint and Nummedal, 2000; Catuneanu, 2006; Catuneanu et al., 2009). These systems tracts are bounded by the following key surfaces (Fig. 1); the LST and TST are separated by the transgressive ravinement surface (TRS). The TST and HST are separated by the maximum flooding surface (MFS). The HST and FRST are separated by the subaerial unconformity/sequence boundary (SU/SB). The distinct stratal geometries of the four individual systems tracts and the sense of shoreline movement reflect the interplay between generation or removal of accommodation and the ability of available sediment to fill that accommodation.

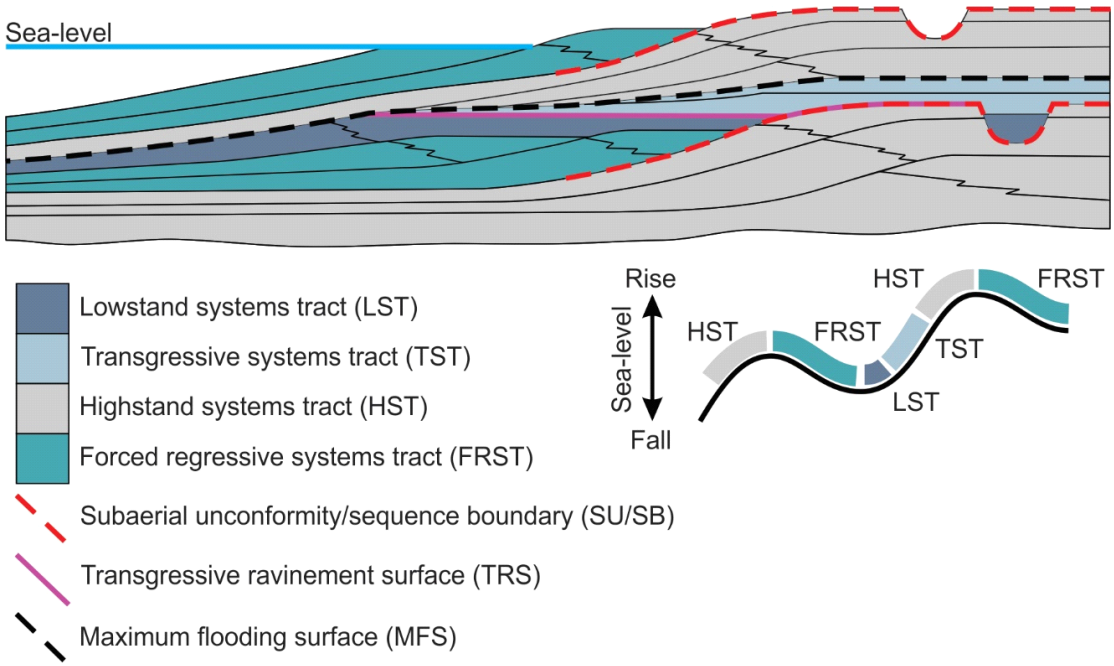

Figure 1 – Simplified sequence stratigraphic model (figure modified from Hunt and Tucker, 1992; Gawthorpe et al., 2000) illustrating the four system tract divisions of Plint and Nummedal (2000) with key sequence stratigraphic surfaces in relation to sea-level interpretation.

Sequence stratigraphic analysis has been extensively applied to coastal and shallow-marine siliciclastic successions (e.g. Allen and Posamentier, 1993; Bhattacharya, 1993: Pemberton and MacEachern, 1995; Garrison and Van den Bergh, 2004) deposited at or near the shoreline, where shifts in depositional trends are more evident and all key sequence stratigraphic surfaces may form (Catuneanu et al., 2009). Although complete sequences preserving all four systems tracts and key bounding surfaces may be present, not all will be necessarily present at any location as they are a function of depositional setting (Catuneanu et al., 2009). In particular, FRST and LST are commonly absent or incompletely preserved because of subsequent subaerial or transgressive ravinement erosion, resulting in cyclic successions that do not preserve the full array of systems tracts and key surfaces as shown by conventional sequence stratigraphic models (e.g. Van

Wagoner et al., 1990). Deltaic successions tend to display a greater variety of process variability, and therefore of facies and stratal stacking pattern complexity, relative to continental fluvial and marine environments, because they are the connective system between those two end-members (Coleman and Wright, 1975: Bhattacharya, 2006). The interplay of allogenic controls such as tectonics, eustasy, and climate (Haq et al., 1987; Gale et al., 2008) and autogenic controls, such as shoreline auto-retreat and delta-lobe switching (Muto and Steel, 1992; Posamentier and Allen, 1999) further complicates analysis.

Existing sequence stratigraphic models (e.g. Vail et al., 1977; Posamentier et al., 1988; Jervey, 1988; Posamentier et al., 1988; Posamentier and Vail, 1988; Posamentier et al., 1992b; Hunt and Tucker, 1992; Hunt and Gawthorpe, 2000) were primarily developed from large-scale, regionally extensive outcrop belts or subsurface seismic imaging of thick continental margin successions in which accommodation was not a limiting factor on sediment accumulation or preservation. These generic models are typically two-dimensional, dip-oriented, display complete sequences containing all systems tracts and key surfaces, and in their original form interpreted patterns in terms of global and regional relative changes in sea-level.

Undoubtedly, the model-driven methodology and framework of sequence stratigraphy provides a powerful tool for correlating and understanding the progression of stratigraphic succession in the context of changing sea-level/accommodation. However, the predicted stratigraphic architecture of these generic models does not fully explain the range of documented stratal geometries and may need adapting in order to be applicable to many stratigraphic successions. Sequence stratigraphic studies conducted on

stratigraphic succession deposited in low-accommodation, continental margin settings (e.g. Upper Cretaceous delta complexes of the western United States and Permian Icehouse successions of western Australia) have shown that basin subsidence regime has a profound effect on the resulting stratigraphy, such that successions accumulated under conditions of low accommodation have markedly different characteristics from those formed in high accommodation settings. In contrast to the architecture predicted by generic sequence stratigraphic models, sequences deposited in low-accommodation setting are relatively thin (tens of meters), condensed, incomplete (in terms of systems tracts), and top-truncated (Zaitlin et al., 2002; Fielding et al., 2006, 2007; Allen and Fielding, 2007). The internal architecture of these sequences has yet to be fully characterized, primarily due to the cryptic nature of key bounding surfaces and complications deciphering incomplete systems tracts within thin, condensed sequences. Understanding the complexities and variabilities of these stratigraphic succession will not only improve sequence stratigraphic understanding, but also provide more efficient hydrocarbon exploration, as these setting host complex and unpredictable, yet attractive exploration targets.

The objectives of this research are to; 1.) Document the facies and stratal stacking patterns of a low-accommodation deltaic succession with the use of Light Detection and Ranging (LiDAR) derived Virtual Outcrop Models (VOM). 2.) Analyze unique depositional geometries or stratigraphic relationships that may aid in identification of low accommodation stratigraphic successions. 3.) Provide a sequence stratigraphic interpretation to explain the locally observed geometries and stratigraphic relationships.

The Turonian Ferron Sandstone Member of the Mancos Shale in south-central Utah, U.S.A is superbly exposed along the western limb of the HMS (Figs. 2; 3A) allowing for relationships among facies, stratal stacking patterns and bounding surfaces to be investigated in great detail. The small (4 km^2) study area (Fig. 2D) contains world-class outcrop quality and exposure, located within vast network of canyons and gullies. Two beautifully exposed, vertical cliff-faces located at the western and eastern margins of the study area have been digitally captured by ground-based LiDAR laser scanning instruments and processed into VOMs (Fig. 4). The study area (Fig. 2C, D) is located near the southwestern corner of the doubly-plunging HMS at the point where two regional transects conjoin (Figs. 2C, D; 5A; Fielding, 2011; Korus and Fielding; In Press), facilitating correlation at all levels of detail.

The application of the sequence stratigraphic method to the fluvial-deltaic Turonian Ferron Sandstone of central and southern Utah has received increasing attention (e.g. Garrison and Van den Bergh, 2004; Fielding, 2010, 2011; Zhu et al., 2012, Akyuz et al., 2016; Famubode and Bhattacharya, 2016; Korus and Fielding, In Press). The consensus sequence stratigraphic interpretation of the Ferron Sandstone is that sediment accumulation took place under strong forcing from relative fall of sea-level, producing a stack of thin, top-truncated sequences dominated by falling-stage deposits (Zhu et al., 2012; Fielding, 2015). High-frequency cycles are nestled within lower-frequency sequences, indicating an overall regressive regime with repeated superimposed, minor transgressions (Fig. 5A).

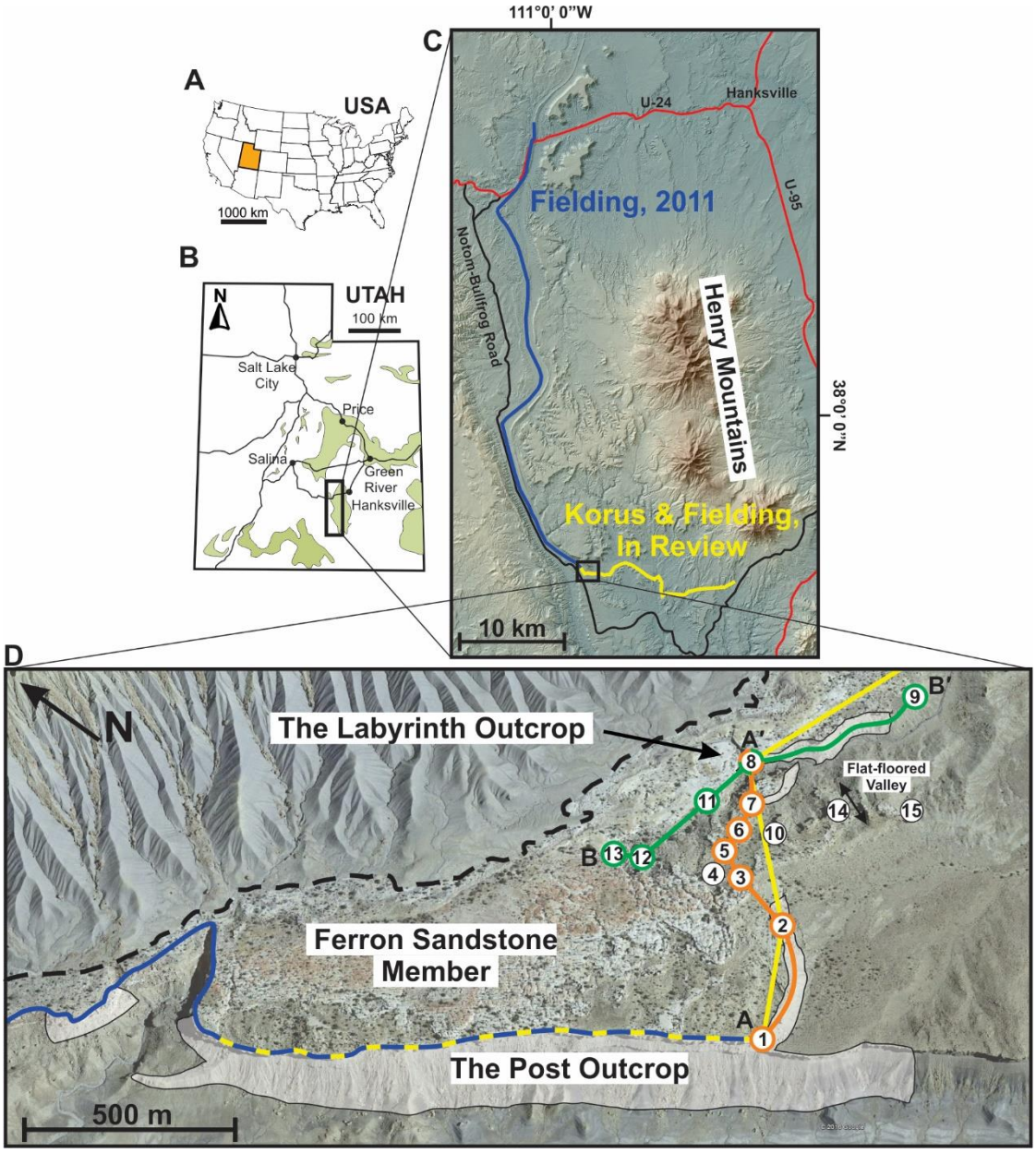

Figure 2 - Study area location in the Henry Mountains Region of south-central Utah. **A)** Map of the United States with Utah highlighted **B)** Map of Utah with major cities, roads, and outcropping Cretaceous strata (Green). Black rectangle outlines the regional study area of Fielding (2011) and Korus and Fielding (In Press) in the western Henry Mountains Region shown in Fig. 1C. **C)** Digital elevation map of the Henry Mountains region showing cross-section extents of Fielding (2011; Blue) and Korus and Fielding (In Press; Yellow). The study area (Black Box) is located at the connecting point of the two regional transects in within the study area. **D)** Aerial image (Google Earth) of the study area with locations of measured sections (MS#), cross-sections and the Post and Labyrinth virtual outcrop models (transparent white). Study area is ~4.0 km^2. Scale bar = 500 m. Black dotted line = extent of Ferron Sandstone Member outcrop.

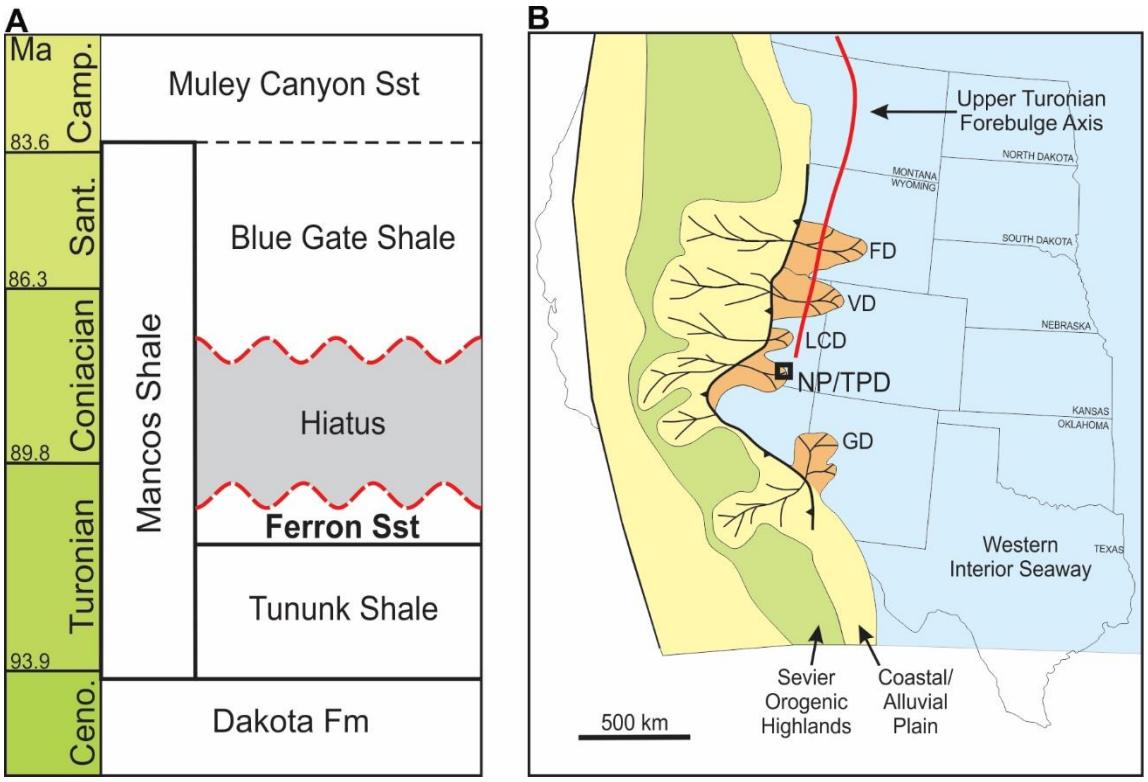

Figure 3 - Stratigraphic context of the Ferron Sandstone member and Upper Turonian paleogeography. **A)** Upper Cretaceous stratigraphic column showing the stratigraphic context and conformable relationship between the Ferron Sandstone and the underlying Tununk Shale. The base of the overlying Blue Gate Shale is marked by a major unconformity (Figure modified from Fielding, 2010, absolute time constraints from Zhu et al., 2012). **B)** Upper Turonian paleogeography map of the Cretaceous Western Interior Seaway showing deltaic complexes and interpreted upper Turonian forebulge position (From Miall et al., 2008). The black box displays the general location of the study area within the Ferron Notom Delta Complex of present day south-central Utah. Map from Hutsky and Fielding, 2017. FD: Frontier Deltas, VD: Vernal Delta, LCD: Last Chance Delta: NP/TPD: Notom/The Post Delta, GD: Gallup Delta.

Our analysis focused on the abrupt upward transition from predominantly deltaic facies of the lower Ferron Sandstone member to coastal-fluvial deposits of the upper Ferron Sandstone member (Fig. 5A), where the two members are separated by a regionally-extensive sequence boundary (referered to herein as SB1). Above SB1 is an ~8 m thick stratigraphic interval containing two unconformity bounded, high-frequency, top-truncated/incompletely preserved sequences, referred to as the Critical Interval. The Critical Interval contains two cyclic successions of small incised distributary channel bodies and thin veneers of delta plain heterolith, the two of which are capped by a laterally extensive shoreface sandstone body. The preserved deposits are interpreted to represent the forced regressive, lowstand, and transgressive systems tracts. A low accommodation setting coupled with high-frequency and low-amplitude sea-level fall associated with the steep gradient of the Ferron Notom Delta Complex (FNDC) delta front slope are considered to be the primary mechanisms behind the observed stratigraphic relationships, moderate fluvial incision depth, and thin-nature of the systems tracts within the Critical Interval.

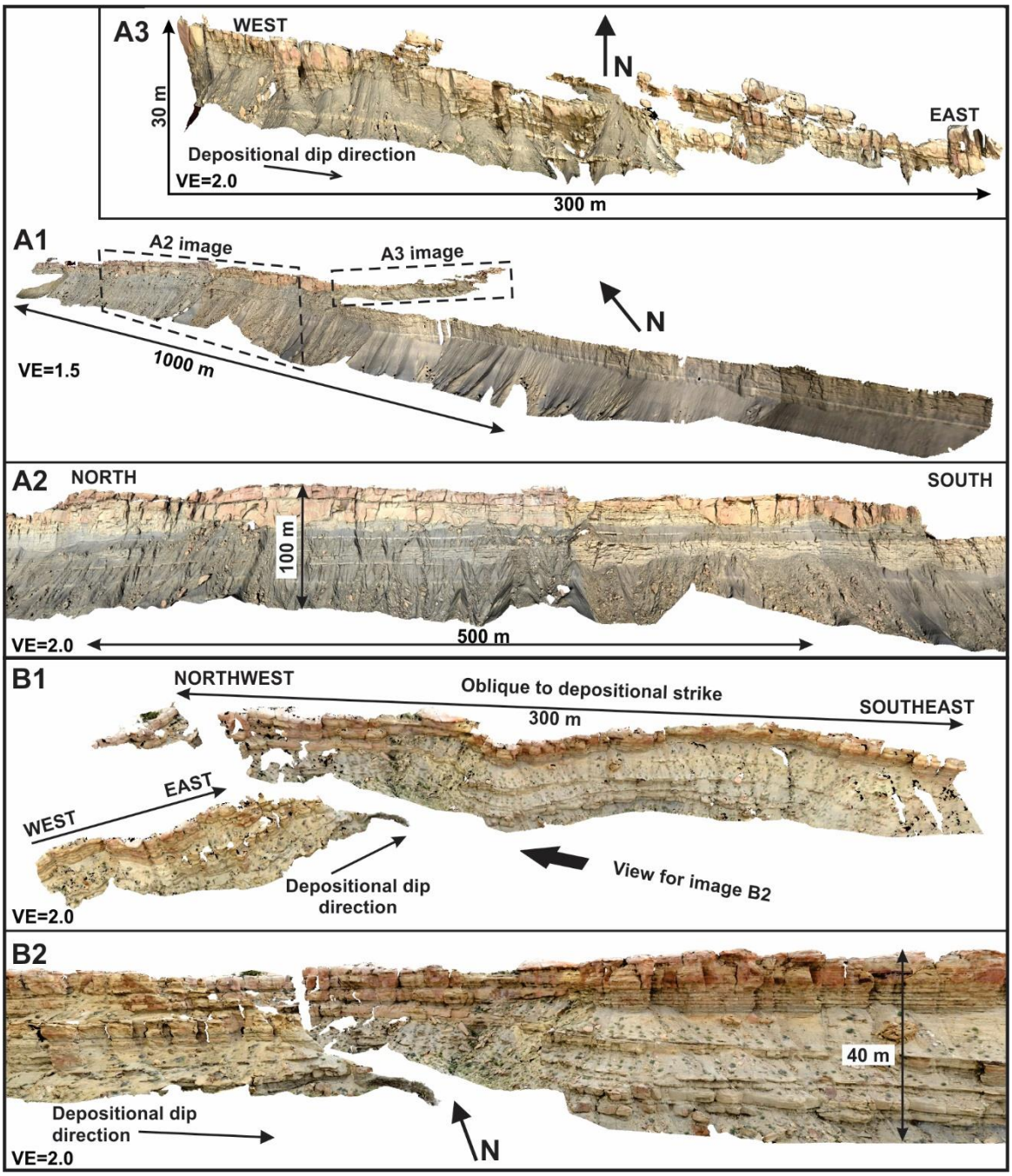

Figure 4 - VOMs used in this study. VOM locations shown in Fig. 2D. VE = Vertical exaggeration. **A1)** Views of the Post VOM looking northeast onto the north-northwest to south-southeast trending, depositional strike-oriented cliff face. Note the boxes represent close-up images of **A2** and **A3**. **A2)** Close up image of the main north-south trending, depositional strike-oriented Post cliff face. **A3)** West-east trending, depositional-dip oriented cliff-face that connect perpendicularly to the main Post cliff. **B1)** Overhead image of the Labyrinth VOM, displaying both the oblique to strike- and dip-oriented cliff facies. **B2)** Northerly view looking into the Labyrinth outcrop canyon, illustrating the exposure within the study area.

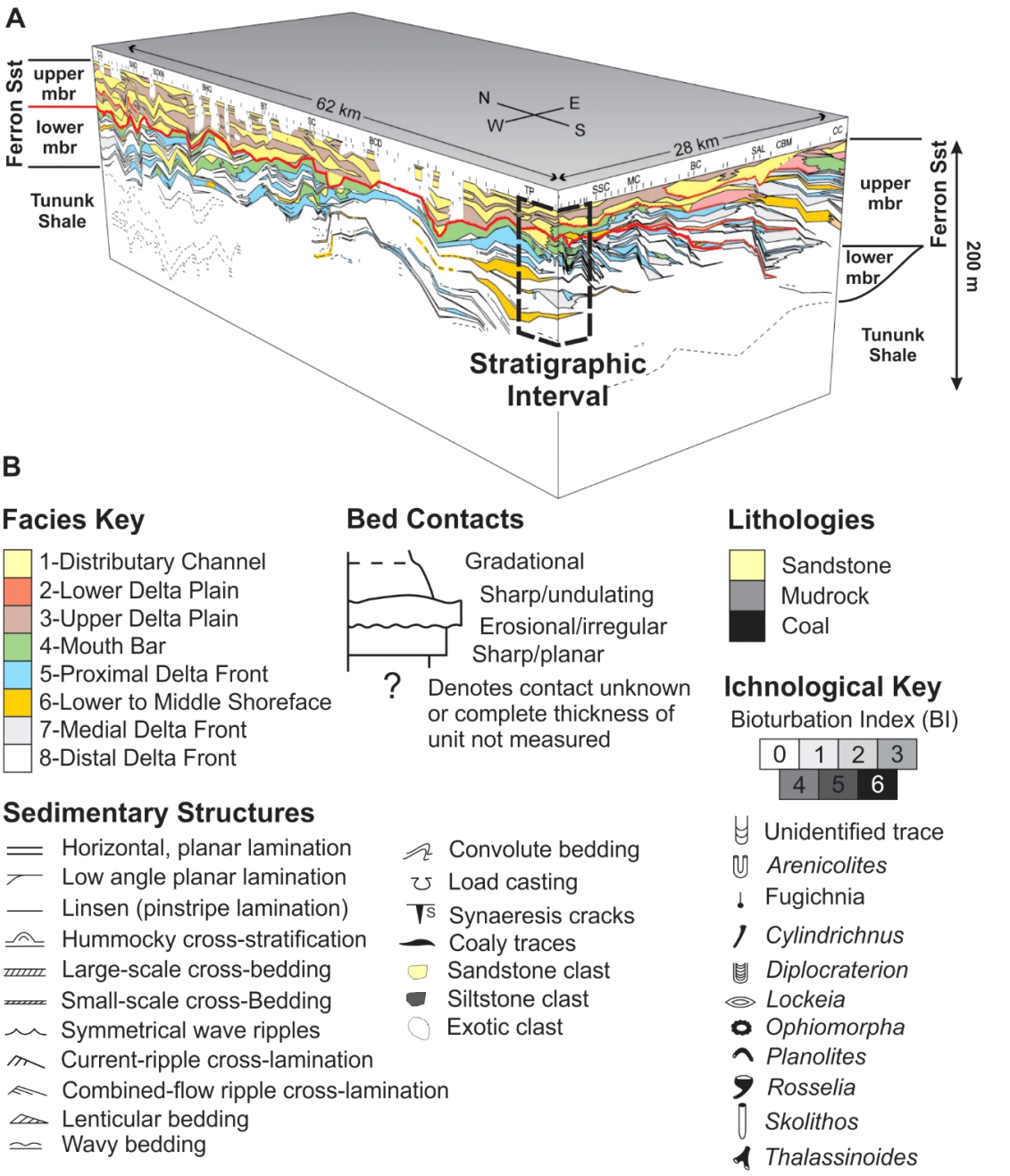

Figure 5 - A) Conjoined cross-sections from Fielding (2011) and Korus and Fielding (In Press) displaying regional stratal stacking patterns and facies architecture of the Ferron Notom Delta Complex in the western Henry Mountains region of south-central Utah. Aerial extent and locations of cross-sections are displayed in Fig. 2C. Note the regionally extensive sequence boundary (SB1; red line) continuously correlated along the 62 km strike-oriented cross-section. Black box represents the study area and stratigraphic interval of the present study. Figure from Korus and Fielding, In Press. **B)** Facies key and log key for measured sections.

GEOLOGICAL BACKGROUND

Beginning in the late Jurassic, a broad foreland basin initiated between the western Cordilleran volcanic arc and eastern North American craton, developing along and east of the Sevier belt (Yonkee and Weil, 2015). The Sevier belt formed as a foreland-propagating (west to east) wedge mostly during Cretaceous to Paleogene time, and included a western thrust system with aerially extensive thrust sheets that carried thick passive margin strata, and an eastern thrust system that carried thinner strata. During the early Cretaceous flexural loading from thrust sheets, load redistribution by erosion and deposition, dynamic subsidence related to subduction, and global sea level changes (DeCelles and Giles, 1996; DeCelles, 2004; Liu et al., 2005), created a north-south elongate, asymmetrical foreland basin forming the epicontinental Cretaceous Western Interior Seaway (KWIS; Yonkee and Weil, 2015)

During the middle-to-late Turonian (at the time of Ferron deposition; Fig. 3A), foredeep subsidence had migrated eastward, the depocenter being located in northern Utah and southwestern Wyoming with an area of lower accommodation on the flank of the forebulge in southern Utah (Fig. 3B; White et al., 2002; Ryer and Anderson, 2004). A regional regression during the middle/late Turonian led to eastward shoreline progradation, depositing a series of coarse clastic wedges (Fig. 3B). Sediments were sourced from growing Sevier orogenic highlands, fluvially dispersed eastward across a narrow coastal plain, and deposited in a series of delta complexes on the western margin of KWIS that faced east-to-northeastward (Fig. 3B; Hale and Van De Graaff, 1964; Hale, 1972; Cotter, 1975; Hill, 1982; Gardner, 1995; Ryer and Anderson, 2004). This regional regression is recorded by the Ferron Sandstone in south-central Utah, the Frontier

Formation in northeast Utah and southwest Wyoming (Kirschbaum and Mercier, 2013; Hutsky and Fielding, 2017), the Gallup Sandstone in northwest New Mexico (Nummedal and Molenaar, 1995), and the Cardium Formation in western Canada (Hart and Plint, 2003). Three known deltaic wedges comprise the Ferron Sandstone member, from north to south; the Vernal, Last Chance, and Notom Delta complexes (Fig. 3B; Hale, 1972; Cotter, 1975; Hill, 1982; Garrison and Van den Bergh, 2004). The Ferron Sandstone member is underlain by the Tununk Shale and is unconformably overlain by the Blue Gate Shale, together constituting the Mancos Shale (Fig. 3A; Lupton, 1916; Hunt, 1946).

During the Turonian, the mid-Cretaceous 'greenhouse' climate is interpreted to have reached peak 'hothouse' conditions (Wilson et al., 2002). Proxy records strongly argue for substantially warmer sea-surface and high-latitude continental temperatures than today (Barron et al., 1983; Herman and Spicer, 1997), leading to the interpretation of an ice-free Earth system at this time (Huber et al., 2002; Norris et al., 2002). Turonian paleogeographic reconstructions indicate 40–50°N paleolatitude and subtropical climate for the region during Ferron accumulation (Sageman and Arthur, 1994; Dean and Arthur, 1998). Recent $^{40}Ar/^{39}Ar$ geochronology of several bentonite beds within and immediately above and below the Ferron-Notom clastic wedge indicate the age of accumulation was from 91.25 Ma to 90.63 Ma, an interval of 600,000 years (Zhu et al., 2012).

Gilbert (1877) was the first to document the Ferron Sandstone in the HMR, initially naming it the Tununk Sandstone. It was not until after Hunt and Miller (1946) correlated the regional stratigraphy to the type Ferron section near the town of Ferron, Utah, that the local formation received its current name. Peterson and Ryder (1975)

informally divided the outcropping Ferron Sandstone Member of the Henry Mountain region into lower and upper members. Facies analysis of Fielding (2010) conducted on the western limb of the HMS, characterized the upper member as fluvial in origin, composed of erosionally based distributary channel sandstones encased in floodplain, mire, and lagoonal sediments. The lower member is marine to deltaic in origin, consisting of prodelta and delta-front facies that are stacked in coarsening-upward, progradational cycles (Fielding, 2010). The upper and lower Ferron Sandstone members are separated by a regionally extensive sequence boundary (hereafter referred to as SB1), mapped along strike by Fielding (2011) and down depositional-dip by Korus and Fielding (In Press) (Fig. 5A). Depositional dip-oriented transects document offlapping and downlapping clinothems with descending, regressive trajectories indicating deposition predominantly during forced regression (Fielding, 2015; Korus and Fielding, In Press).

The FNDC is characterized as the deposits of several flood-dominated, yet wave and tide-influenced, small- to medium sized, asymmetrical deltas that prograded eastward into the KWIS (Fielding, 2010). Although the deposits of the delta front display a dominant eastward progradation direction, paleocurrent data from distal delta front facies indicate southward-deflection presumed due to a cyclonic gyre in the KWIS (Cotter, 1975; Slingerland et al., 1996; Fielding, 2010; Li et al., 2011b; Korus and Fielding, 2015). Allogenic control is suggested to have been the primary influence on stratigraphic architecture (Li et al., 2011a; Zhu et al., 2012; Li and Bhattacharya, 2013, Fielding, 2010, 2011, 2015) with two different mechanisms proposed. Fielding (2011) proposed tectonic forcing through the growth of a synsedimentary structural arch (~50 m amplitude fold structure; Fig. 3A) attributed to Sevier forebulge migration. Glacio-eustatic sea-level

fluctuation driven by the periodic growth and decay of glaciers was suggested by Zhu et al. (2012) as an alternative explanation for interpreted sea-level excursions of < 50 m.

STUDY AREA AND METHODS

The study area is located in Garfield County of south-central Utah, USA on the western limb of the HMS (Fig. 2) beneath the northern backdrop of South Swap Mesa, roughly ~1.5 kilometers to the east of the Notom-Bullfrog access road. Extensive canyon wall exposure and minimal vegetation allow for unobstructed 3D analysis of stratal geometries and internal lithofacies relationships. A dual approach of traditional outcrop methodologies in combination with LiDAR derived VOMs (Fig. 4) analysis is used here in order to gather a robust dataset from the study area and stratigraphic interval of interest. Two VOMs were used for this project (Figs. 2D, 4); 1) The Post VOM (Fig. 4A), a continuously outcropping, 1.5 km long, north-south trending, strike-parallel cliff face (~100 m in height) exposing the stratal stacking patterns of the lower Ferron member. The Post VOM includes a 300 m west-east trending, dip-parallel cliff face (~25 m height) (Fig. 4A) allowing for true 3D analysis. 2) The Labyrinth VOM is located ~700 m to the east, down depositional dip from the Post location at the eastern edge of the study area (Fig. 4B). The Labyrinth VOM displays two ~40 m stratigraphic successions and exhibits truly three-dimensional exposure, oriented obliquely along strike and dip (Fig. 4B).

Both VOMs were interpreted using LIMEv0.64, a research software tool for LiDAR interpretation and manipulation. VOM analysis included outlining lithofacies and key sequence stratigraphic surfaces. LiDAR data collection (see reviews by Buckley et al., 2008; Pringle et al., 2006; Howell et al., 2014) was implemented using a Riegl LMS-

Z420i ground-based terrestrial laser scanner. Point cloud data combined with an overlay of referenced photogrammetry allowed integration of the outcrop coloration into the VOM (see review by Enge et al., 2007).

An intensive, ground-based sedimentological and ichnological investigation was carried out over the small (4 km^2) study area. 15 detailed vertical sections of varying stratigraphic intervals were measured in the field with particular focus on the interval through the regional sequence boundary that separates the lower and upper members of the Ferron Sandstone. Measured section locations (Fig. 1D) were chosen so as to provide distributed data across the study site and to satisfy the need for documentation of stratigraphically important boundaries and facies. All measured sections were located by GPS and cross-referenced with topographic maps and aerial imagery. Measured vertical sections documented lithology, grain size, sedimentary structure, bed contacts, paleocurrent indicators, and trace fossils. Key beds and sequence stratigraphic surfaces were walked-out over the entire study area during fieldwork and outlined on the VOMs and compiled photomosaics. This allowed for the correlation and "ground-truthing" of virtual outcrop interpretations. Paleocurrent data were gathered and corrected for magnetic declination. Paleocurrent analysis utilized the EZ-ROSE program by Baas (2000). Trace fossils were identified where possible, noting size of individual traces, their distribution, and intensity of bioturbation based on the bioturbation index (BI) of Taylor and Goldring (1993). Cross-sections were hung from a laterally persistent TRS, unlike in prior studies that have used the top of the Ferron or the basal bentonites as datums. This is because many of the stratigraphic sections could not be logged through the entirety of the Ferron Sandstone.

Table 1 - Facies of the Ferron Sandstone Member. Table from Fielding (2010) with modifications. Note the new facies scheme changes from this study and the correlation to the Fielding (2010).

Facies	Interpretation (Fielding, 2010)	Lithology	Physical Structures	Biogenic Structures	Interpretation (This Study)
1	Distributary Channel	Erosionally-based, poorly sorted, med.- to v.c.-gr. sandstone bodies (~2-10 m thick) with extraformational gravels, pebbles, and intraformational siltstone clast. Thin (cm-scale) siltstone beds separate multistorey and/or multilateral channel fills.	Sole structures (gutter, flute, and tool marks) and syneresis crack on basal surfaces, large-scale (3–6 m), low-angle cross-bedding (lateral accretion surfaces), trough cross-bedding (0.1–1.5 m thick), local sigmoidal profile and/or mud drapes (paired), minor flat and undulatory lamination, convolute bedding, bed tops show current-ripple cross-lamination	Plant debris (macerated and coalified logs). Sparse bioturbation on basal surfaces, BI = 0–1 (*Lockeia*, *Planolites*), locally absent internally, BI = 0, more abundant at tops of bodies, BI = 0–2 (*Diplocraterion*, *Planolites*, *Cylindrichnus*, *Ophiomorpha*).	**Distributary Channel Variant 1**
		Erosionally-based, mod. sorted, f.- to med.-gr., U-shaped sandstone bodies (~2-7 m thick), minor extra-formational gravels and intra-formational siltstone clast, channel bodies are composed of individual sandstone beds separated by thin (cm-scale) siltstone partings, inclined-heterolithic-strata (IHS) of f.-gr. sandstone and siltstone interbeds located near body margins.	**Sandstone:** sole structures (flute, tool marks), syneresis cracks on basal surfaces, large-scale (2–6 m) low-angle cross-bedding (lateral accretion surfaces), trough cross-bedding (0.1–1.2 m), local sigmoidal profile and/or paired mud drapes, minor flat and undulatory lamination, convolute bedding. **IHS:** siltstones show flat and low-angle lamination, sandstones show flat and low-angle lamination, current-ripple cross-lamination, and trough cross-bedding.	Macerated plant debris locally abundant, bioturbation most abundant on basal surfaces and within siltstone partings, BI = 1–3 (*Lockeia*, *Planolites*, *Cylindrichnus*, and small *Diplocraterion*), sparse internally, BI = 0–1, more abundant at tops of bodies, BI = 0–2 (small *Diplocraterion*, *Planolites Thalassinoides*, *Rosselia*, *Cylindrichnus*, *Ophiomorpha*).	**Distributary Channel Variant 2**
2	Costal Floodplain	Intervals (1-2 m thick) of grey siltstone and black carbonaceous shale, root-penetrated bed, pedogenic alter-ation, gray to orange-mottling, locally sulfur-stained, minor interbeds (<0.15 m thick) of v.f.- to f.-gr. sandstone.	Siltstone and shale are finely-laminated, sandstone beds may contains current-ripple cross-lamination.	*In situ* plant roots, dispersed plant debris (some petrified logs), locally upright *in situ* tree stumps. No bioturbation, BI = 0.	**Upper Delta Plain**
	Coastal Mire	Black carbonaceous shale to locally clean coal (1 m thick).	Flat, parallel stratification, sulfur staining.	*In situ* and drifted plant material. No bioturbation, BI = 0.	

Facies	Interpretation (Fielding, 2010)	Lithology	Physical Structures	Biogenic Structures	Interpretation (This Study)
3	Coastal Lagoon	Interbedded intervals of f.- to crs.-gr. siltstone, laminated coaly siltstone and thicker (0.2-2.0 m thick) individual, erosionally-based, f.- to med.-gr. sandstone beds.	Erosionally-based sandstone bodies contains load casts and syneresis cracks on basal surfaces, planar and low-angle lamination, trough cross-bedding (0.2-0.7 m sets), and swaley- and hummocky-cross-stratification (0.3-1.5 m thick; S/HCS), tops typically current rippled. Siltstones are crudely stratified and may contain organic-rich lamination.	Macerated plant debris and organic-rich laminations, bioturbation on individual sandstone bed bases and tops, BI = 0-4, abundant on bed bases, BI = 0-4 (small *Diplocraterion*, *Planolites*, *Thalassinoides*, *Ophiomorpha*), sparse, yet consistent bioturbation on bed tops BI = 0-2 (large *Diplocraterion*, compound *Arenicolites*, fugichnia).	**Lower Delta Plain**
4	Mouth Bar Complex	Planar, or erosionally-based, f.- to med.-gr. sandstone bodies (2-6 m thick) that typically coarsen upwards, thin (<1.5 m thick) channel forms located the tops of intervals. Bodies are characteristically w.-sorted and contain >95% sandstone.	Sole structures on bed bases, soft-sediment deformed and synsedimentary growth-faulted bodies, displaying large-scale planar-parallel and low-angle discordant lamination, cross-stratification, clinoform-sets, bed tops preserve combined-flow sedimentary structures, channel forms contains trough cross-bedding (<1.0 m in height).	Macerated plant debris common, bioturbation is sparsely observed at the tops of beds, BI = 0-2 (*Planolites*, small and large *Diplocraterion*, *Skolithos Ophiomorpha*, *Cylindrichnus*, *Rosselia*).	**Mouth Bar Complex**
5	Proximal Delta Front	Amalgamated, sharp-based, f.- to med.-gr. sandstone units of highly variable thickness (2-15 m thick), three variants observed: **1**. soft-sediment-deformed, **2**. stratified, **3**. rotated or growth-faulted masses.	**1**. large-scale convolute bedding and load casting, **2**. med.- to large-scale HCS, flat and low-angle lamination with parting lineation, local cross-bedding, syneresis cracks and load casts, symmetrical wave-ripples and interference ripples near bed tops, **3**. stratified as above, massive SSD.	**1**. none. **2**. dispersed, sparse bioturbation throughout bodies, BI = 0–2 (*Thalassinoides*, O*phiomorpha*, *Planolites*, *Diplocraterion*, *Lockeia*, *Cylindrichnus*, fugichnia), tops of beds intensely bioturbated, BI = 2–4 (D*iplocraterion*, *Thalassinoides*, *Cylindrichnus*, *Ophiomorpha*). **3.** none.	**Proximal Delta Front**
6	Delta Lobe Abandonment	Erosionally-based, locally coarsening-upward bodies of orange-tan calcareous med.-gr. sandstone with intraformational siltstone clasts (5-10 mm), appears weathered/mottled due to intensity of bioturbation.	SSD, HCS, current and combined-flow ripple cross-lamination, locally preserved cross-bedding and convolute bedding.	Abundant macerated plant debris ("coffee grounds", organic-rich lamination) locally pervasively bioturbated, BI = 2-6 (*Ophiomorpha*, *Diplocraterion*, *Rosselia*, large *Teichichnus*) dominated by vertical and obliquely orient burrows.	**Lower- to Middle-Shoreface**

Facies	Interpretation (Fielding, 2010)	Lithology	Physical Structures	Biogenic Structures	Interpretation (This Study)
7	Medial Delta Front	Thickly interbedded f.-gr. siltstone, c.-gr. siltstone, and v.f.-gr. to f.-gr. sandstone intervals (<6 m thick; 30–60% sandstone), sandstone beds are sharp- to erosionally-bounded (<0.3 m thick).	**Sandstone**: current and combined-flow ripple cross-lamination, HCS, flat and low-angle lamination, soft-sediment deformation, syneresis cracks, thicker beds preserve sole structures and load casting. **Siltstone**: stratified, intraformational breccias of SSD siltstone clast, imbricated, or concentrated at bed tops.	Abundant macerated plant debris in all lithologies, f.- and c.-gr. siltstones are unbioturbated, BI = 0, sandstones are locally bioturbated on bed bases and tops, BI = 0–2 (small *Diplocraterion*, *Arenicolites*, *Planolites*, *Ophiomorpha*, fugichnia *Cylindrichnus*, and rare *Skolithos*).	**Medial Delta Front**
8	Distal Delta Front	Thinly interbedded heterolithic strata, dominated by f.-gr. siltstone, with thin beds (<0.1 m thick) of v.f.- to f.-gr. sandstone (10–30%) in sharp-bounded beds, c.-gr. siltstone beds are locally present.	Fine- and c.-gr. siltstones are crudely stratified, sandstones contain linsen lamination, lenticular and wavy bedding, current and combined-flow ripple cross-lamination, symmetrical wave and interference ripples, with load casts, sole structures, and syneresis cracks on bed bases.	F.-gr. siltstones are typically unbioturbated, BI = 0-1 (*Planolites*), c.-gr. siltstones are rich in macerated plant debris and unbioturbated. Sandstones are sparsely and irregularly bioturbated, BI = 0–2 (*Planolites*, *Lockeia*, *Thalassinoides*, small *Diplocraterion*, *Gyrochorte*, *Cylindrichnus*)	**Distal Delta Front**
9	Prodelta	Thinly laminated siltstone with minor v.f.-gr. sandstone beds (<5 cm thick), rare thin (5 cm thick) reworked bentonite layers.	Sandstones contain linsen lamination, lenticular and wavy bedding, current and combined-flow cross-lamination, and load casts.	Locally sporadic distribution of bioturbation, BI = 0-3 (*Planolites*, small *Teichichnus*). Locally fossiliferous (bivalves, ammonoids).	**Prodelta**
10	Offshore	Thinly laminated, locally fissile, f.-gr. siltstone and claystone (shale), with local bentonite beds (0.10 m thick).	Parallel lamination.	Largely unbioturbated, locally fossiliferous (bivalves, ammonoids).	**Offshore**

FACIES ANALYSIS

The facies scheme presented herein is largely consistent with the extensive lithofacies analysis of the Ferron Sandstone member conducted by Fielding (2010). The purpose of this section is to emphasize new facies and associations not described by Fielding (2010). See Table 1 for a comprehensive summary of facies based both on the present study and the regional analysis of Fielding (2010).

Facies 1 – Distributary Channel

Description -

Facies 1 consists of erosionally-based (Fig. 6; Table 1) bodies of fine- to coarse-grained sandstone, with minor extraformational gravel and intraformational siltstone clasts. Facies 1 constitutes the volumetric majority of strata within the upper Ferron Sandstone member and only a minor proportion of the lower member (Fig 5A; Fielding, 2011; Korus and Fielding, In Press). Within the local stratigraphic interval of the study area, two variants of Facies 1 are observed, distinguished by the following criteria; sandstone-body dimensions, average grain-size, paleocurrent trends, and presence of bioturbation (Table 1).

Variant 1 -

Distributary Channel Variant 1 (V1) is characterized by erosionally-based, moderately-sorted, medium- to coarse-grained sandstone bodies (2-10 m thick) with extraformational gravels, pebbles and intraformational siltstone clast. Sandstone bodies are locally well-developed in the upper portion of the upper Ferron Sandstone member (Figs. 6C; 5A). Fielding (2010, 2011) correlated these sandstone bodies within the study

area along the western rim of HMS, showing channel widths may extend 5-20 km along depositional strike (perpendicular to paleoflow direction). Locally, sandstone bodies display consistent thickness and show no observable pinch-outs or lateral boundaries. Channel bodies display multistorey and multilateral channel organization (Fielding, 2010). Large-scale (3-6 m in height), low angle cross-bedding (lateral accretion surfaces) and trough cross-bedding are the primary sedimentary structures with individual channel bodies. Local paleocurrent data indicates no dominant modes of paleoflow, displaying a multi-modal distribution (Fig. 7E). Fine-grained material (e.g. siltstone) composes <5% of the total lithological composition, and is only observed at local erosional surfaces separating multistorey channel fills. Inclined heterolithic stratification (IHS; Thomas et al., 1987) is absent from V1. Bioturbation is absent to sparse (BI = 0-2) within V1, preserved bioturbation is typically observed only locally at the tops of channels bodies, usually by a low diversity assemblage of 1 or 2 individual traces (Table 1).

Variant 2 -

Distributary Channel Variant 2 (V2) consists of moderately-sorted, fine- to medium-grained, U-shaped, channel-form sandstone bodies (~2-6 m thick and 150-300 m wide), some of which are incised into underlying strata with up to ~5 m of relief (Fig. 6A). Sandstone bodies are composed of individual channel-form sandstone beds (0.5-2.5 m thick) that are individually stacked upon one another and separated by thin (cm-scale), bioturbated siltstone partings (Fig. 6A). These composite channel sandstone bodies commonly contain three individual erosive-based beds, with a maximum of five individually-stacked beds (Fig. 6A). Interior channel bodies of V2 are predominately characterized by medium-grained sandstone beds with erosional- or planar-bases that are

dominated by flat and low-angle cross-stratification and trough scours. IHS of alternating sandstone and mudstone beds (Fig. 6B) are commonly located at the lateral margins of V2 incised bodies (Fig. 6A, B). IHS interbeds consist of fine- to medium-grained sandstone beds of variable thicknesses (0.1-0.25 m thick) and thin (cm-scale) siltstone beds that gradually amalgamate laterally and transition into the interior channel deposits of medium-grained sandstone (Fig. 6A). The sandstone unit of the IHS interbeds commonly have irregular basal surfaces and internally display planar and low-angle laminations, with current ripple-cross lamination at the tops of beds. IHS beds dip at 6-18° and exhibit an angular discordance with the overlying flat-lying strata (Fig. 6A, B). At the tops of V2 channel body succession are intervals of thinly interbedded (~0.1 m thick) grey siltstones and fine-grained sandstone with abundant macerated plant debris and thin layers of dark-grey carbonaceous siltstones. Locally, V1 displays erosional and transitional lateral relationship with Facies 3, lies above and incises into Facies 7, and is overlain by Facies 6 (Table 1). The basal incision surface marks the regionally extensive SB1 (Figs. 6A; 5A).

Bioturbation is commonly observed at basal surface of individual channel beds and within siltstone partings (BI = 1-3), displaying a consistent assemblage of *Lockeia*, *Planolites*, *Cylindrichnus*, and small *Diplocraterion* that found on surfaces containing syneresis cracks. Bioturbation is less abundant at the tops of beds (BI = 0-1), where only individual, isolated traces are observed. Locally, V1 displays erosional and transitional lateral relationship with Facies 3, lies above and incises into Facies 7, and is overlain by Facies 6 (Table 1). The basal incision surface marks the regionally extensive SB1 (Figs. 6A; 5A).

Interpretation -

In general, Facies 1 contains erosionally-based to incised sandstone bodies with cross-beds in multistorey/multilateral organization which are interpreted as the deposits of distributary channel(s) within the delta-plain setting. V1 deposits are considered to be laterally extensive (km-scale) and substantially wider than V2. V1 bodies are multistorey/multilateral, possess a higher fraction of coarse-grained sediment, lack IHS, shows no paleocurrent evidence of tidal-processes (Fig. 7E), and locally display a lesser degree of bioturbation relative to V2. V1 characterizes the prominent sandstone bodies in upper Ferron Sandstone member (Fig. 5A) and represent the deposits of distributary channels within the upper delta plain (Facies 2; Table 1), located in the most proximal (landward) setting preserved within the fluvial-deltaic Ferron Sandstone depositional system. Variances in channel body size, stacking organization, and lithological composition within individual channels argues against a simple, steady-state depositional history. This depositional setting is interpreted to lie above the point of significant marine- or tidal-influence due to a lack of tidal-indicators and lesser degree of bioturbation and thus deposits are fluvial-dominated. Fielding (2010) suggested that some of the larger channel bodies composed of multistorey, multilateral channels fills along the western rim of the HMS could represent coastal-plain incised valley fills.

The incised channel bodies composed of fine- to medium-grained sandstone are interpreted as the product of distributary channels in the lower delta plain (Facies 3; Table 1) setting where both fluvial- and tidal-processes influenced deposition. Paleocurrent data reveals a well-defined bi-modal paleocurrent distribution (Fig. 7D), displaying a dominant east-northeast (80°) flow direction and minor westward mode,

interpreted to represent tidal-backflow during low outflow periods. Sedimentation and marine-influence was episodic, at times associated with in-channel flow reversal indicated by the minor westward mode, as well as salinity changes, likely under the forcing of tidal processes in the fluvial–tidal transition zone (FTTZ; cf. Dalrymple and Choi 2007; Van den Berg et al. 2007, Dashtgard and La Croix, 2015). IHS near the channel body margins is interpreted as lateral accretion sets at meander bends, suggesting moderate sinuosity within the formative fluvial system. One exposed channel body displays the typical point bar to cut bank cross-sectional geometry associated with sinuous fluvial systems, adding further evidence for sinuosity (Allen, 1963).

Siltstone partings containing syneresis cracks and a consistent trace fossil assemblage of low diversity represent times of little or no discharge and/or sediment accumulation, when the coastal saltwater wedge may have extended upstream, resulting in intrusion of brackish- to marine conditions into distributary channels (Dalrymple and Choi, 2007; Dalrymple et al., 2015). The low-diversity trace fossil assemblage, characterized by *Diplocraterion*, small-diameter *Skolithos*, *Planolites,* and *Lockeia,* is interpreted as the record of opportunistic colonizers that could withstand the stressful environment of the FTTZ.

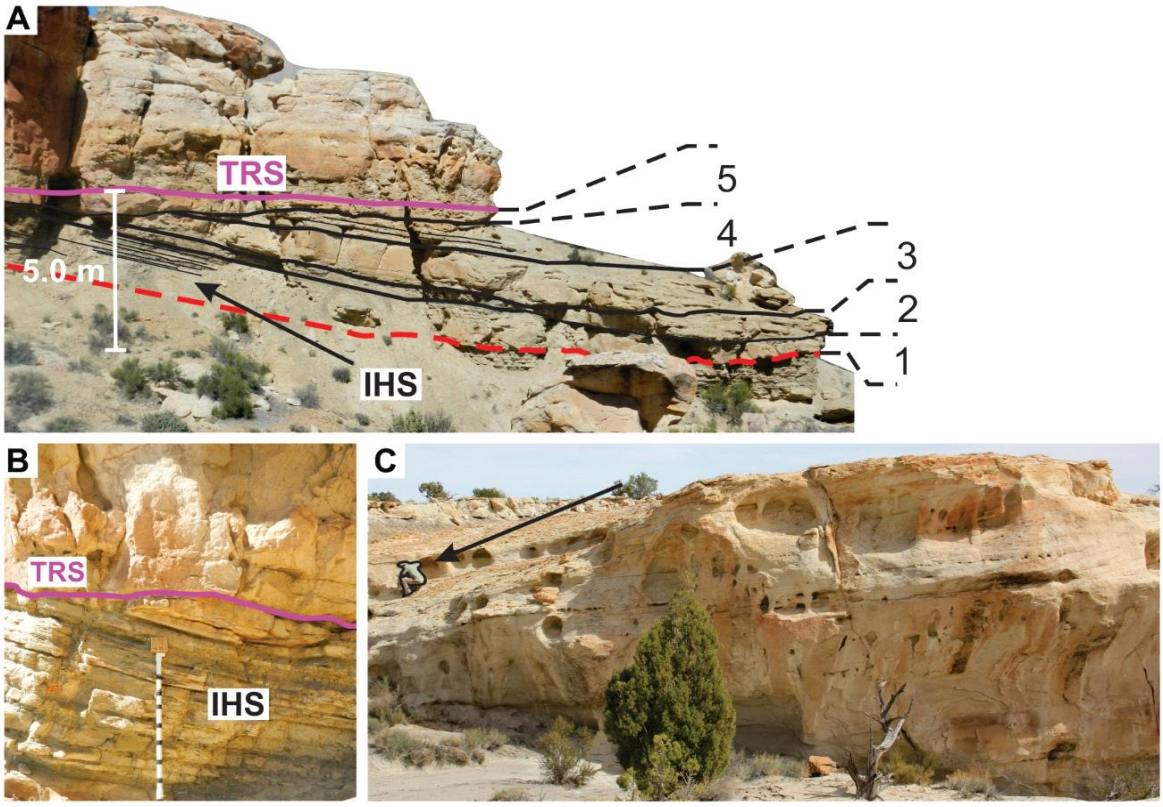

Figure 6 – Images of Facies 1. For measured section (MS#) locations see Fig. 2D. **A)** Variant 2 incised distributary channel body showing five individual, erosionally based sandstone beds. Channel margin IHS grades laterally into the interior sandstone dominated bodies of the axial channel fill. The basal surface of Variant 2 represents a sequence boundary (red line). Image location is at the northwestern margin of the Labyrinth gully network, near MS#4. **B)** IHS composed of fine-grained sandstone and mudstone interbeds (<0.15 m thick) located at the Channel 2 margin near MS#6. Note the angular discordance and truncation with the overlying bioturbated sandstone of Facies 6 (Table 1), this contact marks the TRS. Jacob staff = 1.5 m. **C)** Image of Variant 1, showing a ~8 m thick coarse-grained sandstone body stratigraphically located within the upper portion of the upper Ferron Sandstone member. Image is take at the location of MS#8 atop the Labyrinth outcrop. Arrow points to outline of crouching human = ~1 m in height.

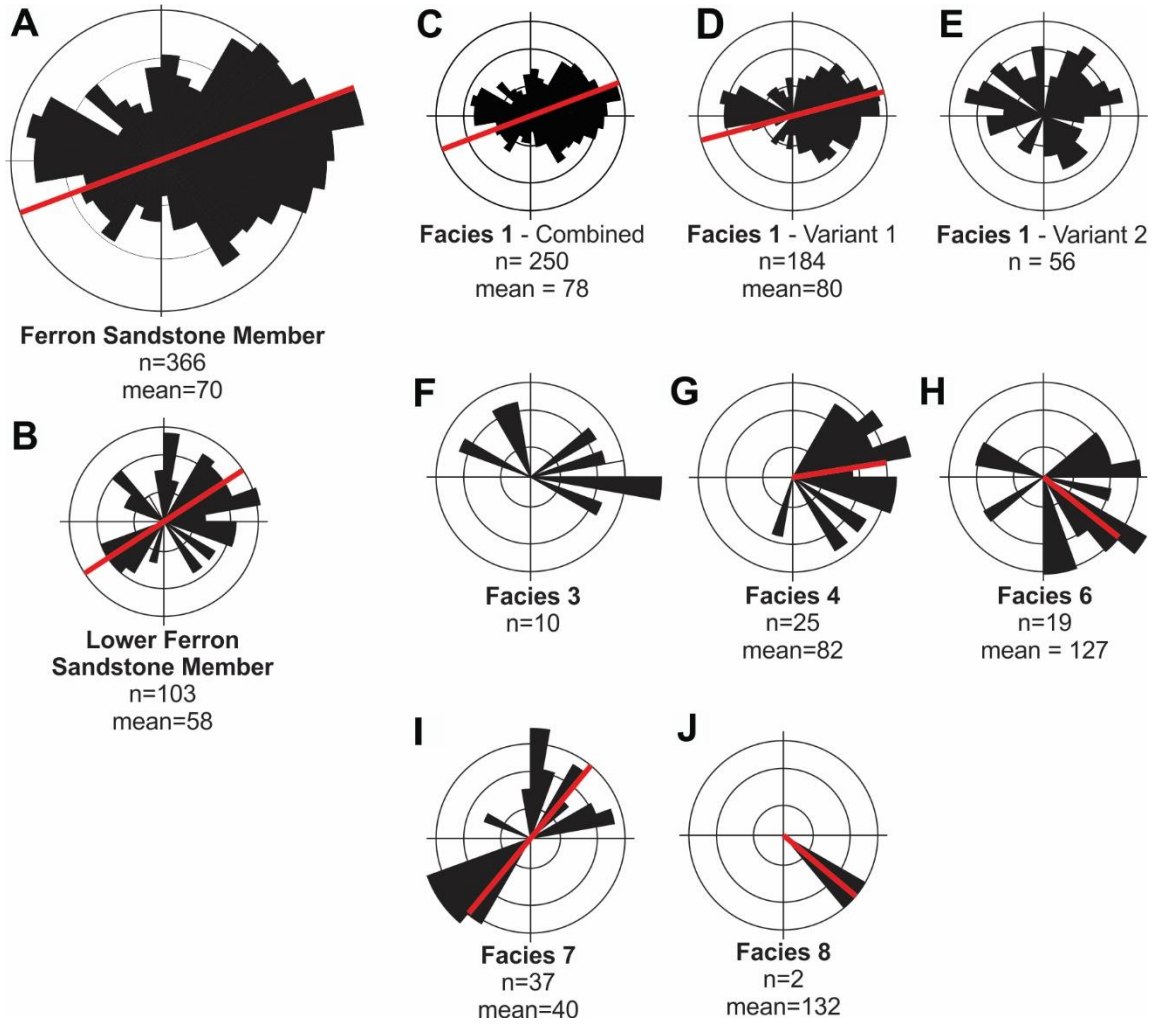

Figure 7 – Paleocurrent data from local stratigraphic interval displayed in rose diagrams. Red lines = dominant paleocurrent trend. n = number of total data points. See appendices 1E for numerical data used to derive diagrams. **A)** Combined paleocurrent data from Ferron Sandstone Member, regardless of facies or variant. Paleocurrent trends indicate a northeast oriented paleoslope direction. **B)** Combined paleocurrent data from only the lower Ferron Sandstone member. **C-E)** Combined paleocurrent data for only Facies 1, with individual diagrams for described Facies 1 variants. **F-J)** Paleocurrent trends for individual facies.

Facies 2 – Upper Delta Plain

Description -

Facies 2 (Table 1) is composed of primarily light-grey siltstone and black carbonaceous shale (Fig. 8) with minor proportions of locally clean coal, and thin beds (5-10 cm thick) of very-fine- to fine-grained sandstone. Facies 2 is stratigraphically confined to the upper fluvial member of the Ferron Sandstone, strongly associated with Facies 1 V1 (Fig. 8). Siltstone and carbonaceous shales are commonly textured with blocky structure and zones of orange-brown staining. Tops of individual beds are root-penetrated and locally sulfur-stained. Carbonaceous shale tend to be highly fissile, organic-rich, and are may interbedded with thin (cm-scale) coaly-horizons or gradually pass upward into clean coal horizons (~1 m thick). Depending on the degree of weathering, carbonaceous shale beds may appear brown (weathered exposure) or black (fresh exposure) at outcrop. Sedimentary structures are almost entirely absent within the finer-grained faction of lithologies in Facies 2, only fine (mm- to cm-thick) laminae are evident in siltstone and shale intervals.

Facies 2 contains very little sandstone (10-20%), represented in the form of very-fine-to fine-grained sandstone “stringers”, sporadically interbedded within the previously described lithologies. Sandstone stringers are thin (5-10 cm), planar- to irregular-based beds containing current-ripple cross-lamination. Plant debris is abundant within all lithologies of Facies 2, including; detrital material and *in situ* plant stems, axes, and roots. No bioturbation or paleocurrent indicators were observed within Facies 2.

Interpretation -

Black carbonaceous shales record deposition in waterlogged floodplains or shallow lake environments that occupied the relatively flat area outside the active distributary channels on the coastal plain. Thin sandstone “stringers” are interpreted as splay or distal overbank deposits formed during high-discharge events that breached channel levees. The light-gray to black color variation, orange-brown mottling and plant roots within the siltstones indicate pedogenic modification or gleying of the substrate typically associated with waterlogged environments. Coal deposits represent the formation of coastal mires, where vegetation growth was unimpeded by sedimentation in a distal location to the active sedimentation processes associated with distributary channels. The absence of marine ichnotaxa indicates sediments accumulated in a setting out of reach from marine-influence or inundation of marine waters. The absence of non-marine traces may be the result of the result of inhospitable or highly stressed conditions, a lack of colonization substrate, or indicate that traces were simply not preserved. No syneresis cracks, wave- or tidal-influenced sedimentary structure or other forms of evidence supporting periodic marine flooding or marine- to brackish-water conditions are evident, indicating this environment was situated above the limit of tidal inundation (Wright, 1978). Vegetation preserved as detrital or *in situ* plant roots, trunks, stems, or macerated plant debris indicate local growth of vegetation. Gleyed siltstones and weakly developed paleosols, deposits related to standing bodies of water (e.g. interdistributary lake carbonaceous shales), and vegetation imply both submerged and emergent surfaces. In conclusion, the unbioturbated, organic-rich siltstones and carbonaceous shales, presence of thin (>1.0 m) locally developed coal beds, lack of marine-influence

sedimentary structures, and absence of tidal indicators argue in favor of deposit formed in an upper delta plain (UDP) setting.

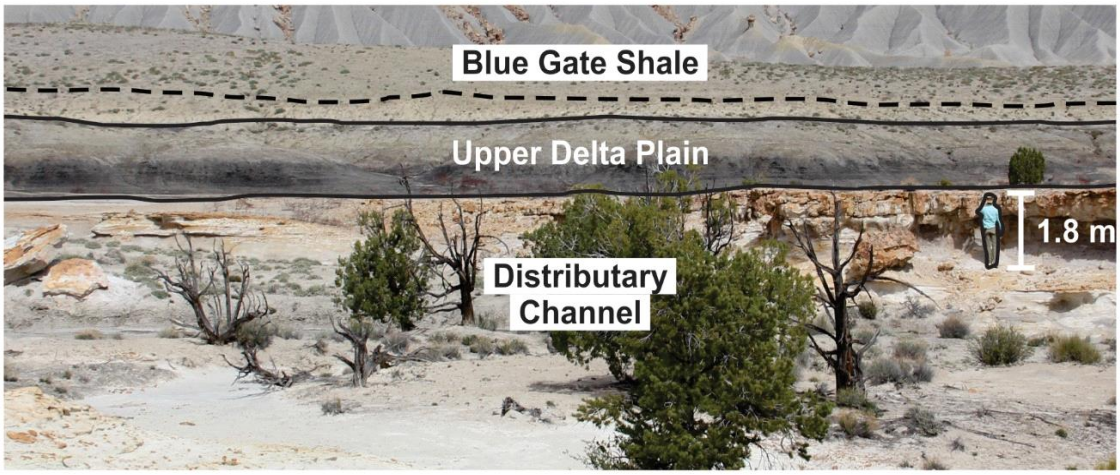

Figure 8 - Laterally extensive interval of Facies 2, displaying characteristic grey mudstones and black carbonaceous shales in between distributary channel sandstones. Black dotted line represents the Ferron Sandstone unconformable contact with the overlying Blue Gate Shale member. Location of picture is at MS#8. Human is outlined in black and white = 1.8 m.

Facies 3 – Lower Delta Plain

Description -

Facies 3 (Table 1) consists of individual fine- to medium-grained sandstone beds (Fig. 9C), and interbedded intervals of fine-grained sandstone, fine- to coarse-grained light-grey siltstone and rhythmically laminated (cm-scale) coaly shale and very-fine-grained sandstone (Fig. 9A-C). Individual sandstone beds show variable thickness changes over short distances (0.4-2.0 m thick; Fig 9C), are erosionally based, and locally tabular to channel-form in cross-sectional geometry (Fig. 9C). At the location of MS#10, an individual sandstone bed bifurcates from the well-defined edge of a distributary channel margin and extends laterally outward. Sandstone bases are marked locally by

large load casts, syneresis cracks and bioturbation (Fig. 9D-E). Internally, beds contain planar to low-angle lamination, cross-bedding, and swaley (SCS) and hummocky cross-stratification (HCS). The tops of sandstone beds are characterized by combined-flow ripple cross-lamination and wave ripples. Bioturbation is sparse to moderately intense (BI = 0-3), but preserved only at basal (Fig. 9E) and top (Fig. 9D) contacts of sandstone beds; bioturbation is entirely absent from mudrocks (BI = 0). A low diversity, low intensity trace assemblage of dwelling traces characterize sandstone bed tops (BI = 0-1) including; small and large *Diplocraterion*, compound *Arenicolites* (Fig. 9D), and fugichnia. Bed bases display greater trace diversity and intensity (BI = 1-3) relative to tops, with *Thalassinoides,* small *Diplocraterion, Lockeia, Planolites,* and *Ophiomorpha* characterizing the assemblage (Fig. 9E).

Fine- to coarse-grained siltstone beds of variable thickness (10-30 cm) and organic content commonly appear blocky in texture (Fig. 9A, B), show mottled coloration, and some are interbedded with thin fine-grained sandstone beds (<0.10 m thick). Siltstone intervals are typically finely laminated or structureless, whereas interbedded sandstone beds commonly contain abundant ripple cross lamination. Intervals of rhythmically laminated (mm-cm-scale) very-fine-grained sandstone and coaly organic-rich laminae are also present in facies 3 (Fig. 9B). Laminations are primarily planar to low-angle, with minor undulations present. The thickness and spacing of coaly organic-rich lamellae are variable within deposits (Fig. 9A, B).

Interpretation –

The presence of a consistent marine trace fossil assemblage, lack of *in situ* plant material and coal beds, presence of wave and tidally-influenced sedimentary structures and relationship with Facies 1 suggest that deposition took place in the lower delta plain (LDP) setting, likely within subaqueous interdistributary bays. Facies 3 is strictly observed in lateral proximity to, and on top of, sandstone distributary channel fills of facies 1. The presence of syneresis cracks on the bases of prominent sandstone bodies indicates changing physio-chemical conditions from mixing of fresh and saline water. Based on the presence of a trace fossil suite that lacks diversity and abundance, this environment was probably highly stressed (MacEachern et al., 2005), with constantly changing salinity and abrupt episodes of sedimentation during flooding events.

The LDP environment lies within the realm of fluvial and marine influences and extends landward from the shoreline to the limit of tidal inundation (Wright, 1978; Coleman and Prior, 1982). In modern settings, interdistributary bays are semi-connected, fluvially and marine-influenced environments that fill the space between distributary channels. These environments are considered the main LDP depocenter for distributary channel overbank and flood deposits.

Laminated siltstone intervals probably reflect suspension fall-out of fines from the water column during normal conditions or after flooding events in the low-energy interdistributary areas. The presence of abundant macerated plant debris further indicates quiet, low-energy conditions dominated. Absence of rootlets and large plant debris within siltstone beds further support the depositional interpretation of a subaqueous environment. Thin, sandstone beds within siltstones were deposited by periodic, higher-

energy events where coarser material was transported into this environment. The thicker individual sandstone bed exhibiting a branching relationship with the adjacent distributary channel is interpreted as a crevasse splay deposit formed by a channel breaching during flood or storm periods. Rhythmically laminated fine-grained sandstone and coaly shale represent tidally reworked organic rich material during sea-level transgression. The rhythmical nature of laminations (Fig. 9B) and channel form geometry (Fig. 9A) of these unique deposits suggest sediments accumulated within smaller abandoned distributary channel during sea-level transgressions.

Figure 9 – Images of Facies 3. For referenced measured section locations see Fig. 2D. **A)** Exposure at MS#10 displaying interbedded coaly-shale and rhythmically laminated organic-rich siltstone within previously cut channel bodies. White box represents the outline of Fig. 9B. Scale = 15 cm. **B)** Close-up view of the fine-grained sandstone with organic-rich laminations shown in Fig. 9A. Organic laminae are 2-3 mm thick and display low-angle and planar stratification. This lithological expression of Facies 3 is interpreted to record reworking of organic material during transgressions or periodic inundation of marine-waters. **C)** Erosionally based fine-grained sandstone beds that display channel-form basal surfaces and characteristic conjoining and amalgamation of individual sandstone beds. Composite sandstone body is outlined in black, reaching a thickness of 1.5 m. Note that sandstone bed (black outline) at the base of the Facies 6 interval overlies heterolithic strata of Facies 7 (Table 1) marking the unincised expression of SB1. Image is located at the southernmost cliff face of outcropping strata, down-dip from MS#15. **D)** View of the bioturbation and syneresis cracked surface found at the bottom of erosionally-based sandstone beds. Ichnotaxa include; *Planolites* (P), *Lockeia* (L), and *Thalassinoides* (Th). Image is located at the southeastern most limit of outcropping strata, down-dip from MS#15. **E)** Compound *Arenicolites* (Ar) at the top of a sandstone bed. A restricted trace fossil suite of robust dwelling and filter-feeding structures is typically found at the tops of such beds. Image is roughly 20 m up-dip (west) of Fig. 6E within the sandstone bed outlined in black.

.

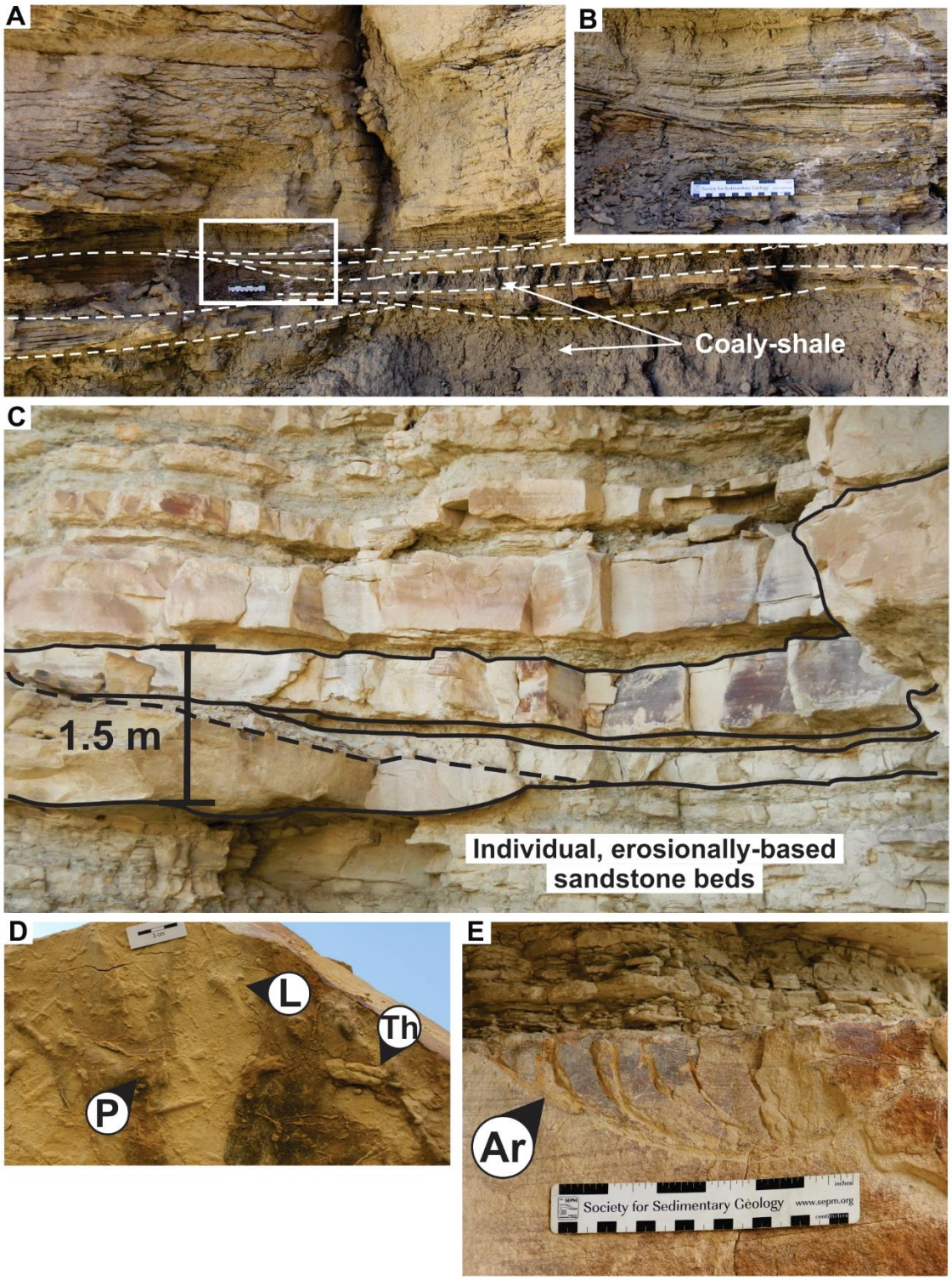

Facies 4 – Mouth Bar Complex

Description -

Facies 4 (Table 1) consists of planar- or erosionally-based, fine- to medium-grained sandstone bodies (2.0-6.0 m thick; Fig. 10A). Basal surfaces preserve sole structures, soft-sediment deformed bed boundaries (Fig. 10C), and synsedimentary faulting (Fig. 10A). Bodies may be growth-faulted, preserving rotated, internal fills of planar and low-angle cross-stratification. Internally, bodies are dominated by large-scale planar and low-angle cross-stratification and trough cross-bedding, with local intervals of soft-sediment-deformation (Fig. 10B) and occasional synsedimentary faulting (Fig. 10A). Smaller-scale current and climbing-ripple cross-lamination, and wave ripples are most commonly present at the tops of individual sandstone beds (Fig. 10C). The tops of these composite bodies display parallel-stratified to low-angle cross-stratification (macroform inclined bedding; Fig. 10A) and scour surfaces associated with lensoid channel forms. Macerated plant debris is common within Facies 4 deposits, while bioturbation is sporadically distributed atop individual beds (BI = 0-2). The observed trace fossil assemblage consists of small and large *Diplocraterion*, *Ophiomorpha*, *Cylindrichnus*, *Planolites*, *Rosselia*, and deep *Skolithos* (Fig. 10C). Paleocurrent data indicate an east-northeastward flow direction of unimodal distribution (Fig. 7G).

Interpretation -

Facies 4 is interpreted as the deposits of river mouth bars (MB) that amalgamated to form mouth bar complexes. This environment lies at the seaward terminus of the distributary channel (Facies 1) in modern deltas, where the confined flow decreases in velocity as it reaches the open basin, leading to sediment deposition (Bates, 1953; Coleman and Wright, 1975; Wright, 1977; Coleman and Prior, 1980). This depositional

setting is typically down-dip of facies 1, while the delta slope lies down depositional dip from the terminus of the mouth bar environment. Sharp-based, planar sand bodies are interpreted as the result of friction-dominated flows from riverine output. Macroform inclined parallel stratification represents the progradation of bedforms down the delta front slope. Channel forms atop mouth bar bodies are relatively small (20-30 m wide, show minimal relief (<1 m thick), and display characteristics similar to 'terminal distributary channels' as described by Olariu and Bhattacharya (2006). Facies 4 displays absent to low bioturbation intensities (BI = 0–2), represented by a low diversity *Skolithos* ichnofacies assemblage. This is considered to be due to high-sediment accumulation rates and constant substrate reworking by both marine and riverine processes not allowing for extended colonization or support of bottom-dwelling ichnogenera. Instead, colonization developed during periods of low sediment delivery, indicating an intermittent sediment dispersal regime.

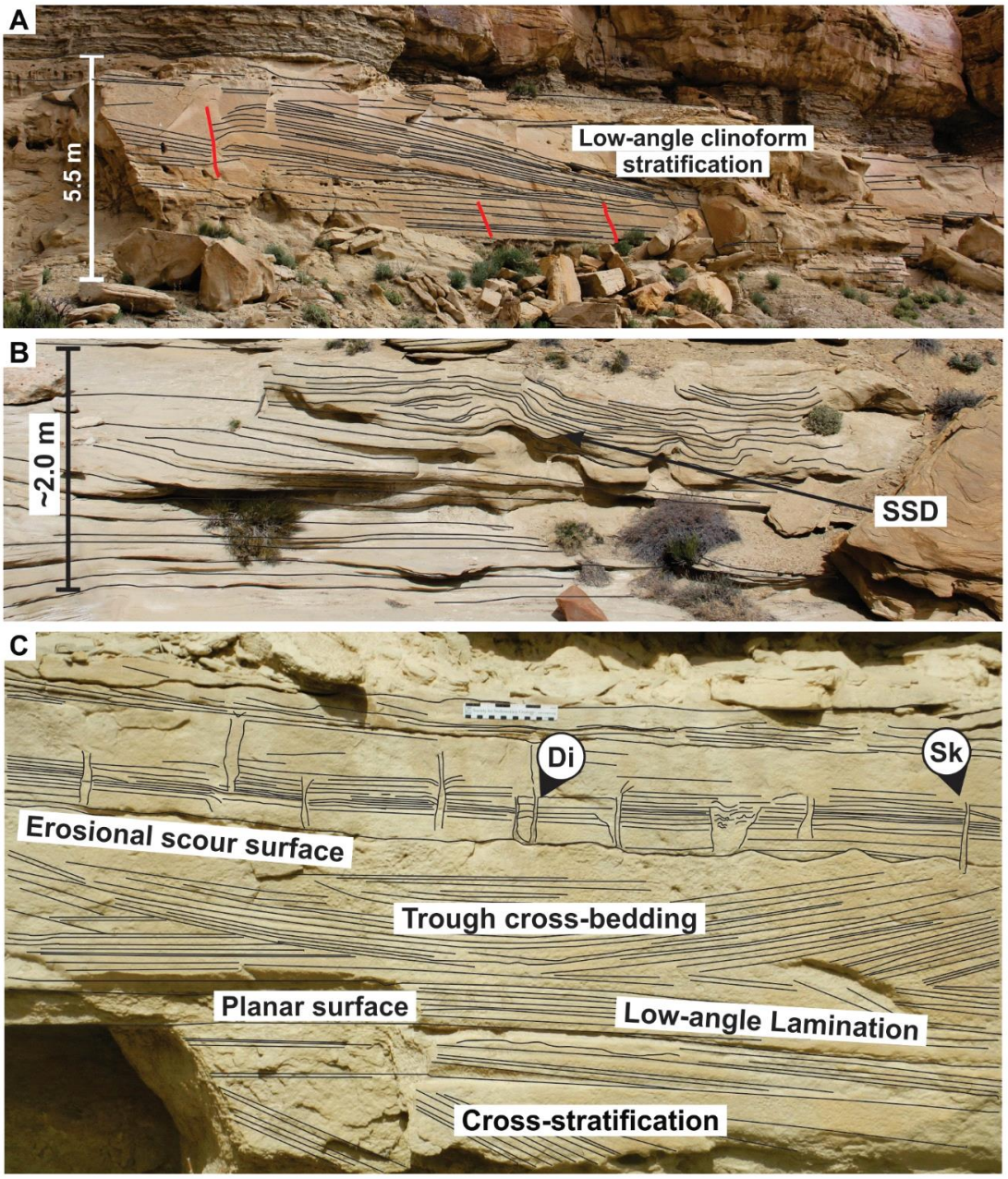

Figure 10 – Views of Facies 4. For referenced measured section locations, see Fig. 2D. **A)** Facies 4 sandstone body exposed at the Labyrinth outcrop at the location of MS#8. The sandstone body displays a maximum thickness of 5.5 m and is dominated by low-angle and planar cross-stratification. Note the low-angle clinoform stratification. Red lines are synsedimentary faults. **B)** Soft-sediment-deformation (SSD; outlined in black with arrow pointing) within Facies 4 deposits. Image location is at MS#11. **C)** Facies 4 bed highlighting the internal stratification and the erosional surface that characterizes the tops of some mouth bar deposits. Image is taken at the halfway point between MS#8 and MS#11. A variety of ichnogenera were identified including *Diplocraterion* (Di) and *Skolithos* (Sk) at individual bed tops. Scale = 15 cm in width.

Facies 5 – Proximal Delta Front

Description -

Facies 5 consists of fine to medium-grained sandstone (~95% sand content) bodies with sharp, erosional, or irregular soft sediment deformed bases. Three depositional variants were noted by Fielding (2010) and observed within this study; 1) Soft-sediment deformed sandstone bodies with large-scale convolute bedding and load casts (Fig. 11A), 2) Stratified sandstone beds with hummocky cross-stratification and flat- to low-angle stratification, with a variety of current and wave generated sedimentary structures (Fig. 11B) 3) Growth-fault controlled, rotated sandstone bodies with planar-to-low-angle stratification, and small-to-large soft-sediment deformation (Fig. 11A). Variants 1 and 2 are preserved as irregular sandstone bodies of variable thickness (1.0-2.2 m thick), typically isolated within marine heterolithic strata (Facies 7 and 8). Variants 2 and 3 are highly variable in thickness (2.0-15.0 m thick), including some deeply incised, growth-faulted and channelized forms. The thicker sandstone bodies are locally observed in lateral proximity to Facies 4. Bioturbation is absent (BI = 0) from Variant 1 (soft-sediment deformed and convoluted sandstone beds) and Variant 3 (rotated or growth-faulted sandstone masses) but present within Variant 2 (hummocky cross-stratified sandstone) in the form of sparse internal bed bioturbation (BI = 0-1) and intensive bioturbation at tops of beds (BI = 0-3).

Figure 11 - Images of Facies 5, 7, and 8 (Table 1). For referenced measured section locations see Fig. 2D. **A)** Thick sandstone body of Facies 5, displaying abrupt termination (dotted line) and rotated strata at the western edge of the body. Note the underlying chaotic deformed sandstone bodies of both sandstone stringers and elongate pillow bodies. Image is located between MS#1-2 on the exposed west-east trending, down-dip oriented cliff face of the Post outcrop. **B)** Facies 5 sandstone bed displaying characteristic sedimentary structures of Variant 2. Image located at MS#9. **C)** Thickly

interbedded heterolithic strata of Facies 7, displaying characteristic sand/silt ratio (70/30) with fine-grained sandstone beds (0.1-0.2 m thick). Camera case = 0.2 m. **D)** Thin-bedded heterolithic strata of Facies 8 at MS#1. Note the thinner sandstone beds and decrease in sandstone percentage for relative to Facies 7. Red line represents a growth fault that penetrated into Facies 8 from the overlying sandstone body of Facies 5. Human for scale =1.8 m.

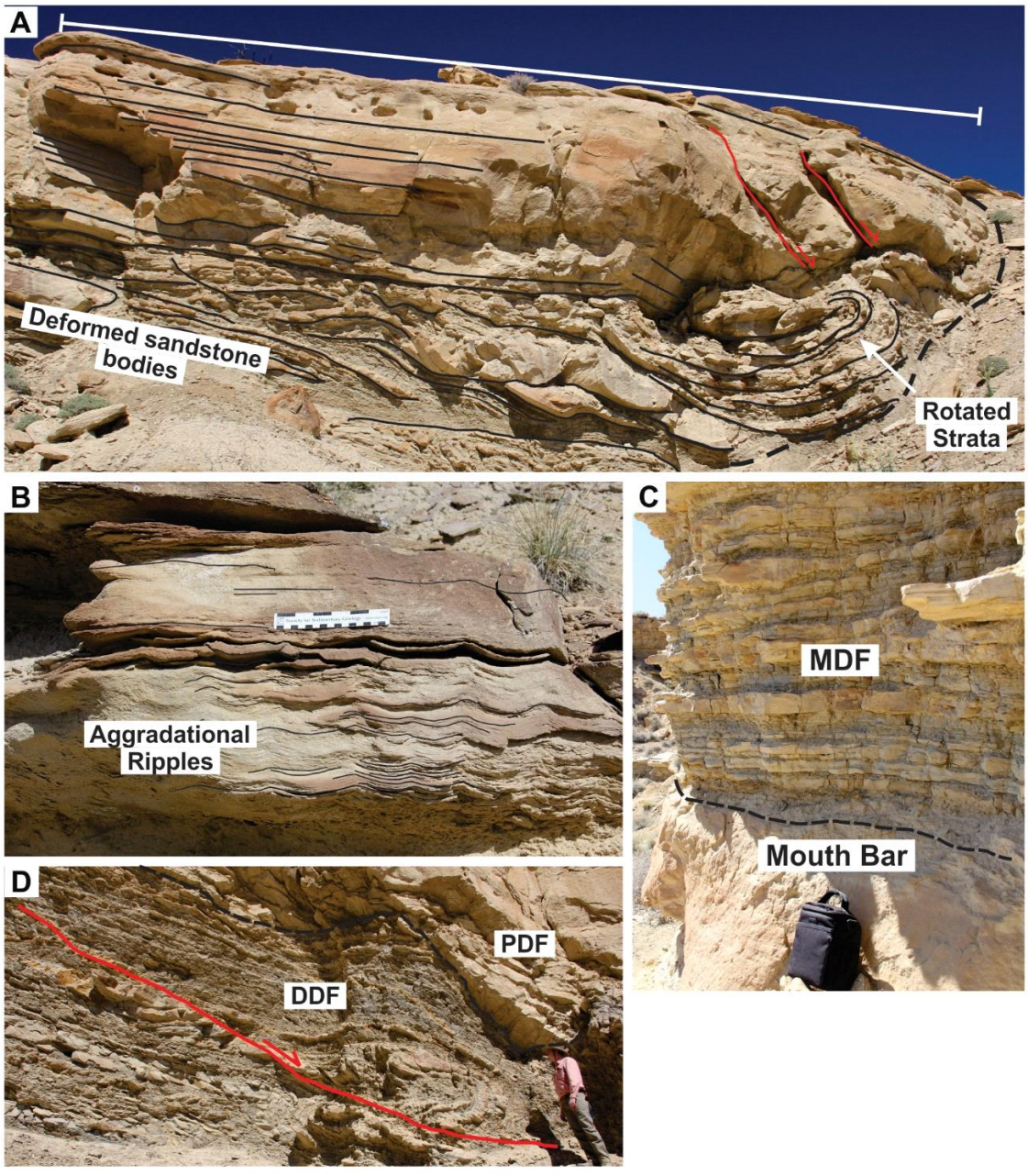

Interpretation -

Facies 5 is interpreted as the deposits of the proximal delta front (PDF), accumulating fine- to medium-grained sand within the upper delta-front slope environment, down-dip from mouth bars. Basal boundaries are highly erosional indicating outflows were friction-dominated. Flows may have been short-lived or may have persisted for longer periods (days or weeks), reflecting storm or seasonal floods. Flows deposited upon the heterolithic substrate of the subaqueous lower delta slope predisposed that surface to failure and liquefaction, creating the pervasive soft-sediment deformation and growth faulted and rotated bodies observed in Variants 1 and 3. Failures may have been produced by the gradual buildup and failure (autogenic) of sediment deposited within mouth bar complexes (Mulder and Cochonat, 1996) or seismic events (allogenic).

Silt is locally absent or a minor component (due to possible lack of preservation or bypass) within PDF bodies. The preserved emplacement sandstone bodies and soft-sediment deformation indicate deposition upon mobile substrate, which is challenging for infaunal colonization (MacEachern and Bann, 2005). Variant 2, the only bioturbated variant observed, most likely reflects an environment away from active delta deposition where delta-front stability was more likely. Variants 1 and 3 show limited evidence of physical sedimentary structure that support typically marine processes (e.g. waves or storms) suggesting that depositional events were rapid and derived from slope-failure, substrate instability, and friction-dominated flow.

Facies 6 – Lower to Middle Shoreface

Description -

Facies 6 (Table 1) is characterized by a pervasively bioturbated (Fig. 12A, C), weathered (Fig. 12B), orange-yellow, fine- to medium-grained sandstone bed (Fig. 12A), averaging 1.0 - 1.5 m in thickness. This distinct sandstone beds is found in both the lower and upper Ferron Sandstone members and are laterally extensive throughout the study area. Bed bases are sharp and locally erosional, typically overlying distributary channel sandstones (Facies 1 – V2) or LDP (Facies 3) heterolithic strata. Facies 6 deposits are defined by three characteristics; 1) intense bioturbation (BI = 2-6) with vertical and obliquely-oriented burrows displaying cross-cutting relationships, completely homogenizing the sandstone (Fig. 12A-B), 2) relict to locally well-preserved cross-bedding (Fig. 12A, C-D), 3) weathered appearance, typically blocky or mottled texture, displaying various shades of grey, yellow, and orange, coloring (Fig. 12A-B). At the base of the upper Ferron member, an individual planar sandstone bed of Facies 6 truncates underlying inclined strata of Facies 1 – V2 (Figs. 12C; 6A-B). Sandstone bodies display upwards decrease in intensity of bioturbation (BI = 2-6), ranging from thoroughly homogenized to locally sparse. A suit of *Cylindrichnus*, *Planolites*, *Thalassinoides*, *Ophiomorpha*, and *Diplocraterion* define a *Skolithos* ichnofacies assemblage. Paleocurrent data indicate a southeast mode of sediment dispersal (Fig. 7H).

Interpretation -

This facies is interpreted as non-deltaic deposits of the lower to middle shoreface (LMSF) environment. Similar deposits of non-deltaic environments have been interpreted in other regional locations of the Ferron Sandstone, including central Utah (Ryer and

Anderson, 2004) on the northern rim of the HMS (Zhu et al., 2012). Relict and preserved trough-cross-stratification and local small-scale cross-bedding is indicative of wave-generated currents. Pervasive bioturbation indicates an environment isolated from active delta sedimentation and records dominance of stable, fair-weather conditions allowing continued colonization of sandy-substrate. The angular truncation with the underlying strata suggests deposits are associated with transgressions and wave ravinement. This facies is similar to the interpretation by Korus and Fielding (In Press) and equivalent to the abandoned delta lobe facies of Fielding (2010), both of which are associated with non-deltaic deposition, reworked substrate, and colonization by trace-forming organisms.

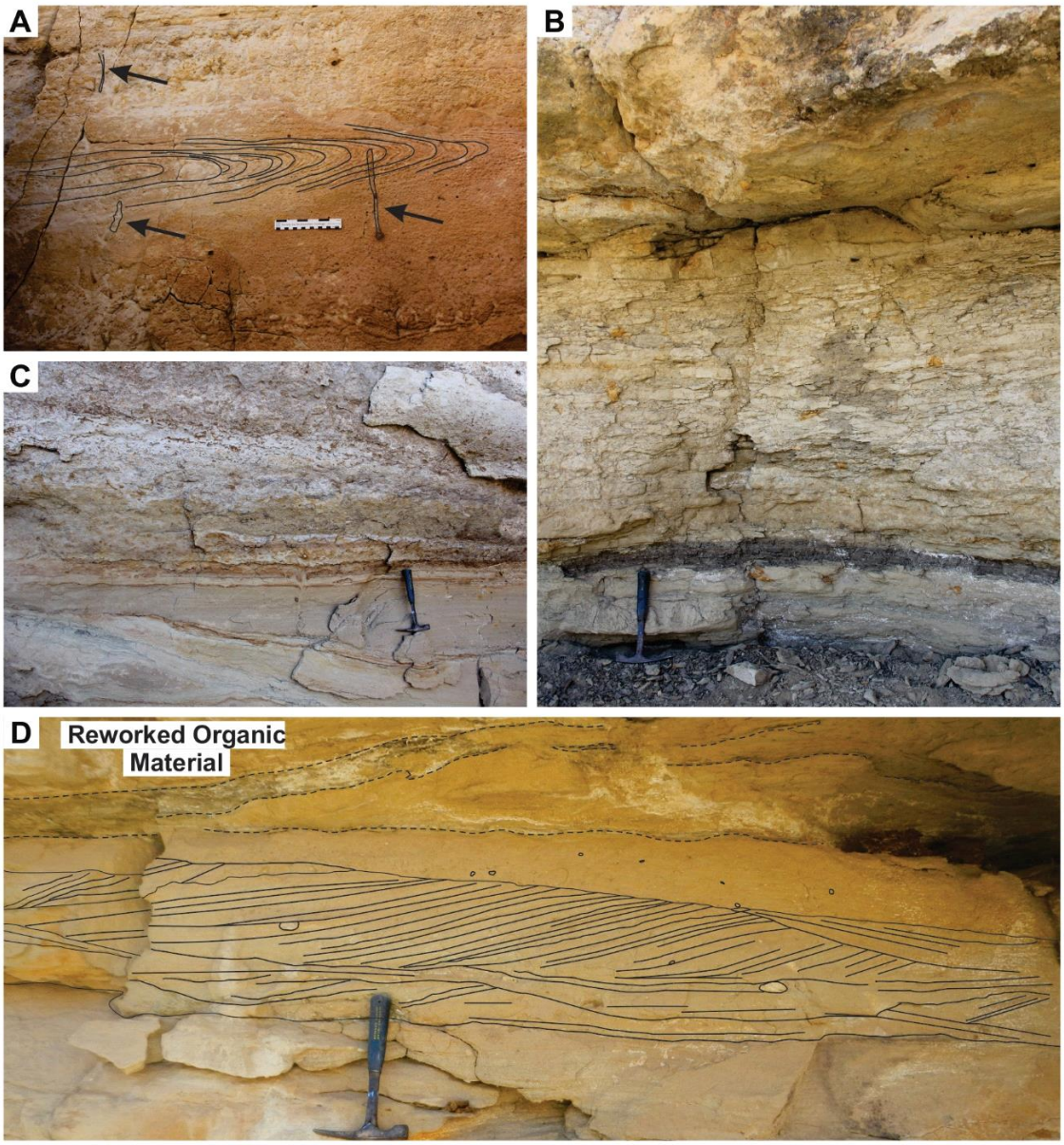

Figure 12 – Images of Facies 6 (Table 1). For referenced measured section locations see Fig. 2D. **A)** Overturned cross-bedding (outlined in black) within bioturbated medium-grained sandstone of Facies 6. Black arrows point towards vertical burrows (5-20 cm long). Note the pervasive bioturbation and cross-cutting burrows that locally homogenize substrate and destroy stratification. Image location is ~20 m up-dip from MS#12. **B)** Characteristic weathered/rubbly appearance of Facies 6 due to thorough bioturbation. Hammer is 0.3 m. **C)** Bioturbated sandstone of Facies 6 overlying Facies 1 sandstone bodies. Note the angular discordance between the underlying strata and thorough bioturbation of the overlying sandstone of Facies 6. Image is located within an alcove between MS#3 and MS#4. **D)** Preserved cross-stratification (outlined in black) within Facies 6 in a relatively unbioturbated bed. Reworked organic debris is present at the top of image (outlined by dotted line). Image location is at MS #12. Hammer = 0.3 m.

Facies 7 – Medial Delta Front

Description -

Facies 7 (Table 1) is characterized by thickly-interbedded very fine-to-fine-grained sandstone and fine-to coarse-grained siltstone (Fig. 11C), with sand constituting ~60% of the total lithology. Sandstone beds (0.1-0.25 m thick) are sharp-bounded with common syneresis cracks at their bases; thicker beds may preserve sole structures and may be soft-sediment-deformed. Within and on top of sandstone beds, current- and combined-flow ripples, symmetrical ripples, flat- and low-angle lamination, ripple-scale hummocky cross-stratification, and low-angle cross-bedding are present. Siltstone intervals are generally stratified or finely-laminated, soft-sediment deformed, and contain mm-scale stringers of very-fine sandstone. Macerated plant debris is abundant within deposits, regardless of lithology. Fine-grained siltstones are generally unbioturbated (BI = 0-1), coarse-grained siltstones are completely unbioturbated (BI = 0), and sandstones show variable bioturbation on bed bases (BI = 0–2). The sandstone trace assemblage consists of *Thalassinoides*, *Arenicolites*, *Planolites*, *Skolithos*, *Ophiomorpha*, *Lockeia*, small and large *Diplocraterion*, *Cylindrichnus*, and fugichnia. Paleocurrent data indicate a bi-modal distribution, with a dominant northeastward mode (Fig. 7I)

Interpretation -

Facies 7 records deposition on the middle (medial) part of the delta front slope (MDF), down-dip from Facies 5 sandstones and up-dip from the thin-bedded heterolithic strata of Facies 8. Periodic increases in fluvial discharge and delta front scouring generated flows that are recorded by the sharp-based sandstone beds. Wave- and

combined-flow generated sedimentary structures preserved at the tops of beds indicate sediment reworking between and after flow events. Silts accumulated by fallout from suspension after turbulent plume-bodies dissipated. Individual sandstone beds with low bioturbation intensities and trace diversity, and inference of plume-related suspension fall-out, unbioturbated siltstone bed indicate stressed environmental conditions likely from increased water turbidity (MacEachern et al., 2005). Syneresis cracks interpreted as a result from outflow freshwater and saline marine water indicate fluctuating salinity levels, further hampering biotic colonization.

Facies 8 – Distal Delta Front

Description -

Facies 8 (Table 1) consists primarily of fine- to medium-grained siltstones interbedded with thin beds (<0.15 m) of very-fine- to fine-grained sandstone (Fig. 11D). Silt is the majority lithological constituent (60-90%) of these deposits, the minority being fine-grained sand (10-30%). Siltstones are characteristically dark grey to black in color, fissile, and finely laminated with fine particles of macerated plant debris. Sandstone beds are very-fine to fine-grained with erosional, irregular, or planar contacts and display thin flat and low-angle lamination. Sedimentary structures commonly observed within sandstone beds include small-scale HCS, ripple cross-lamination, rolling grain ripples, and combined-flow cross-lamination, and syneresis cracks. Sandstone beds exhibit sparse to locally moderate bioturbation (BI = 0-2) on bed tops. Bioturbation intensity is variable from bed to bed, with typically only one or two traces present. Identified ichnogenera include *Diplocraterion* and *Planolites*. Facies 8 is similar to Facies 7, but displays thinner bedded intervals and a lower sandstone/siltstone ratio. Two paleocurrent measurements

were taken from one rippled sandstone bed top indicating a southeast oriented dispersal direction (Fig. 7J).

Interpretation -

Facies 8 thin-bedded heteroliths are largely similar to MDF heterolithic strata but show a lower sandstone proportion and individual bed thickness. Observed trends argue for deposition down-dip of MDF in the distal delta front (DDF) near the lowermost part of the delta front slope. Sediment was sourced and received through the same processes as the MDF, however the thin-bedded nature suggest sediment-laden flows had diminished at the lowermost part of the delta front slope. The down-dip increase (relative to the PDF and MDF) in silt and macerated plant debris suggest that flows were largely transporting fine-grained material and suspension fallout was an important depositional mechanism.

KEY SURFACES

Recognition of key bounding surfaces is central to sequence stratigraphy and chronostratigraphic interpretation (Catuneanu et al., 2009). Two types of key stratigraphic surface were identified within the study interval, the subaerial unconformity/sequence boundary (SU/SB) and the transgressive ravinement surface (TRS). Surfaces are distinguished on the basis of underlying and overlying facies, vertical stacking pattern and along-strike relationships of strata, stratal terminations, and substrate-controlled ichnofossil suites. Surfaces in the Ferron Sandstone member are erosionally truncated or amalgamated with overlying (younger) surfaces (Korus and Fielding, In Press).

The SU/SB occurs as both an incised and an unincised erosion (Fig. 13A, B) surfaces. The incised expression occurs as a basal channel scour marking (SB1), and is identified by moderate (<5 m) truncation of underlying delta front deposits. Unincised surfaces are generally planar to irregular and are overlain by LDP deposits (Facies 3). Subaerial exposure surfaces can be difficult to identify where lithologically similar heterolithic strata of the MDF are overlain by LDP deposits. The LDP contains evidence of marine influence (e.g. combined-flow structures, bioturbation) and reworking of the substrate, indicating periodic flooding and close marine proximity. Since the LDP displays no preserved evidence of extended subaerial exposure (e.g. roots, coal beds) placement of the boundary is based on the presence of thin (cm-scale) coaly-laminated siltstone and thick (0.5-1.0 m) sandstone beds with channel-forms at the base (Fig. 13B).

The TRS is located at the distinct planar to erosional boundary between underlying distributary channel or LDP facies and overlying LMSF deposits (Fig. 13C-D). The TRS is marked by pervasive bioturbation in the form of distinctive large diameter (1–2 cm), typically vertical- to obliquely-oriented trace fossils of the LMSF that penetrating into underlying strata. Placement of the TRS is straightforward due the noticeable lithofacies change and may be identified from afar at locations where LMSF sandstone beds erosionally overlie channel margin IHS creating an obvious angular truncation that defines the surface (Figs. 9B; 13C-D). At exposure locations where distributary channel deposits are not present, LDP coaly-shale and organic-rich siltstone beds underlie the bioturbated sandstone, marking the TRS (Fig. 13C). The observed TRS is consistent with literature describing a diachronous erosional surface cut during transgression by waves in shallow-marine settings (Swift, 1968; Demarest and Kraft,

1987; Nummedal and Swift, 1987). For a detailed description of the key bounding surfaces and associated variations in the Ferron Sandstone member, refer to Korus and Fielding (In Press).

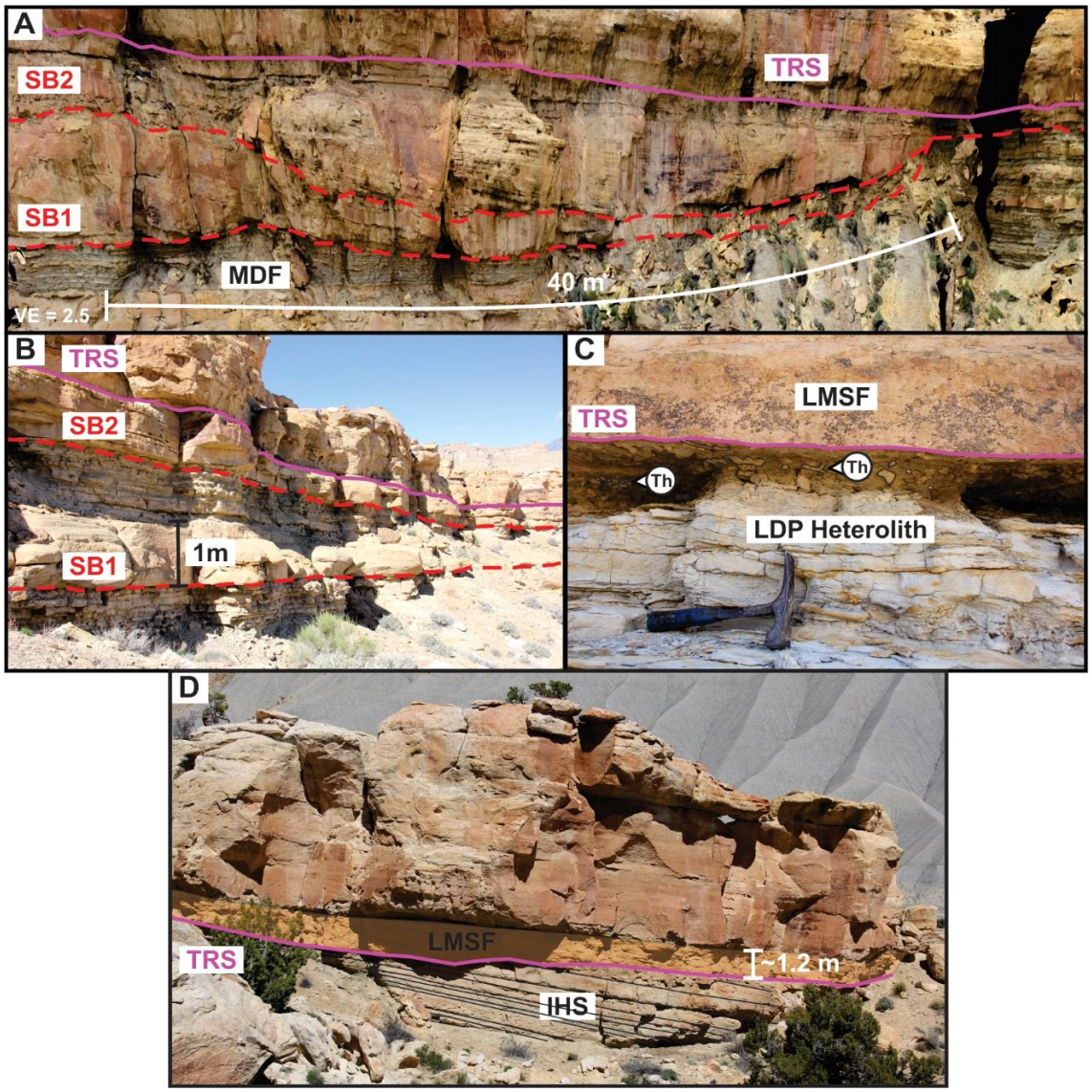

Figure 13 – Annotated images of key sequence stratigraphic bounding surfaces. For measured section locations see Fig. 2D. **A)** Incised distributary channel located on main north-south, depositional strike-parallel cliff face of the Labyrinth VOM in the eastern extent of the study area at the location of MS#8. Channel body is incised into the underlying MDF (Facies 7) heterolith, displaying up to 5 m of erosional-relief. At the Labyrinth outcrop, the incised channel displays a well-defined southern boundary where channel sandstone is juxtaposed against eroded MDF deposits. SB1 marks the initial incision surface, correlating to the regional extensive sequence boundary of Fielding

(2011). SB2 is marked by the erosional surface of a second channel (CH2) that incises down into channel body 1 (CH1). The TRS is placed atop the channel body at the base of a bioturbated LMSF sandstone (Facies 6). VE = 2.5. **B)** Cyclic overbank deposits with corresponding sequence boundaries (SB1 and SB2). Sequence boundaries are placed at the base of fining-upward sequences at the basal surface of thick crevasse splay sandstone beds. Image take at the location of MS#14. **C)** Transgressive Ravinement Surface (TRS) separating the overlying bioturbated LMSF sandstone (Facies 6) from the underlying LDP (Facies 3) heterolith. The TRS is marked by abundant *Thalassinoides* (Th) burrows. Image location is at the northwestern channel margin in the western (up-dip) portion of the study area. Hammer is 0.3 m long. **D)** Typical facies stacking pattern and bounding surfaces surrounding Facies 6 (highlighted in orange). Distributary channel sandstone and HIS interbeds (Facies 1 – V2) are overlain by LMSF sandstone. Note the angular truncation of underlying IHS. Image is located at MS #4.

FACIES ARCHITECTURE AND STACKING PATTERNS

The complex stratal stacking patterns and facies associations of the lower Ferron Sandstone member and the critical interval that separates the lower and upper members is documented here in great detail through VOM analysis (Fig. 14) of the Post (Fig. 14A) and Labyrinth (Fig. 14B) outcrops in combination with a 700 m west-east trending depositional-dip-parallel cross-section (Fig. 15A), and an 800 m north-south trending, oblique to strike transect (Fig. 15B) allowing for a tightly constrained interpretation with correlation between VOMs. For describing purpose and ease of identification, major sandstone bodies and stratal packages discussed in the following section are numbered. The local stratigraphic interval described correlates to allomembers 7 and 8 of Fielding (2011, 2015) and parasequences within sequence II to IV of Korus and Fielding (In Press). For further description and regional Ferron Sandstone stratal stacking patterns, refer to those documents.

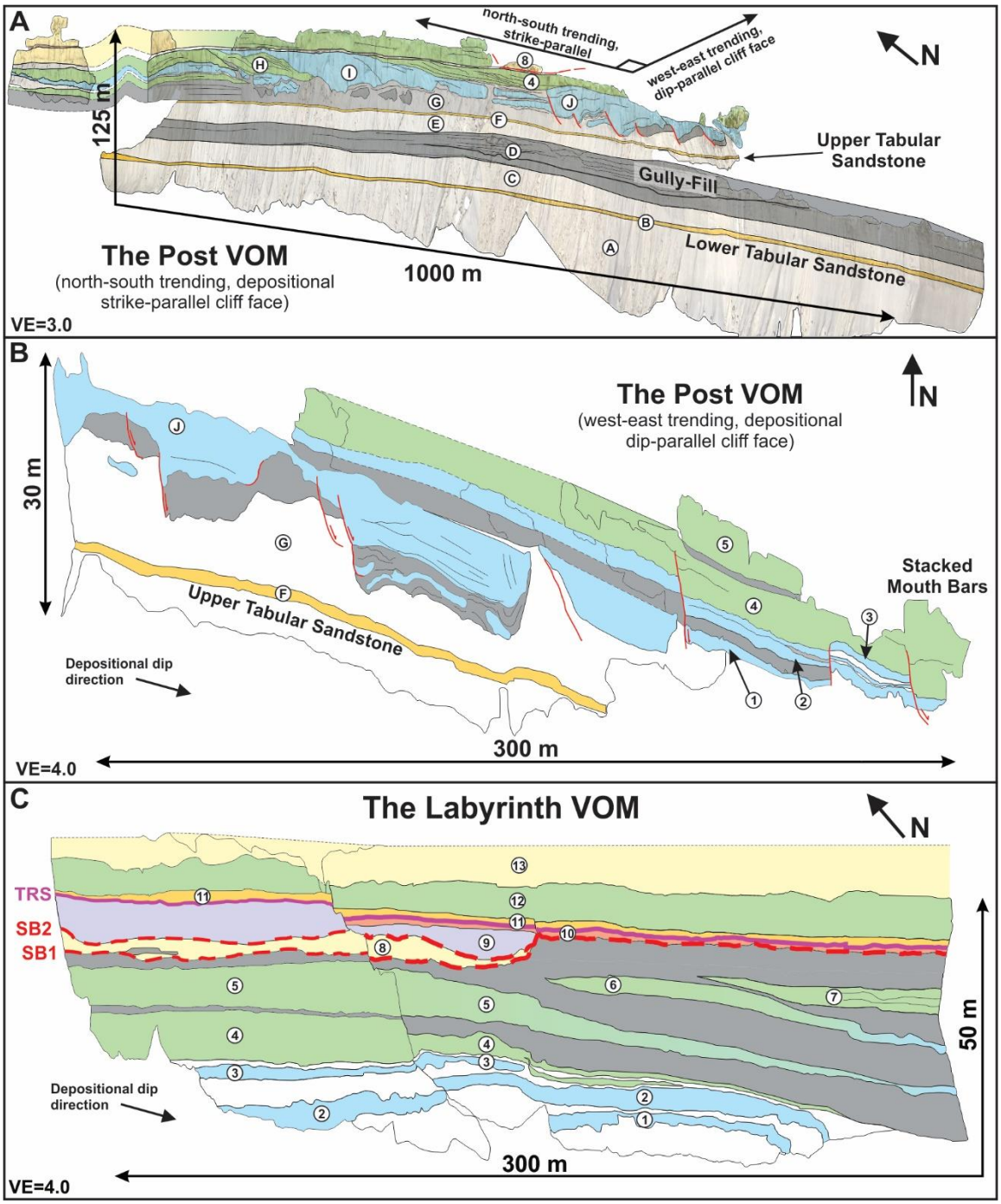

Figure 14 – VOMs with facies interpretations and key bounding surfaces. Key beds and intervals that are correlated within the study area are numbered (1-12), other beds of note are lettered (A-J). See Fig. 2D for location of VOMs. **A)** VOM of the Post, displaying 3D geometries of several steep-sided, stratified sandstone-filled gullies associated with rotated or growth-faulted basal contacts. MB deposits laterally grade into PDF sandstones or terminate against growth faulted gully-fills. Note the tabular-bed geometries of the lower half of the succession in comparison to the chaotic and variable dimensions of the bodies near the top. **B**) The Post VOM (west-east trending, depositional dip-parallel cliff

face) displaying the down-dip geometries of several steep-sided, stratified sandstone-filled gullies associated with rotated or growth-faulted basal contacts. Note the density of growth faulted bodies and the effect on bed continuity and thickness. **C**) Labyrinth VOM at the eastern end of the study area showing a succession equivalent to that at the "Post." The lower Ferron Sandstone member is composed of cycles of MB and delta front sandstone bodies which are separated by MDF/DDF heterolithic strata. Note that the MB bodies show offlapping relationships and thin rapidly to the southeast. The lower/upper Ferron Sandstone member boundary is represented by SB1.

Figure 15 – Measured section transects displaying the correlated bodies of the exposed strata in the study area. Transect path and measure section locations are shown in Fig. 2D. **A**) A-A′ (orange), west-east trending depositional-dip parallel transect displaying lithofacies correlation from the Post to the Labyrinth. Note the two MB bodies in the lower Ferron member correlated throughout the study area and that thick PDF and MB bodies are strongly associated with growth-faulting. **B)** B-B′ (green), northwest-southeast trending, oblique to strike transect. PDF and MB bodies thin to the southeast, with corresponding increase in DDF deposits. Note the abrupt down-dip thickening of new MB bodies and their off-lapping relationships. The multi incised channel body lies at the boundary between the lower/upper Ferron Sandstone members.

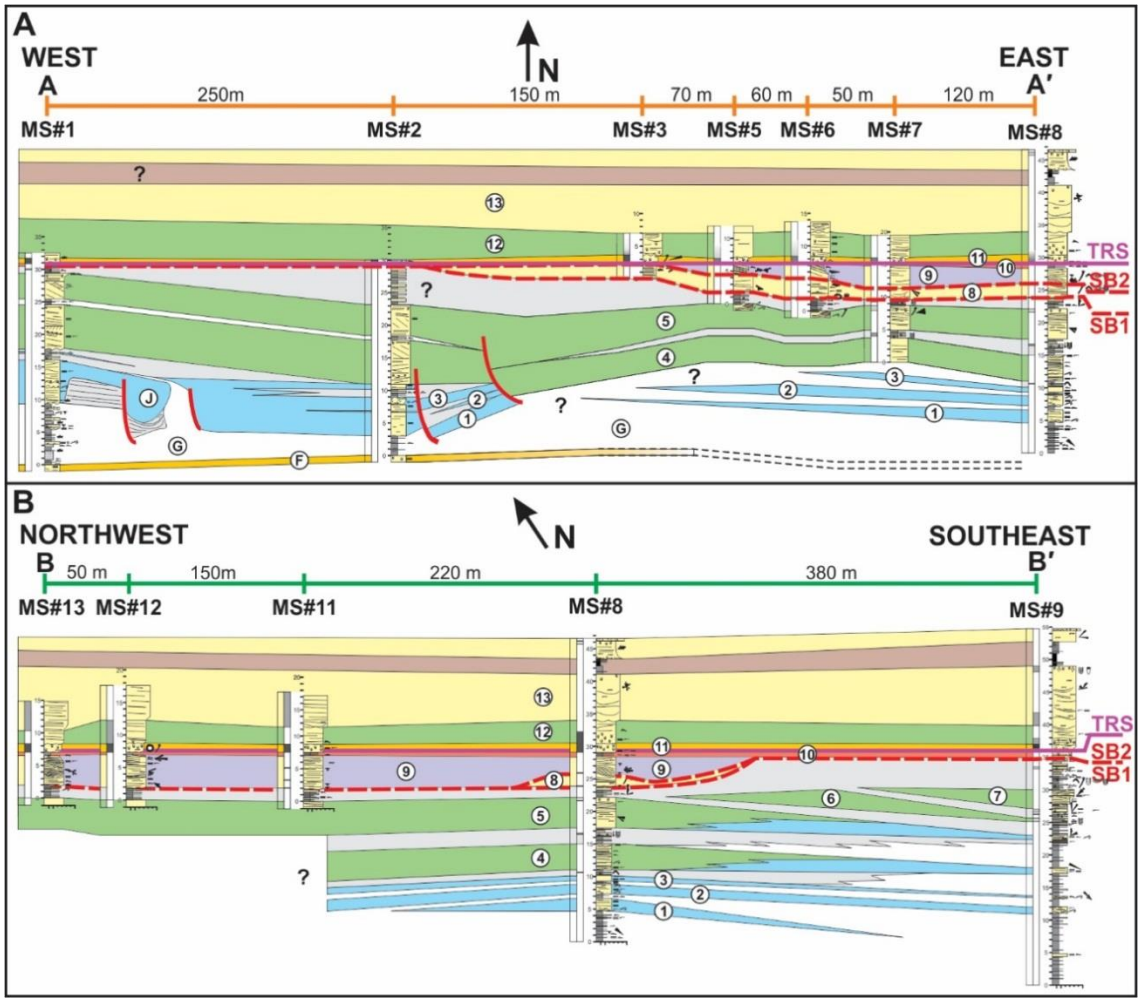

VIRTUAL OUTCROP MODEL DESCRIPTION

The Post VOM

The western margin of the study area is marked by the Post outcrop which the Post VOM captures. This 1.5 km north-south trending, 60-80 m high cliff face exposes the proximal stratigraphic expression of strata within the study area relative to the local northeastward prograding paleoshoreline. Figure 14A displays the facies architecture of the main north-south trending cliff face and should be referred to for the following description unless explicitly noted otherwise. At the base of the succession, multiple progradational cycles of laterally extensive, tabular-packaged strata (Fig. 14A:A-F) in strike-perpendicular cross-sectional view characterize the lowermost 50 m of strata. Tabular bodies of increasingly more proximal settings relative to the delta front are stacked upon one another. Described in stratigraphic order, at the base a ~30 m thick interval (Fig. 14A:A) of thinly-bedded DDF heterolithic is sharply-capped by a tabular, laterally extensive, bioturbated sandstone bed (Fig. 14A:B; labeled as 'Lower Tabular Sandstone' on Fig. 14A). Fielding (2010) interpreted this enigmatic, stratigraphically isolated, DDF deposit-bounded sandstone bed as the preserved record of delta lobe abandonment. Very-fine to medium-grained sand originally accumulated in shallow-water, most-likely MB or PDF environments. However, pervasive bioturbation and abundant bivalve shells indicate a post-depositional environment cut-off from active sediment dispersal and subject to marine re-working before being drowned (Fielding, 2010). The lower tabular sandstone bed averages 2.3 m in thickness, ranging from 1.5 – 3.1 m, locally displaying a thickness increase northward.

A second cycle starts above the lower tabular bed, beginning with a ~10 m thick DDF body (Fig. 14A:C) displaying a coarsening- and thickening-upward sequence before gradually passing into the thickly-interbedded deposits of the MDF. This MDF interval (Fig. 14A:D) averages ~12.0 m in thickness, ranging from 8.2 – 15.5 m, increasing in thickness to the south. Within this MDF interval, sandstone-siltstone inter-beds are primarily organized as a tabular succession of sheet-like units repeating sandstone-siltstone, but also preserve a ~350 m wide, 6 m thick broad, trough-like body (Labeled as 'Gully Fill' on Fig. 14A) containing inclined and horizontal sandstone beds, channel forms, soft-sediment deformation, and amalgamated bodies. The density of these features decreases towards the edge of the trough-form with sand-silt interbeds returning gradually returning to the horizontal orientation. The top of this complicated MDF deposit is overlain by another tabular interval (Fig. 14A:E) of DDF before being capped being abruptly capped by a second abandoned delta lobe body (Fig. 14A:F; labeled as 'Upper Tabular Sandstone' on Fig. 14A). This upper tabular sandstone bed is also laterally extensive, bioturbated, and bounded by DDF deposits, averaging 1.0 m in thickness.

Above the upper tabular sandstone, a facies succession typical of the lower Ferron member begins (Fig. 14A:G-J); a gradual coarsening-upward sequence of DDF-to-MDF heteroliths that is erosionally capped by sandstone-dominated deposits of the PDF and MB facies (Fig. 14A). The MDF-to-PDF and MB lithofacies boundary is characterized by preserved growth-faulting that penetrate through prominent sandstone bodies and into underlying heterolith, synsedimentary thrust faults with displacements of 1-3 m, and soft-

sediment-deformation sandstone pillows (see Fielding, 2015 for a comprehensive description of the delta front instability in the Ferron Sandstone).

Preserved at the top of the lower Ferron member, is a complex succession of thick MB and PDF (Fig. 14A:H-J) sandstone bodies of variable geometries, some of which are associated with syn-depositional growth-faulting (Fig. 14A:J). The sequence of MB (Fig. 14A:H, 4) and PDF (Fig. 14A:I-J) deposits to the north of the growth-fault cluster located at the Post corner display a similar sigmoidal body trend, with offlapping initiation points and downlapping terminations. As shown in Figure 14A, the series of north-south trending lateral prograding MB and PDF bodies initiate from thin, offlapping beds increasing in thickness towards the south. Once maximum thickness is reached, bodies thin to south before pinching out and downlapping onto the delta front heterolith.

PDF bodies are strongly influenced by preserved growth faulting and pervasive soft-sediment-deformation in the underlying strata (Figs. 11D; 14B:J, 1-5). PDF sandstone bodies display highly variable geometries in 3D, irregular bases, abrupt terminations, and modified beds dismembered into elongate pillow forms (Fig. 14B:J). At the Post corner (Fig. 14A-B) and preserved along the west-east trending, depositional dip-parallel cliff faces, where several steep-sided, stratified sandstone-filled gullies associated with rotated or growth-faulted basal contacts are preserved (Fig. 14B:J). The impressive gully fill sandstone bodies and synsedimentary growth faults directly overlie delta front heterolithic strata (Fig. 14B:G) that were prone to liquefaction and subsequent slope-failures.

PDF and associated gully-fills exposed along the depositional-dip cliff face (Fig. 14B) display eastward-thickening bodies that abruptly terminate down-dip and overlie

rotated and deformed masses of the underlying medial-distal delta front deposits (Figs. 11A; 14B:J). Down-dip from the Post corner (Stratigraphic architecture in Figs. 14B; 15A), faulting begins to propagate into MB bodies (Fig. 14B:4-5) containing offset beds and abrupt changes in thickness as growth faulting continues. One large growth fault at the eastern edge of the depositional dip-parallel VOM displaces two MB bodies (Fig. 14B:4-5), with enough offset to stack the sandstone bodies directly on top of one another (Figs. 14B; 15A).

The Labyrinth VOM

The Labyrinth outcrop is located near the eastern margin of the study area (Fig. 2D) showing a true 3D exposure of a ~40 m stratigraphic succession (Fig. 14C) equivalent to the up-dip succession along the depositional dip-parallel cliff face (Fig. 14A-B) at the Post. Correlation of sediment bodies between the two VOMs is shown in Figure 15A. The Labyrinth VOM captures portions of both the lower and upper Ferron members including the two sequence boundaries (SB1 and SB2) within the critical interval at the lower/upper member interface (Figs. 14C; 15A).

The stratigraphic succession at the Labyrinth outcrop displays a succession of thicker sandstone bodies of proximal facies interfingering with heterolithic deposits of more distal facies. Distal-, medial-, and proximal-delta front (Fig. 14C:1-3), MBs (Fig. 14C:4-7), distributary channel(s) (Fig. 14C:8-9, 13), delta plain (Fig. 14C:10) and shoreface (Fig. 14C:11) facies are exposed within the stratigraphic interval. The large syndepositional deformational features preserved at the Post are absent from the stratigraphic succession here. MB and PDF bodies are also much thinner in comparison to their equivalents up-dip. Description of the Labyrinth stratal stacking pattern and

facies architecture will precede in ascending stratigraphic order and will reference Figure 14C unless otherwise noted.

At the base of the outcrop, a succession of three prominently soft-sediment-deformed PDF beds (Fig. 14C:1-3) is separated by thin intervals of DDF heterolithic deposits. A succession of MB bodies (Fig. 14C:4-7) and MDF deposits overlies this basal PDF succession. A total of four individual MB sandstone bodies are identified. The lower two (Fig. 14C:4-5) correlate up-dip (Fig. 15A:4-5) where they maintain a relatively consistent thickness, although they are shown here to thin down-dip before passing into PDF deposits (Fig. 14C:4-5). The upper two MB bodies (Fig. 14C:6-7) of the lower member abruptly pinch-in down-dip and display an offlapping relationship (Figs. 14C; 15B). Bodies increase in thickness over a short distance before reaching maximum thickness and thinning out over a much longer distance (Figs. 14C; 15A). Capping the lower member is an interval of thickly bedded MDF heterolithic strata below the erosional surface of SB1.

Above SB1 lies an incised channel body (Fig. 14C:8-9) that downcuts into the underlying MDF deposit. Above the channel bodies is a thin veneer of LDP heterolith (Fig. 14C:10) that lies beneath the laterally extensive LMSF bioturbated sandstone body (Fig. 14C:11). This ~ 8 m thick succession represents the Critical Interval and will be expanded up in the following sections. Topping the section is a thick (~10-12 m) succession of locally developed MBs (Fig. 14C:12), overlain by a laterally extensive distributary channel body, representing V1 (Facies 1; Fig. 14C:13).

Lower Member

Three-dimensional exposure of the lower member facilitates new insights into lithofacies geometry, stacking patterns, and facies relationships that are worthy of specific focus. Locally, the lower member displays a progradational, coarsening-upwards succession comprising; offshore and prodelta mudstones, DDF and MDF heterolith, and PDF and MB complex sandstones. The ~120 m thick interval is bounded at its base by the Tununk Shale and the top is marked by SB1. Stratigraphic analysis (Fielding, 2015; Korus and Fielding, In Press) eastward on the down depositional-dip equivalent (present study interval) stratigraphic succession shows clinoforms arranged into eastward-dipping, downlapping and offlapping clinoform sets of descending-regressive trajectory. The observed clinoform set stratal relationships and trajectory are definitive characteristics of forced-regressive systems tracts (Plint and Nummedal, 2000; Posamentier and Morris, 2000), indicating the lower member was predominantly deposited under base-level fall. Paleocurrent measurements within the lower member indicate paleoslope and sediment dispersal direction was east-northeast (Fig. 7B).

Critical Interval

This section describes the facies architecture and stratal stacking patterns of the critical interval enclosing SB1. The Critical Interval is bounded by SB1 at its base and by the locally extensive TRS at the top that lies beneath the prominent fluvial deposits of the upper Ferron member (Fig. 15). The Critical Interval is roughly ~8 m thick, containing two cryptic cycles of transgression and regression each associated with subaerial unconformities/sequence boundaries. Each cycle contains an incompletely preserved sequence with a narrow (100-300 m), moderately incised, channel body, associated with

a sequence boundary; SB1 underlies Channel 1 (Fig. 14C:8), SB2 underlies Channel 2 (Fig. 14C:9). The two separate channel systems display well-defined margins within the study area where the stratigraphic interval cropped out (Fig. 16). Channel extents were identified from IHS margins, angular discordances from overlying stratal truncations, and channel sandstone body pinch-outs. Paleocurrent data and channel margins show the two channel bodies flowing into the same accommodation pathway, converging at the location of the main Labyrinth outcrop cliff-face (Figs. 14C; 16). Preserved above and laterally to the distributary channel bodies lies relatively thin deposit of poorly developed, reworked LDP deposits (Figs. 14C; 15B). The top of the interval is marked by the TRS, which truncates the underlying angular deposits creating an easily observed angular discordance (Fig. 16D).

Incised Distributary Channel Bodies

Channel 1 –

Channel 1 (CH1) is the stratigraphically lowermost distributary channel body of the two channels, and its basal surface of erosion correlates to SB1 (Figs. 17C; 14C). Paleocurrent data from CH1 indicate a dominant east-northeast (mean=75°) paleoflow direction (Fig. 16B). CH1 has a maximum width of ~300 m, maximum thickness of 6.5 m, and a west-east channel body trend (Fig. 16). Where the basal surface outcrops, CH1 incises into as much as ~5.5 m of underlying MDF heterolithic strata (Figs. 16A; 17A, C) The basal fill of CH1 is typically laterally confined by this erosional MDF contact (Figs. 16A; 13A), the upper portion is locally confined by either MDF heterolith or gradually transitions into LDP heterolith, with crevasse sandstone bodies bifurcating away from the main channel deposits (Fig. 17A). CH1 internal fill is almost entirely well sorted,

medium-grained sandstone internally dominated by flat and low-angle cross-stratification, with trough cross-stratification observed less frequently. Internal scour surfaces with up to 1 m of erosional relief, horizons of imbricated siltstone clasts, ripple cross-lamination, and combined flow ripple cross-lamination are also present. A consistent stacking pattern of three individual sandstone beds (1.0-3.1 m thick), each with an erosional boundary marked by a thin (cm-scale) siltstone layer containing abundant small syneresis cracks and a limited diversity, yet consistently present trace fossil assemblage of *Planolites*, *Diplocraterion*, small-diameter *Skolithos*, and *Lockeia*.

The westernmost extent of CH1 subtly crops out at the top of the Post cliff-face (Fig. 14A), from which the channel body maintains a broadly straight planform down-dip where it can be physically "walked-out" eastward across the study area and onto the vertical cliff-face of the Labyrinth outcrop (Fig. 16), the last down-dip exposure of the channel body (Figs. 13A; 15). The northeasternmost margin of CH1 is shown in Fig. 16A, where the body of CH1 gradually thins before pinching-out (Fig. 16B). The northwest linear boundary of CH1, at the most up-dip location displays channel body thinning and lateral transition into LDP overbank heterolith.

CH1 has a well-defined, yet complex southern margin (Fig. 15), where the margin of CH1 can correlated sporadically almost a kilometer from the most down-dip, southeastern exposure at the Labyrinth, up-dip to the location of MS#10 (Figs. 15), continuing all the way to the western most extent of CH1 at the Post (Fig. 16A). The up-dip southern boundary is not explicitly observed in outcrop, but the outcropping channel body exposure is discontinuous with the next stratigraphically equivalent deposit being a thin coaly shale, located at the top of MS#1 (Fig. 15A). At the Labyrinth, the southeast

margin is an abrupt termination against eroded MDF (Fig. 14C). Up-dip at the location of MS#10, the channel extent is clearly-defined by IHS transitioning into horizontal beds of the LDP heterolith (Figs. 17A; 16B). At this margin, an erosionally-based, fine- to medium-grained, tabular sandstone body branches away from CH1 deposits, extending laterally southward (Figs. 17A: 16). This sandstone body is relatively thin compared to the main channel body, but displays variable thickness (0.7-2.0 m), thinning and thickening as it extends southward away from the exposed channel margin. Small channel forms, 1 m deep and 20 m wide are preserved on the base and through internal scour-surfaces within the sandstone body. Unidirectional flow structures such as flat and low-angle lamination and minor crossbedding with ripple cross-lamination are commonly observed within the body in proximity to CH1. Combined-flow structures in the form of large scale hummocky (1.5 m) and swaley cross-stratification, increase in abundance southward from relative to bifurcation point. Changes in the nature of bioturbation also follow this southerly trend, with increasing intensity and more pervasive distribution on the base and top of the sandstone body (Fig. 9D, F). This body is interpreted as a crevasse splay (Fig. 16). The deposits of CH1 display very little evident of tidal influence, and considered to be fluvially-dominated from the unimodal paleocurrent distribution (Fig. 16B), low mud content, and general lack of tidal sedimentary structures.

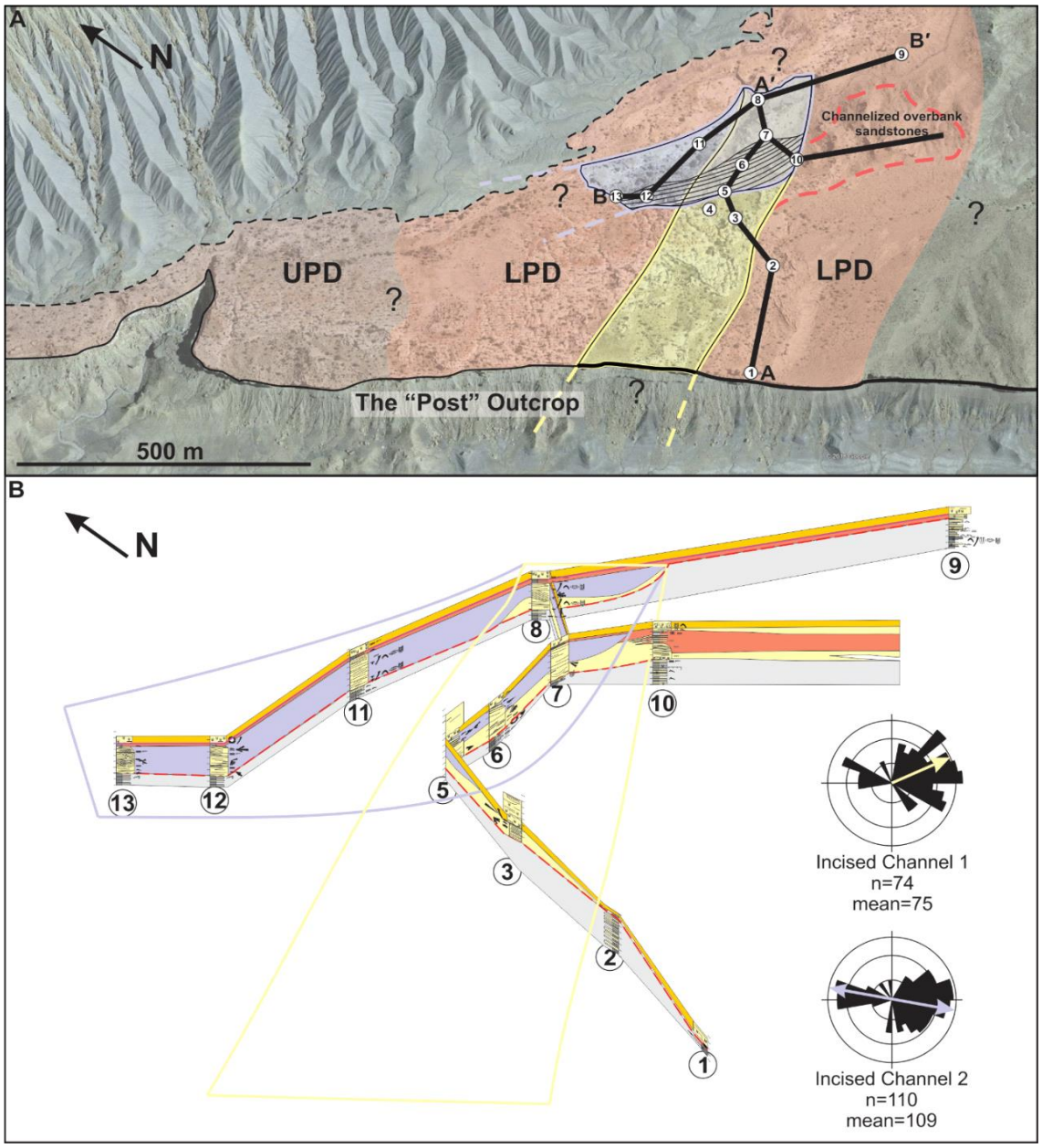

Figure 16 – A) Plan view reconstruction of Critical Interval displaying the extents of CH1 (yellow), CH2 (purple), LDP (salmon), and UDP (brown) deposits. Measured section and cross-section transects of 16B are shown for reference. Black dotted line denotes extent of Ferron Sandstone Member. ? = areas of unknown due to lack of outcrop exposure. **B)** Measured sections and correlation through the exposed Critical Interval strata illustrating the true body correlation in three dimensions. Paleocurrent data for CH1 and CH2 are also displayed with the dominant and minor modes shown by the arrows.

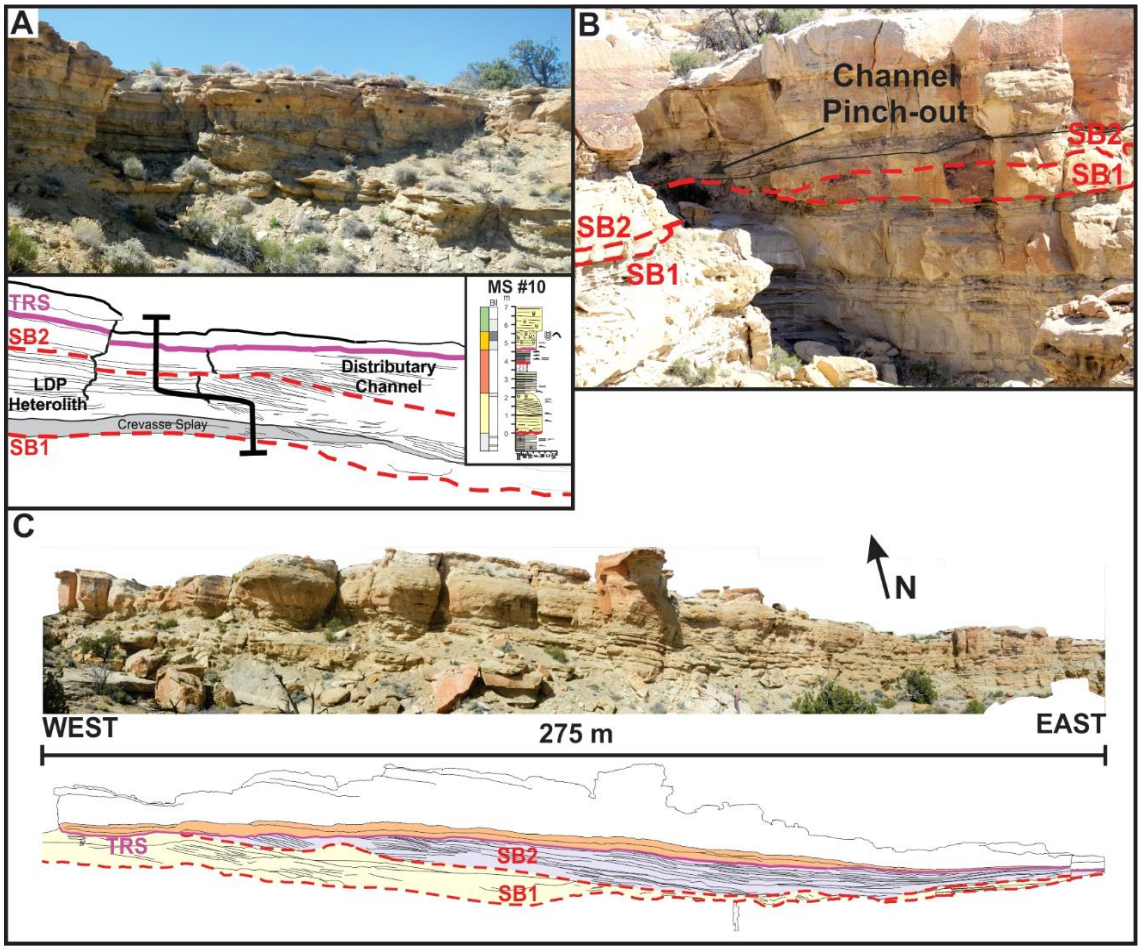

Figure 17 – **A**) Complex channel body relationship with LDP strata at the location of MS#10 displaying angular distributary channel beds transitioning into flat-lying LDP heterolith. Note the lower crevasse splay sandstone body that bifurcates from the base of the distributary channel. Black line represents the location of MS#10. **B**) Labyrinth channel body pinch-out at the location of MS#8. **C)** Photomosaic of channel fill architecture and internal bedding of CH1 and CH2; CH1 = Yellow. CH2 = Purple. Photomosaic located between MS#5-7 along a west-east trending, linear canyon wall. Note that CH2 pinches in and erodes into the underlying CH1 body, the basal boundary marking SB2.

Channel 2 –

Channel 2 (CH2) overlies CH1 and occupies the top channel fill of the incised distributary sequence. CH2 differs from CH1 in flow direction, dimensions, sand/mud content, interpreted sinuosity, and number of channel fill stories. CH2 paleocurrent data indicate a dominant east-southeast (mean=102°) paleoflow direction (Fig. 16B), a

difference of 27° from CH1, with a minor westward paleocurrent mode interpreted as tidal backflow during periods of low out-flow due to proximity to the marine-environment. The composite channel body dimensions display a maximum central body width of ~250 m and maximum measured thickness of 6 m (Fig. 16). The basal boundary of CH2 incises into CH1 where the separate incised distributary channel bodies overlap one another (Fig. 14C; 15A-B; 16C). In plan view CH2 trends northwest-southeast (Fig. 16), first outcropping up-dip in the northwest head of the Labyrinth gully network near MS#14. The channel fill consists of up to five (Fig. 6A) identifiable erosional-based beds, each with a distinctive bioturbated siltstone parting. The western boundary of CH2 is well-constrained through the angular discordance of the channel margin IHS and overlying strata (Figs. 13D; 16). The last down-dip exposure of CH2 at the Labyrinth location shows an erosional surface (SB2) separating the underlying CH1 and marking SB2 (Figs. 13A: 14C; 16B). The channel displays an asymmetric point-bar to cut-bank geometry infilled by single sandstone body of lateral accretions sets (3.5 m high) spanning half of the cross-sectional width of the channel (Fig. 13A).

Higher mud-content and decreased bed thickness is observed within body of CH2. Each of the individual channel-beds is associated with an interval of IHS at the channel margin (Figs. 6A) that grades into the sandstone dominated, axial channel fill. Mudstone partings are more prominent in CH2 and are not only observed at the margin of channel stories but extending into the central channel fill. CH2 IHS is sand-dominated and irregular with respect to interbed thickness, ranging from 0.1-1.0 m thick with relatively thin cm-scale mudstone beds (Fig. 6B). Sandstone bases of CH2 IHS are erosional and some contain syneresis cracks at the sand-mud interface and internally dominated by

current ripple-cross and flat lamination with weakly developed mud-drapes. Bioturbated (BI = 0-1) bed bases and tops are characterized by a low diversity of traces, typically individual *Planolites* burrows. IHS mudstones are not bioturbated (BI = 0), but siltstone partings associated with channel separating erosional surface display moderate bioturbation intensity (BI = 0-3) comprising a similar assemblage to that which characterizes such surfaces in CH1.

DISCUSSION

Compound Incised Distributary Channel Fill

The two channels within the Critical Interval show distinct characteristics with implications for depositional influences. The most significant distinction between the separate channel systems is that CH1 appears to be fluvial-dominated with no evidence of tidal-influence, while CH2 contains evidence of tidal processes in the form of bimodal paleocurrent distribution (Fig. 16B) and IHS. IHS deposits are common elements of modern tidal channels and depositional systems (Nio and Yang, 1991; Dalrymple and Choi, 2007; Choi 2010; Dalrymple, 2010; Davis, 2012) and are often used to interpret tidal-influence in ancient deposits. However, IHS may form in fluvial-dominated or mixed-energy environments due to temporal variations in river discharge at a seasonal or shorter time scales (Thomas et al., 1987). Difficulties arise when distinguishing between seasonal- and tidal-influenced IHS deposits because river discharge fluctuation is a fundamental characteristic of modern rivers and may temporally and spatially coexist with tidal-processes in the lower reaches of rivers (e.g. Fraser River delta distributary channel; Sisulak and Dashtgard, 2012; Johnson and Dashtgard, 2014).

Many deltaic distributary channels containing IHS are interpreted to lie within the fluvial-tidal transition zone (FTTZ; Van den Berg and Boersma, 2007; Dalrymple and Choi, 2007: Dashtgard and La Croix, 2015,). Within this zone, dominant seaward-directed transport occurs during normal river conditions and flooding events, while landward transport in the form of tidal-process may take place during periods of low flow. The majority of the FTTZ contains fresh water, although an influx of brackish water may dominate at the seaward-end of the FTTZ, extending further inland at times of low river flow (Dalrymple and Choi, 2007). Literature concerning IHS of mixed tidal-fluvial distributary channels document two notable sedimentological trends reflecting tidal and/or fluvial controls on sedimentation. 1) Increased mud-content seaward (Thomas, 1987; Ranger and Pemberton, 1992; Dalrymple and Choi, 2007; Hubbard et al., 2011; Johnson and Dashtgard, 2014). 2) Interbed rhythmicity increases with tidal-influence (Choi et al., 2004; Dalrymple and Choi, 2007, Sisulak and Dashtgard, 2012; Johnson and Dashtgard, 2014). Regardless of the trends and degree of tidal-influence, if the fluvial system is strongly seasonal, then the subsequent deposit will reflect this more than any other depositional factor (Dalrymple and Choi, 2007). Seasonal high-flow events rapidly deposit sand during flooding, followed by mud during the waning stages. Sand deposition is associated with freshwater conditions that are inhospitable for marine life, with deposits typically remaining unbioturbated (Sisulak and Dashtgard, 2012). The absence or lack of thoroughly bioturbated sand and mud beds indicates that sedimentation most likely overwhelmed infauna, and that salinity levels were not high enough to sustain marine organisms. Unbioturbated sand and mud interbeds typically reflect low salinity

environments, and may enable recognition of increasing fluvial- or seasonal-influences in ancient deposits.

The IHS within CH2 is highly irregular and displays poor rhythmicity between sandstone and mudstone interbed deposits. Sandstone beds are erosionally-based, highly variable in thickness (0.1-1.0 m), and have a low bioturbation intensity (BI = 0-1) typically represented by a low-diversity of individual *Planolites* burrows. The irregular bed thickness most likely indicates sedimentation was primarily during flooding events related to seasonal variations. Tidal-influence existed during low flow stage as indicated by westward paleocurrent directions, but the likelihood of such deposits being preserved was low due to the erosion associated with seasonal events.

Both CH1 and CH2 are considered tidally-influenced, fluvial-dominated distributary channels within the FTTZ. CH1 is considered to be within the upper limits of the FTTZ, representing Facies 1 - V2. CH2 is the primary example of Facies 1 – V2, and was deposited under strong marine- and tidal-influence near the lower limit in proximity to the marine environment. Although bioturbation is absent to minimal in IHS interbeds and within sand bodies, thin (mm-scale), bioturbated (BI = 2-3), siltstone partings with syneresis cracks separate individual channel stories, indicating extended periods of low river flow and increased salinity. The lithology, limited trace fossil assemblage and paleocurrent trends are similar to descriptions of distributary channels of prominent seasonal river discharge near the limit of tidal limit (Dalrymple and Choi, 2007; Van den Berg and Boersma, 2007).

In summary, two separated distributary channel bodies were identified (CH1 and CH2). The lower CH1 is interpreted as primarily fluvial deposited near the limit of tidal

inundation due to its unimodal paleocurrent distribution, lack of IHS and indicators of marine influence. CH2 erosionally incises into CH1, and is interpreted as a fluvial-dominated, tidally-influenced distributary channel located down-dip of the tidal inundation limit. Each channel deposit displays evidence for variable flow regimes related to tidal fluctuations allowing for deciphering proximity to the marine-environment.

Critical Interval Sequence Stratigraphy

Incision by fluvial-deltaic distributary channels is often driven by relative fluctuations in sea-level (Zaitlin et al., 1994; Blum and Aslan, 2006). This is certainly the case with the incised channel body documented in this study area. Figure 18 summarizes the sequence of events and sea-level fluctuations interpreted from the preserved facies, stratigraphic architecture, and key bounding surfaces observed in the critical interval and will be referred to within the following section unless noted otherwise.

SB1 separates the lower and upper Ferron Sandstone members and has been directly linked to allogenic control recorded by the syndepositional growth of a structural arch (Fig. 5A; Fielding, 2011). Related base-level fall and subsequent forced regression are recorded by a regionally extensive, roughly planar erosional surface that truncates the crest of a broad anticline in the lower Ferron Sandstone (Fig. 5A). Physical correlation of SB1 along strike over 67 km by Fielding (2011) noted SB1 was marked by thin veneer of coastal plain facies and a few small-scale fluvial incisions, similar to those documented in this study. The initial episode of channel incision associated with SB1 occurred near the end of the FRST after sea-level stabilized and the fluvial channel re-equilibrated to base

level. The local distributary channel incised into a subaerially exposed delta slope parasequence at the top of the lower Ferron member.

Channel filling began during base-level stillstand and subsequent rise, spanning the LST and early TST. Channel deposits are interpreted to have filled the incised topographic low and deposited a significant amount of overbank deposits, but subsequent erosion and reworking from transgressive wave ravinement only preserved locally reworked transgressive facies within small previously cut and abandoned sub-channels adjacent to channel margins.

The second episode of incision was driven by base-level fall and forced regression, shifting the depositional profile seaward. The incision surface associated with SB2 cut into CH1, eroding and carrying away the exposed sandy-substrate. Channel filling followed, beginning in the LST and continuing into early TST. CH2 occupies the SB2 incision displaying evidence for increased marine-influence suggesting deposition took place closer to the marine-environment relative to CH1. The stratigraphic succession associated with SB2, including the well-developed LDP deposits containing abundant plant material, was transgressed and subject to extensive erosion and reworking by wave ravinement. Evidence of these organic-rich LDP deposits lies within overlying LMSF body that contains abundant plant debris. This reworked organic material (Fig. 12D) created an environment perfectly suited for invertebrate colonization leading to the pervasively bioturbated LMSF sandstone preserved today (Fig. 12).

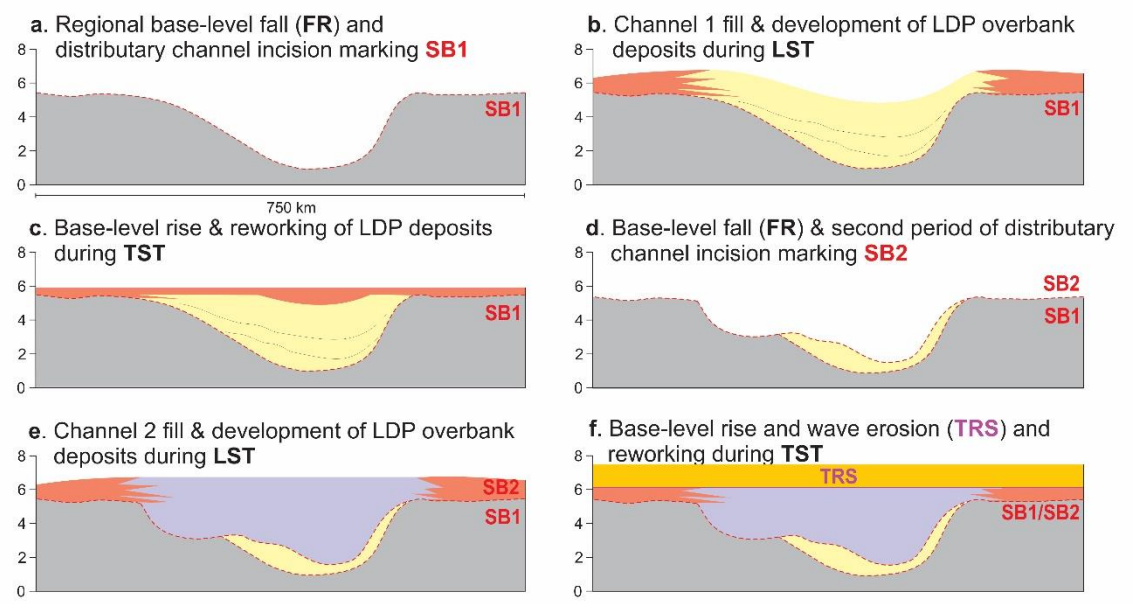

Figure 18 – Sequence of events leading to the preserved deposits of the critical interval. Two complete cycles of base-level are interpreted, associated with Forced Regression (FR) incision, Lowstand channel fill and overbank deposits, Transgression and transgressive systems tract (TST) erosion and reworking. Diagram is modelled from a north-south trending, strike-perpendicular view. Colors correspond to facies scheme in Fig. 5B and CH1 and CH2 colors from Fig. 15. Sequence boundary = SB. Transgressive ravinement surface = TRS

Channel Incision and Response to Sea-Level Fall

Sequence stratigraphic models predict that during sea-level fall, progradation occurs shifting the depositional profile basinward, including fluvial and deltaic distributary channel systems. Base-level and the downstream portion of the fluvial profile typically have a process-response relationship in which the system is anchored by and responds to base-level fluctuations (Posamentier and Allen, 1999; Catuneanu, 2006). If the lowering of base-level exposes a surface that is steeper than the local fluvial equilibrium grade, local fluvial incision of the coastal–delta plain–shelf results in the development of incised valleys as the fluvial system incises to attain a new fluvial equilibrium profile (Posamentier et al., 1992; Leeder and Stewart, 1996; Posamentier and Allen, 1999). Fluvial erosion and sediment bypass during periods of adjustment create

degradational landscapes resulting in regional unconformities that demarcate depositional sequence boundaries (Mitchum et al., 1977; Posamentier and Vail, 1988; Van Wagoner et al., 1990). Due partly to the hydrocarbon potential of incised valley fill deposits, they are well documented (e.g. Zaitlin et al., 1994; Shanley and McCabe, 1994; Dalrymple et al., 1994; Hampson et al., 1997; Dalrymple, 2006; Fielding, 2007: Blum et al., 2013). These large-scale subaerial erosion surfaces form sequence bounding unconformities, a key surface almost exclusively interpreted to be a consequence of relative sea-level fall (Posamentier et al., 1988; Posamentier, 2001; Catuneanu, 2006; Catuneanu et al., 2009). Reynolds (1999) and more recently, Gibling (2006) and Blum et al. (2013) compiled a record of documented ancient incised valley dimensions, reporting an average width of ~10 km, ranging from 0.5 - 63 km, averaging 30 m in depth. A series of review papers (Hampson et al., 1997; Fielding, 2007; Gibling et al., 2011, Blum et al., 2013) published diagnostic criteria for incised valley fill deposits, namely; 1) association with a regionally-extensive sequence boundary, 2) facies dislocation across the sequence boundary, 3) significant erosion of underlying strata, and 4) multistorey organization recording base-level transgression and associated fill. Incised valleys are generally filled during the subsequent base-level rise and may contain sediments deposited continuously during late lowstand to highstand deposition (Zaitlin et al., 1994; Martinsen, 1994) and, possibly, subsequent sea-level cycles.

Incised valleys in the Ferron Sandstone member are documented in the FNDC from the northeast rim of the HMS (Li et al., 2010; Zhu, 2012; Li and Bhattacharya, 2013), some 70 km to the northeast of the study area, and also within the older Last Chance delta complex in east-central Utah (Schwans, 1995; Garrison and van den Bergh,

2004; 2006; Barton et al., 2004). Li et al. (2010) interpreted a compound incised valley (>10 km wide) containing high-frequency (Milankovitch-scale) cut-and-fill sequences, with up to 30 m of incision (Li et al., 2010; Li and Bhattacharya, 2013). Each of the valley fill sequences displays a vertical facies trend of fluvial, to tidal, and back to fluvial facies (Li et al., 2010; Zhu et al., 2012; Li and Bhattacharya, 2013). Garrison and van den Bergh (2004, 2006) reported four fourth-order depositional sequences, each marked by 30 m deep multistorey valley systems within Last Chance delta complex of the Ferron Sandstone in east-central Utah. A total of six incised valley fills have been reported from the Last Chance delta complex (Schwans, 1995; Garrison and van den Bergh, 2004; Barton et al., 2004). One reported valley from Barton et al. (2004) was documented to be only 150 m wide, but displays incised, multistorey channel bodies with a relatively simple fill. Several authors have interpreted such small-scale examples as stable distributary channels that presumably eroded as a result of upstream variables or a newly avulsed channel, opposed to a valley cut during a significant drop of sea-level (Garrison and van den Bergh, 2004; Moiola et al., 2004). Along the western-limb of the HMS near the present study area, no incised valleys have been documented in the Ferron Sandstone member, but that does not mean that they may not be present.

The argument of whether smaller-scale incised channel bodies with organized and cyclic channels fill are distributary channels or incised valleys is relevant to the findings of this study. The incised channel body succession of this study is associated with two sequence boundaries, including a regionally-extensive sequence boundary (SB1), demonstrates a well-defined facies change from marine- to non-marine, and has internal organization related to fluctuations in marine-and fluvial-influence, our example does not

satisfy the criteria of significant incision (considered relatively modest, ~5 m of relief). Furthermore, the incised fluvial channel bodies documented in the paper is dwarfed in size by previously documented examples of incised valley systems (see review by Gibling, 2006). Incised valley interpretation requires incision depth exceeding the thickness of two or more of the encased channel belts (Holbrook, 2001; Gibling, 2006; Strong and Paola, 2008).

Falling sea-level from forced regression, or simple progradation of the shoreline during the HST, may cause lengthening of the river profile. Transgression of the shoreline, during rapid sea-level rise (TST), will cause a shortening of the river profile. Rivers will typically either aggrade or erode, depending on whether the new profile lies above or below the natural equilibrium profile of the river. Blum and Tornqvist (2000) emphasize that downstream changes in sea-level will propagate up-dip only as far as the coastal onlap point. Holbrook et al. (2006) and Blum and Tornqvist (2000) also hypothesize the importance of upstream controls, including uplift and climate-driven changes in discharge, in controlling river erosion and aggradation. These upstream effects define the preservation space, which is determined by the lowest level to which a stream may erode and the highest level to which it may aggrade. Shanley and McCabe (1994), Wright and Marriott (1993), Amorosi et al., (1999) and Van Wagoner (1995) proposed models for how fluvial systems might respond to changes in base-level, these models suggest that early phases of incision fill are composed of amalgamated multistorey channel belts, with later stages developing estuarine or tidal deposits, depending on distance upstream (Zaitlin et al., 1994). Work from Garrison and van den Bergh (2004, 2006) on the Last Chance delta complex of the Ferron Sandstone member in central Utah

concluded that the small magnitudes of sea-level fluctuations had minimal effect on fluvial erosion and that changes in sediment supply were an important control.

Magnitude of incision depends on a number of factors; distance from the shoreline, length and amplitude of base-level fall, and the gradient of the exposed shelf. As illustrated in this paper, the local stratigraphic architecture is composed of high-frequency sequences deposited during high-frequency and low-amplitude sea-level cycles. One explanation of the incised channel bodies of the Critical Interval is that repeated high-frequency and low-amplitude sea-level fluctuations did not allow for significant erosion and development of an incised valley, preserving the entrenched succession of distributary channel deposits. During high-frequency relative sea-level falls, fluvial systems will have less time to adjust themselves and incise into the underlying strata. Fluvial incision during such high-frequency relative sea-level falls, if it occurred, would probably diminish over short distances both up dip and down dip (Holbrook et al., 2006). Thus, low-amplitude relative sea-level falls would favor small-scale distributary channel incision down-dip and poorly developed incised valleys systems up-dip past the nodal avulsion point.

Holbrook and Bhattacharya (2012) describe similar processes through a *Buttress valley* model, where valley formation is controlled by a downstream buffer (e.g. sea-level change) along with upstream controls (e.g. climate and tectonics), as well as citing the gradient of the underlying strata as an important factor. During sea-level fall, a knickpoint initiates at the shoreline that propagates up-dip, linking the higher and lower river profiles and forming an incision surface over time (Posamentier and Vail, 1988; Holbrook and Bhattacharya. 2012). It is noted that knickpoint formation requires a drop

in sea-level over a slope that is steeper than the normal river slope gradient (Schumm, 1993; Muto et al., 2007), typically associated with forced regression exposing the shelf delta front, or some topographical element (Blum and Tornqvist, 2000; Holbrook et al., 2006). The previous work of Korus and Fielding (In Press) illustrates the down-dip stratigraphic architecture and gradient changes in clinoform set geometries associated with the Ferron Sandstone delta front (Fig. 5A). Relatively flat clinothem topsets and steeply-dipping foresets display a significant gradient-change, thus allowing for controlled incision given base-level fall of substantial magnitude and duration.

The strata of the lower Ferron Sandstone member preserve a high-density of syndepositional growth faults, growth-fault bounded gully-fills, soft sediment deformed bodies, as well as other deposits associated with liquefaction-related deformation. The overlying succession of entrenched, erosionally-based distributary channel bodies lies almost directly above these features. It is proposed that a pre-existing topographic low created by these features facilitated the initial accommodation pathway for the fluvial channel to flow through. It has been documented that rivers commonly occupy pre-existing topographic lows caused by structural subsidence related to fold and faulting (Schumm et al., 2000; Burbank and Anderson, 2001).

CONCLUSIONS

1. The dual approach of laboratory-based VOM analysis and field-based outcrop data allowed for tightly constrained documentation and illustration of facies relationships, stratal stacking patterns and key sequence stratigraphic surfaces within the Ferron Sandstone member in the HMS area of south-central Utah. The use of VOMs facilitated study of inaccessible vertical-cliff face exposures through high-resolution, three-

dimensional models that can be accessed without visiting outcrop locations. This paper illustrates how survey technology and geological software facilitate detailed 3D visualization of true bed and body geometries and aid in sequence stratigraphic interpretation.

2. Detailed facies analysis throughout the Ferron Sandstone member shows vertical stacking patterns and lateral relationships of deposits associated with high-frequency, low-amplitude sea-level cycles. Within the predominantly deltaic succession of the lower Ferron Sandstone member, high-frequency cycles are shown as thin (2.5-5.0 m) clinothem sets of regressive and transgressive deposits, interpreted to be the result of high-frequency and low-amplitude sea-level fluctuations within a low-accommodation delta front environment. The Critical Interval was primarily deposited in a semi-subaqueous delta plain setting in proximity to the delta front, where accommodation and marine-influence limited the preservation potential of the original deposits. The sequences within the Critical Interval are thin (~5 m), incomplete (Low preservation potential of LST delta plain deposits), and top-truncated (HST missing).

3. The incised channel body of the Critical Interval displays many characteristics of incised valley systems, yet the moderate incision depth (~5 m) and small dimensions do not meet previous definitions of incised valley systems. Instead the documented example is interpreted as the seaward-end of an entrenched distributary channel system, containing two separate cycles of transgression and regression. Fluvial incision was influenced by downstream controls; sea-level and the gradient of the exposed delta front slope. Although the exposed delta front gradient may be steep, moderate incision depths are credited to the low duration and magnitude of sea-level fluctuations under which the

Ferron Sandstone Member accumulated. Regional transects from Fielding (2011) and Korus and Fielding (In Press), show that the local expression of SB1 can be correlated to a regionally extensive sequence boundary. The small-scale incised channel bodies associated with this regionally extensive sequence boundary differs from previously documented incised bodies within the Ferron Sandstone Member. Although no incised valley systems have been identified on the western rim of HMS, the described of the Critical Interval may represent the cryptic, down-dip expression of incised valley systems.

5. Initial accommodation and development of the incised fluvial channels was most likely provided by pre-existing growth-fault reactivation in the underlying delta-front strata, creating a paleo-topographic low. The stratigraphic interval beneath the channel bodies is interpreted to be at or near the delta front, where high sedimentation rates and underlying substrate prone to failure and liquefaction created a high-density of synsedimentary faulting and soft-sediment-deformed bodies.

6. The proposed sequence stratigraphic model for the critical interval provides insight into the formation of thin, incomplete, and top-truncated sequences of low-accommodation settings. Our model illustrates the processes associated with individual phases of sea-level change that lead to the preserved deposits. The FRST is not directly recorded by deposition, but rather erosion in the form of fluvial incision surfaces related to downcutting and sediment bypass from the fluvial system as it adjust to the new base-level. During the LST, distibutary channel sandstone infilled the accommodation space and mature lower delta plain deposits accumulated outside of the channel confines. During times transgression (TST), overbank deposited were eroded and reworked by

wave ravinement. Coastal platform deposits within the critical interval were likely well-developed prior to transgressive ravinement. Evidence for this lies in the form of thin, preserved beds of transgressively reworked, rhythmically laminated macerated plant debris and organic-rich siltstone deposits located adjacent to and at the tops of channel bodies. Furthermore, the LMSF sandstone base marks the TRS, and the overlying deposit contains abundant macerated plant debris, interpreted to represent wave ravinement during transgression. However, the relative brevity of these RSL highs limited accommodation creation and meant that the preservation potential of HST deposits was very low and are thus not recorded in the Critical Interval.

REFERENCES

Akyuz, I., Warny, S., Famubode, O., and Bhattacharya, J.P., 2015, Palynology of the Upper Cretaceous (Turonian) Ferron Sandstone Member, Utah, USA: Identification of marine flooding surfaces and Milankovitch cycles in subtropical, ever-wet, paralic to non-marine palaeoenvironments: Palynology, v. 40, p. 122–136.

Allen, J.R., 1963, The Classification of Cross-Stratified Units. With Notes on Their Origin: Sedimentology, v. 2, p. 93-114.

Allen, J. P., and Fielding, C. R., 2007, Sequence architecture within a low-accommodation setting: An example from the Permian of the Galilee and Bowen Basins, Queensland, Australia: AAPG Bulletin, v. 91, p. 1503–1539.

Allen, G.P., and Posamentier, H.W., 1993, Sequence stratigraphy and facies model of an incised valley fill: the Gironde estuary, France: Journal of Sedimentary Petrology, v. 63, p. 378-391.

Amorosi, A., Colalongo, M.L., Pasini, G, and Preti, D., 1999, Sedimentary response to Late Quaternary sea-level changes in the Romagna coastal plain (northern Italy): Sedimentology, v. 46, p. 99–121.

Barron, E.J., 1983, A warm, equable Cretaceous: the nature of the problem: Earth-Science Reviews, v. 19, p. 305-338.

Baas, J.H., 2000, EZ-ROSE: a computer program for equal-area circular histograms and statistical analysis of two-dimensional vectorial data: Computers and Geosciences, v. 26, p. 153-166.

Bates, C.C., 1953, Rational theory of delta formation: AAPG Bulletin, v. 37, p. 2119-2162.

Bhattacharya, J.P., 1993, The expression and interpretation of marine flooding surfaces and erosional surfaces in core; examples from the Upper Cretaceous Dunvegan Formation, Alberta foreland basin, Canada, *in* Posamentier, H.W., Summerhayes, C.P., Haq, B.U., and Allen, G.P., eds., Sequence Stratigraphy and Facies Associations, p. 125-160.

Bhattacharya, J. P., 2006, Deltas, *in* H. W. Posamentier and R. G. Walker, eds., Facies models revisited: SEPM Special Publication 84, p. 237–292.

Bhattacharya, J.P., and MacEachern, J.A., 2009, Hyperpycnal rivers and prodeltaic shelves in the Cretaceous seaway of North America: Journal of Sedimentary Research, v. 79, p. 184-209.

Buckley, S.J., Howell, J.A., Enge, H.D., and Kurz, T.H., 2008, Terrestrial laser scanning in geology: data acquisition, processing and accuracy considerations: Journal of the Geological Society, v. 165, p. 625-638.

Blum, M.D., and Aslan, A., 2006, Signatures of climate vs. sea-level change within incised valley-fill successions: Quaternary examples from the Texas Gulf Coast: Sedimentary Geology, v. 190, 177-211.

Blum M., Martin J., Milliken K., and Garvin M., 2013, Paleovalley systems: insights from Quaternary analogs and experiments: Earth-Science Reviews, v. 116, p. 128–169.

Blum, M.D., and Törnqvist, T.E., 2000, Fluvial responses to climate and sea-level change: a review and look forward: Sedimentology, v. 47, p. 2-48.

Burbank, D.W., and Anderson, R.S., 2011, Tectonic geomorphology: Blackwell: Malden, MA.

Catuneanu, O., 2006, Principles of sequence stratigraphy: Oxford, UK, Elsevier, 375 p.

Catuneanu, O., Abreu, V., Bhattacharya, J., Blum, M., Dalrymple, R., Eriksson, P., Fielding, C., Fisher, W., Galloway, W., Gibling, M., Giles, K., Holbrook, J., Jordan, R., Kendall, C.G.S.C., Macurda, B., Martinsen, O., Miall, A.D., Neal, J., Nummedal, D., Pomar, L., Posamentier, H.W., Pratt, B., Sarg, J., Shanley, K.W., Steel, R.J., Strasser, A., Tucker, M., and Winker, C., 2009, Towards the standardization of sequence stratigraphy: Earth-Science Reviews, v. 92, p. 1-33.

Choi, K.S., and Dalrymple, R.W., 2004, Recurring tide-dominated sedimentation in Kyonggi Bay (west coast of Korea): similarity of tidal deposits in late Pleistocene and Holocene sequences: Marine Geology, v. 212, p. 81-96.

Coleman, J.M., and Wright, L.D., 1975, Modern river deltas: Variability of processes and sand bodies, *in* Broussard, M.L., eds., Deltas: Models for exploration: Houston, Texas, Houston Geological Society, p. 99–149.

Coleman, J.M., and Prior, D.B., 1980, Deltaic sand bodies: American Association of Petroleum Geologist Short Course, No. 15.

Cotter, E., 1975, Late Cretaceous sedimentation in a low-energy coastal zone: the Ferron Sandstone of Utah: Journal of Sedimentary Petrology, v. 45, p. 669-685.

Dalrymple, R.W., and Choi, K., 2007, Morphologic and facies trends through the fluvial–marine transition in tide-dominated depositional systems: a schematic framework for environmental and sequence-stratigraphic interpretation: Earth-Science Reviews, v. 81, p. 135-174.

Dalrymple, R. W., Kurcinka, C. E., Jablonski, B. V. J., Ichaso, A. A., and Mackay, D. A., 2015, Deciphering the relative importance of fluvial and tidal processes in the fluvial–marine transition: Fluvial-tidal sedimentology, Oxford, United Kingdom, Elsevier, Developments in Sedimentology, v. 68, p. 3-45.

La Croix, A.D., and Dashtgard, S.E., 2015, A synthesis of depositional trends in intertidal and upper subtidal sediments across the tidal–fluvial transition in the Fraser River, Canada: Journal of Sedimentary Research, v. 85, p. 683-698.

Dean, W.E., and Arthur, M.A., 1998, Cretaceous Western Interior Seaway drilling project: An overview, *in*, Dean, W.E., and Arthur, M.A., eds., Stratigraphy and Paleoenvironments of the Cretaceous Western Interior Seaway, USA, Concepts in Sedimentology and Paleontology, v. 6, p. 1–10.

DeCelles, P. G., and Giles, K. A. (1996). Foreland basin systems: Basin research, v. 8, p. 105-123.

DeCelles, P. G. (2004). Late Jurassic to Eocene evolution of the Cordilleran thrust belt and foreland basin system, western USA: American Journal of Science, v. 304, p. 105-168.

Demarest, J.M., and Kraft, J.C., 1987, Stratigraphic record of Quaternary sea levels: Implications for more ancient strata *in* Nummedal, D., Pilkey, O.H., and Howard, J.D., eds., Sea-level Fluctuation and Coastal Evolution. SEPM Special Publication, v. 41, p. 223-239.

Famubode, O.A., and Bhattacharya, J.P., 2016, Sequence Stratigraphic Analysis of the Youngest Nonmarine Sequence In the Cretaceous Ferron Notom Delta, South Central Utah, USA: Journal of Sedimentary Research, v. 86, p. 168-198.

Fielding, C.R., Trueman, J.D., and Alexander, J., 2005, Sharp-based, flood-dominated mouth bar sands from the Burdekin River Delta of northeastern Australia: extending the spectrum of mouth-bar facies, geometry, and stacking patterns: Journal of Sedimentary Research, v. 75, p. 55-66.

Fielding, C. R., K. L. Bann, J. A. MacEachern, S. C. Tye, B. G. Jones, 2006b, Cyclicity in the nearshore marine to coastal, Lower Permian, Pebbley Beach Formation, southern Sydney Basin, Australia: A record of relative sea-level fluctuations at the close of the late Paleozoic Gondwanan Ice Age: *Sedimentology*, v. 53, p. 435–463.

Fielding, C.R., K.L. Bann, and J.D. Trueman, 2007, Resolving the architecture of a complex low-accommodation unit using high-resolution sequences stratigraphy and ichnology: The Late Permian Freitag Formation in the Denison Trough, Queensland, Australia, in J. A. MacEachern, K. L. Bann, M. K. Gingras, and S. G. Pemberton, eds., Applied ichnology: SEPM Short Course Notes 52, p. 1–30.

Fielding, C. R., 2008, Sedimentology and stratigraphy of large river deposits: Recognition in the ancient record, and distinction from “Incised Valley Fills”.: Large Rivers: Geomorphology and Management, John Wiley and Sons, Ltd, 97-113.

Fielding, C.R., 2010, Planform and facies variability in asymmetric deltas: facies analysis and depositional architecture of the Turonian Ferron Sandstone in the western Henry Mountains, south-central Utah, USA: Journal of Sedimentary Research, v. 80, p. 455-479.

Fielding, C.R., 2011, Foreland basin structural growth recorded in the Turonian Ferron Sandstone of the Western Interior Seaway Basin, USA: Geology, v. 39, p. 1107-1110.
Fielding, C.R., 2015, Anatomy of falling-stage deltas in the Turonian Ferron Sandstone of the western Henry Mountains Syncline, Utah: growth faults, slope failures, and mass transport complexes: Sedimentology, v. 62, p. 1-26.

Enge, H.D., Buckley, S.J., Rotevatn, A., and Howell, J.A., 2007, From outcrop to reservoir simulation model: Workflow and procedures: Geosphere, v. 3, p. 469-490.
Gale, A.S., Voigt, S., Sageman, B.B., and Kennedy, W.J., 2008, Eustatic sea-level record for the Cenomanian (Late Cretaceous) - extension to the Western Interior Basin, USA: Geology, v. 36, p. 859-862.

Galloway, W. E. (1975). Process framework for describing the morphologic and stratigraphic evolution of deltaic depositional systems, *in* Broussard, M.E., ed., Deltas, Houston Geological Society, Houston, Texas, p. 87–98.

Gardner, M.H., 1995, Tectonic and eustatic controls on the stratal architecture of Mid-Cretaceous stratigraphic sequences, central Western Interior foreland basin of North America, *in* Dorobek, S.L., and Ross, G.M., *eds.,* Stratigraphic Evolution of Foreland Basins, SEPM Spec. Publ., no. 52, p. 243–281.

Gardner, M. H., Cross, T. A., and Levorsen, M, 2004, Stacking patterns, sediment volume partitioning, and facies differentiation in shallow-marine and coastal-plain strata of the Cretaceous Ferron Sandstone, Utah: Regional to wellbore analog for fluvial-deltaic reservoir modeling: The Ferron Sandstone of Utah: AAPG Studies in Geology, v. 50, p. 95-124.

Garrison, J.R., and van den Bergh, T.C.V., 2004, High-resolution depositional sequence stratigraphy of the upper Ferron Sandstone Last Chance delta: an application of coal-zone stratigraphy, *in* Chidsey, T.C., Adams, R.D., and Morris, T.H., eds., Regional to Wellbore Analog for Fluvial-Deltaic Reservoir Modeling: Ferron Sandstone of Utah, American Associaton of Petroleum Geologists, p. 125-192.

Garrison, J.R., and van den Bergh, T.C.V., 2006, Effects of sedimentation rate, rate of relative rise in sea level, and duration of sea-level cycle on the filling of incised valleys: examples of filled and ‘‘overfilled’’ incised valleys from the Upper Ferron Sandstone,

Last Chance Delta, east-central Utah, USA, *in* Dalrymple, R.W., Leckie, D.A., and Tilman, R.W., eds., SEPM Special Publication 85, p. 239-279.

Gibling, M.R., 2006, Width and thickness of fluvial channel bodies and valley fills in the geological record: a literature compilation and classification: Journal of Sedimentary Research, v. 76, p. 731-770.

Gibling, M.R., Fielding, C.R., and Sinha, R., 2011, Alluvial valleys and alluvial sequences: towards a geomorphic assessment, *in* Davidson, S.K., Leleu, S., and North, C.P., eds., SEPM Special Publication 97, p. 423-447.

Gilbert, G.K., 1877, Geology of the Henry Mountains. *US Geographical and Geological Survey of the Rocky Mountain region: Washington, DC, US Government Printing Office*.

Hale, L.A., and Van de Graaff, L.A., 1964, Cretaceous stratigraphy and facies patterns: northeastern Utah and adjacent areas: Intermountain Association of Petroleum Geologists, 13th Annual Field Conference, Guidebook, p. 115– 138.

Hale, L.A., 1972, Depositional history of the Ferron Formation, central Utah, *in* Baer, J.L., and Callaghan, E., eds., Plateau-Basin and Range Transition Zone, Central Utah, Utah Geological Association, p. 29-40.

Hampson, G. J., and Storms, J. E., 2003, Geomorphological and sequence stratigraphic variability in wave-dominated, shoreface-shelf sequences: Sedimentology, v. 50, p. 667-701.

Hart, B.S., and Plint, A.G., 2003, Stratigraphy and sedimentology of shoreface and fluvial conglomerates: insights from the Cardium Formation in NW Alberta and adjacent British Columbia: Bulletin of Canadian Petroleum Geology, v. 51, p. 437-464.

Haq, B.U., Hardenbol, J., and Vail, P.R., 1987, Chronology of fluctuating sea levels since the Triassic: Science, v. 235, p. 1156-1167.

Hill, R. B., 1982, Depositional environments of the Upper Cretaceous Ferron Sandstone south of Notom, Wayne County, Utah. Brigham Young University, Geology Studies, v. 29, p. 59-83.

Holbrook, J.M., 2001, Origin, genetic interrelationships, and stratigraphy over the continuum of fluvial channel-form bounding surfaces: an illustration from middle Cretaceous strata, southeastern Colorado: Sedimentary Geology, v. 144, p. 179-222.

Holbrook, J., Scott, R.W., and Oboh-Ikuenobe, F.E, (2006), Base-level buffers and buttresses: a model for upstream versus downstream control on fluvial geometry and architecture within sequences: Journal of Sedimentary Research, v. 76, p. 162-174.

Holbrook, J.M., and Bhattacharya, J.P., 2012, Reappraisal of the sequence boundary in time and space: case and considerations for an SU (subaerial unconformity) that is not a sediment bypass surface, a time barrier, or an unconformity: Earth-Science Reviews, v. 113, p. 271-302.

Howell, J. A., Martinius, A. W., and Good, T. R.., 2014, The application of outcrop analogues in geological modelling: A review, present status and future outlook: Geological Society, London, Special Publications, v. 387, p. 1-25.

Hubbard, S.M., Smith, D.G., Nielsen, H., Leckie, D.A., Fustic, M., Spencer, R.J., and Bloom, L. (2011). Seismic geomorphology and sedimentology of a tidally influenced river deposit, Lower Cretaceous Athabasca oil sands, Alberta, Canada: AAPG bulletin, v. 95, p. 1123-1145.

Huber, B.T., Norris, R.D., and MacLeod, K.G., 2002, Deep-sea paleotemperature record of extreme warmth during the Cretaceous: Geology, v. 30, p. 123-126.

Hunt, C.B., and Miller, R.L., 1946, General geology of the region-stratigraphy, Guidebook to the Geology and Geography of the Henry Mountain Region, Utah Geological Society, p. 6-10.

Hunt, D., and Tucker, M.E., 1995, Stranded parasequences and the forced regressive wedge systems tract: deposition during base-level fall—reply: Sedimentary Geology, v. 95, p. 147-160.

Hutsky, A.J., and Fielding, C.R., 2017, Tectonic control on deltaic sediment dispersal in the middle to upper Turonian Western Cordilleran Foreland Basin, USA: *Sedimentology*.

Johnson, S.M., and Dashtgard, S.E., 2014, Inclined heterolithic stratification in a mixed tidal–fluvial channel: differentiating tidal versus fluvial controls on sedimentation: Sedimentary Geology, v. 301, p. 41-53.

Kauffman, E.G., 1977, Geological and biological overview: Western Interior Cretaceous Basin: The Mountain Geologist, v. 14, p. 75-99.

Korus, J.T., and Fielding, C.R., 2015, Enhanced bioturbation on the down-drift flank of a Turonian asymmetrical delta: Implications for seaway circulation, river nutrients and facies models: Sedimentology, v. 62, p. 1899-1922.

Li, W., Bhattacharya, J.P., and Campbell, C., 2010, Temporal evolution of fluvial style in a compound incised-valley fill, Ferron "Notom Delta," Henry Mountains region, Utah (U.S.A.): Journal of Sedimentary Research, v. 80, p. 529-549.

Li, W., Bhattacharya, J.P., and Zhu, Y., 2011a, Architecture of a forced regressive systems tract in the Turonian Ferron "Notom Delta", southern Utah, U.S.A.: Marine and Petroleum Geology, v. 28, p. 1517-1529.

Li, W., Bhattacharya, J.P., Zhu, Y., Garza, D., and Blankenship, E., 2011b, Evaluating delta asymmetry using three-dimensional facies architecture and ichnological analysis, Ferron 'Notom Delta', Capital Reef, Utah, USA: Sedimentology, v. 58, p. 478-507.

Liu, L., 2015, The ups and downs of North America: Evaluating the role of mantle dynamic topography since the Mesozoic: Reviews of Geophysics, v. 53, no. 3, p. 1022–1049.

Lupton, C.T., 1916, Geology and coal resources of Castle Valley in Carbon, Emery, and Sevier Counties, Utah, U.S. Geological Survey, p. 88.

MacEachern, J.A., Bann, K.L., Bhattacharya, J.P., and Howell Jr, C.D., 2005, Ichnology of deltas: organism responses to the dynamic interplay of rivers, waves, storms, and tides, *in* Gioson, L., and Bhattacharya, J.P., eds., River Deltas: Concepts Models and Examples. SEPM Special Publication 83, p. 49–85

Martinsen, O.J., 1994, Evolution of an incised-valley fill, the Pine Ridge Sandstone of southeastern Wyoming, U.S.A.: systematic sedimentary response to relative sea-level change, *in* Dalrymple, R.W., Boyd, R., and Zaitlin, B.A., eds., Incised Valley Systems, Origin and Sedimentary Sequences: SEPM, Special Publication 51, p. 109–128.

Miall, A.D., 1985, Architectural-element analysis: a new method of facies analysis applied to fluvial deposits: Earth-Science Reviews, v. 22, p. 261-308.

Miall, A.D., Catuneanu, B.K., Vakarelov, B.K., and Post R., 2008, The Western Interior Basin, *in* Miall, A.D., eds., The Sedimentary Basins of the United States and Canada: Amsterdam, Elsevier Science, p. 329– 362

Mitchum Jr, R.M., Vail, P.R., and Thompson III, S., 1977, Seismic stratigraphy and global changes of sea level, part 2: the depositional sequence as a basic unit for stratigraphic analysis, *in* Payton, C., ed., Seismic Stratigraphy - Application to Hydrocarbon Exploration, American Association of Petroleum Geologists, p. 53-62.

Moiola, R.J., Welton, J.E., Wagner, J.B., Fearn, L.B., Farrell, M.E., Enrico, R.J., and Echols, R. J., 2004, Integrated analysis of the Upper Ferron deltaic complex, southern Castle Valley, Utah: Analog for Fluvial–Deltaic Reservoir Modeling, p. 79-91.

Mulder, T., and Cochonat, P., 1996, Classification of offshore mass movements: Journal of Sedimentary research, v. 66.

Muto, T., and Steel, R.J., 1992, Retreat of the front in a prograding delta: Geology, v. 20, p. 967–970.

Muto, T., Steel, R. J., and Swenson, J. B., 2007, Autostratigraphy: a framework norm for genetic stratigraphy: Journal of Sedimentary Research, v. 77, p. 2-12.

Nio, S.D., and Yang, C.S., 1991, Diagnostic attributes of clastic tidal deposits: A review: Canadian Society of Petroleum Geologists Clastic Tidal Sedimentology Memoir 16, p. 3–28.

Norris, R.D., Bice, K.L., Magno, E.A., and Wilson, P.A., 2002, Jiggling the tropical thermostat in the Cretaceous hothouse: Geology, v. 30, p. 299-302.

Nummedal, D., and Swift, D.J.P., 1987, Transgressive stratigraphy at sequence-bounding unconformities: some principles derived from Holocene and Cretaceous examples, *in* Nummedal, D., Pilkey, O.H., and Howard, J.D., eds., Sea-Level Fluctuation and Coastal Evolution: SEPM, Special Publication 41, p. 241–260.

Nummedal, D., and Molenaar, C.M., 1995, Sequence Stratigraphy of ramp-setting strand plain successions: The Gallup Sandstone, New Mexico, *in* Van Wagoner, J.C., and Bertram, G.T., eds., Sequence Stratigraphy of Foreland Basin Deposits, Outcrop and Subsurface Examples from the Cretaceous of North America, Am. Assoc. Petrol Geol. Memoir, 64, p. 277–307

Olariu, C., and Bhattacharya, J. P., 2006, Terminal distributary channels and delta front architecture of river-dominated delta systems: Journal of sedimentary research, v. 76, p. 212-233.

Pemberton, S.G., and MacEachern, J.A., 1995, The sequence stratigraphic significance of trace fossils: examples from the Cretaceous foreland basin of Alberta, Canada, in Van Wagoner, J.C., and Bertram, G., eds., Sequence Stratigraphy of Foreland Basin Deposits—Outcrop and Subsurface Examples from the Cretaceous of North America: American Association of Petroleum Geologists, Memoir 64, p. 429–475.

Peterson, F., and Ryder, R.T., 1975, Cretaceous rocks in the Henry Mountains region, Utah and their relation to neighboring regions, *in* Fasset, J.E., ed., Canyonlands Country, Four Corners Geological Society, p. 167-189.

Plint, A.G., and Nummedal, D., 2000, The falling stage systems tract: recognition and importance in sequence stratigraphic analysis, *in* Hunt, D., and Gawthorpe, R.L., eds., Sedimentary Responses to Forced Regressions, Geological Society of London, p. 1-17.

Posamentier, H.W., and Vail, P.R., 1988, Eustatic controls on clastic deposition II - sequence and systems tracts models, *in* Wilgus,
C.K., Hastings, B.S.,Kendall, C.G.St.C., Posamentier, H.W., Ross, C.A. & Van Wagoner, J.C., eds., Sea-Level Changes: An Integrated Approach. SEPM, Special Publications, v. 42, p. 125–154.

Posamentier, H.W., Allen, G.P., James, D.P., and Tesson, M., 1992, Forced regressions in a sequence stratigraphic framework: concepts, examples, and exploration significance (1): AAPG Bulletin, v. 76, p. 1687-1709.

Posamentier, H.W., and Allen, G.P., 1999, Siliciclastic Sequence Stratigraphy: SEPM Concepts in Sedimentology and Paleontology, v. 7.

Posamentier, H.W., Jervey, M.T., and Vail, P.R., 1988, Eustatic controls on clastic deposition I - conceptual framework, *in* Wilgus, C.K., Hastings, B.S., Kendall, C.G.S.C., Posamentier, H.W., Ross, C.A., and Van Wagoner, J.C., eds., Sea Level Changes - An Integrated Approach, Society of Economic Paleontologists and Mineralogists (SEPM), p. 110-124.

Posamentier, H.W., and Morris, W.R., 2000, Aspects of the stratal architecture of forced regressive deposits, *in* Hunt, D., and Gawthorpe, R.L., eds., Sedimentary Responses to Forced Regressions, Geological Society of London, p. 19-46.
Pringle, J. K., Howell, J. A., Hodgetts, D., Westerman, A. R., and Hodgson, D. M. (2006). Virtual outcrop models of petroleum reservoir analogues: a review of the current state-of-the-art: First break, v. 24, p. 33-42.

Ranger, M.J. and Pemberton, S.G., 1992, The sedimentology and ichnology of estuarine point bars in the McMurray Formation of the Athabasca Oil Sands deposit, northeastern Alberta, Canada, *in* Pemberton, S.G., eds., Applications of Ichnology to Petroleum Exploration: Society of Economic Paleontologists and Mineralogists, Core Workshop, v. 17, p. 401–421.

Reynolds, A.D., 1999, Dimensions of paralic sandstone bodies: AAPG bulletin, v. 83, p. 211-229.

Rodriguez, A.B., Hamilton, M.D., and Anderson, J.B., 2000, Facies and evolution of the modern Brazos Delta, Texas: wave versus flood influence: Journal of Sedimentary Research, v. 70, p. 283-295.

Ryer, T.A., and Anderson, P.B., 2004, Facies of the Ferron Sandstone, east-central Utah, *in* Chidsey, T.C., Adams, R.D., and Morris, T.H., eds., Regional to Wellbore Analog for Fluvial-Deltaic Reservoir Modeling: Ferron Sandstone of Utah, American Association of Petroleum Geologists, p. 59-78.

Sageman, B.R., and Arthur, M.A., 1994, Early Turonian paleogeographic/paleobathymetric map, Western Interior, US, in Caputo, M. V., Peterson, A., and Franczyk, K.J., eds., Mesozoic systems of the Rocky Mountain Region, USA: Rocky Mountain Section, Society for Sedimentary Geology (SEPM), p. 457–469.

Schumm, S., 1993, River response to baselevel change: implications for sequence stratigraphy: The Journal of Geology, p. 279-294.

Schwans, P. (1995) Controls on sequence stacking and fluvial to shallow-marine architecture in a foreland basin, *in* Van Wagner, J.C., and Bertram, G.T., eds., Sequence Stratigraphy of Foreland Basin Deposits, AAPG Mem., v. 64, p. 55– 102.

Shanley, K.W., and McCabe, P.J., 1994, Perspectives on the sequence stratigraphy of continental strata: AAPG bulletin, v. 78, p. 544-568.

Sisulak, C.F., and Dashtgard, S.E., 2012, Seasonal controls on the development and character of inclined heterolithic stratification in a tide-influenced, fluvially dominated channel: Fraser River, Canada: Journal of Sedimentary Research, v. 82, p. 244-257.

Slingerland, R.L., Kump, L.R., Arthur, M.A., Fawcett, P.J., Sageman, B.B., and Barron, E.J., 1996, Estuarine circulation in the Turonian Western Interior seaway of North America: Geological Society of America Bulletin, v. 108, p. 941-952.

Strong, N., and Paola, C., 2008, Valleys that never were: time surfaces versus stratigraphic surfaces: Journal of Sedimentary Research, v. 78, p. 579-593.

Swift, D.J., 1968, Coastal erosion and transgressive stratigraphy: The Journal of Geology, v. 76, p. 444-456.

Taylor, A.M., and Goldring, R., 1993, Description and analysis of bioturbation and ichnofabric: Journal of the Geological Society, v. 150, p. 141-148.

Thomas, R.G., Smith, D.G., Wood, J.M., Visser, J., Calverley-Range, E.A., and Koster, E.H., 1987, Inclined heterolithic stratification—terminology, description, interpretation and significance: Sedimentary Geology, v. *53*, p. 123-179.

Vail, P. R., Mitchum Jr, R. M., and Thompson III, S., 1977, Seismic Stratigraphy and Global Changes of Sea Level: Part 4. Global Cycles of Relative Changes of Sea Level: Section 2. Application of Seismic Reflection Configuration to Stratigraphic Interpretation.

Van den Berg, J.H., Boersma, J.R., and Gelder, A.V., 2007, Diagnostic sedimentary structures of the fluvial-tidal transition zone–Evidence from deposits of the Rhine and Meuse: Netherlands Journal of Geosciences/Geologie en Mijnbouw, v. 86.

Van Wagoner, J.C., Posamentier, H.W., Mitchum, R.M. J., Vail, P. R., Sarg, J. F., Loutit, T. S., and Hardenbol, J., 1988, An overview of the fundamentals of sequence stratigraphy and key definitions, *in* Wilgus, C.K., Hastings, B.S., Kendall, C.G.St.C., Posamentier, H.W., Ross, C.A., and Van Wagoner, J.C., eds., Sea Level Changes—An Integrated Approach, SEPM Special Publication 42, p. 39–45.

Van Wagoner, J.C., Mitchum, R., Campion, K., and Rahmanian, V., 1990, Siliciclastic sequence stratigraphy in well logs, cores, and outcrops: concepts for high-resolution correlation of time and facies, American Association of Petroleum Geologists Methods in Exploration Series, p.55.

White, T., Furlong, K., and Arthur, M., 2002, Forebulge migration in the Cretaceous Western Interior basin of the central United States: Basin Research, v. 14(1), p. 43-54.
Wilson, P.A., Norris, R.D., and Cooper, M.J., 2002, Testing the Cretaceous greenhouse hypothesis using glassy foraminiferal calcite from the core of the Turonian tropics on Demerara Rise: Geology, v. 30, p. 607-610.

Wright, L.D., 1977, Sediment transport and deposition at river mouths: a synthesis: Geological Society of America Bulletin, v. 88, p. 857-868.

Wright, V.P., and Marriott, S.B., 1993, The sequence stratigraphy of fluvial depositional systems: the role of floodplain sediment storage: Sedimentary Geology, v. 86, p. 203–210
Yonkee, A., Weil, A.B., 2015, Tectonic evolution of the Sevier and Laramide belts within the North American Cordillera Orogenic system: Earth-Science Reviews, v. 150, p. 531–593

Zaitlin, B.A., Dalrymple, R.W., and Boyd, R.O.N., 1994, The stratigraphic organization of incised-valley systems associated with relative sea-level change, *in* Dalrymple, R.W., Boyd, R., and Zaitlin, B.A., eds., Incised-Valley Systems: Origin and Sedimentary Sequences, Spec. *Publishers Soc. Econ. Paleont. Miner*, v. 51, p. 45–60.

Zaitlin, B.A., M.J. Warren, D. Potocki, L. Rosenthal, and R. Boyd, 2002, Depositional styles in a low accommodation foreland basin setting: An example from the Basal quartz (Lower Cretaceous), southern Alberta: Bulletin of Canadian Petroleum Geology, v. 50, p. 31–72.

Zhu, Y., Bhattacharya, J., Li, W., Lapen, T.J., Jicha, B.R., and Singer, B.S., 2012, Milankovitch scale sequence stratigraphy and stepped forced regressions of the Turonian Ferron Notom deltaic complex, south-central Utah, U.S.A.: Journal of Sedimentary Research, v. 82, p. 723-746.

APPENDIX

Appendices 1A – Measured Sections #1-6

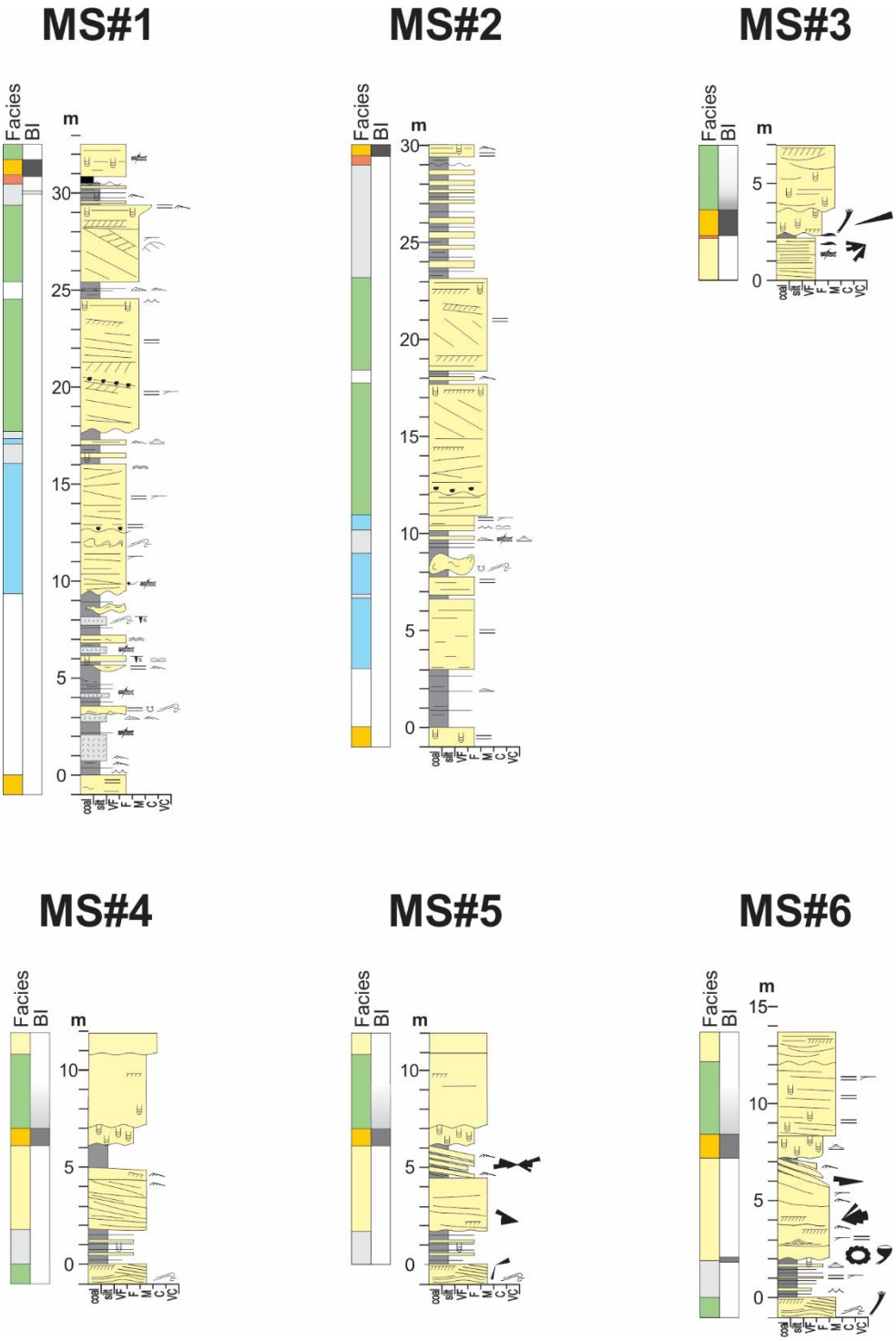

Appendices 1B – Measured Sections #7-9

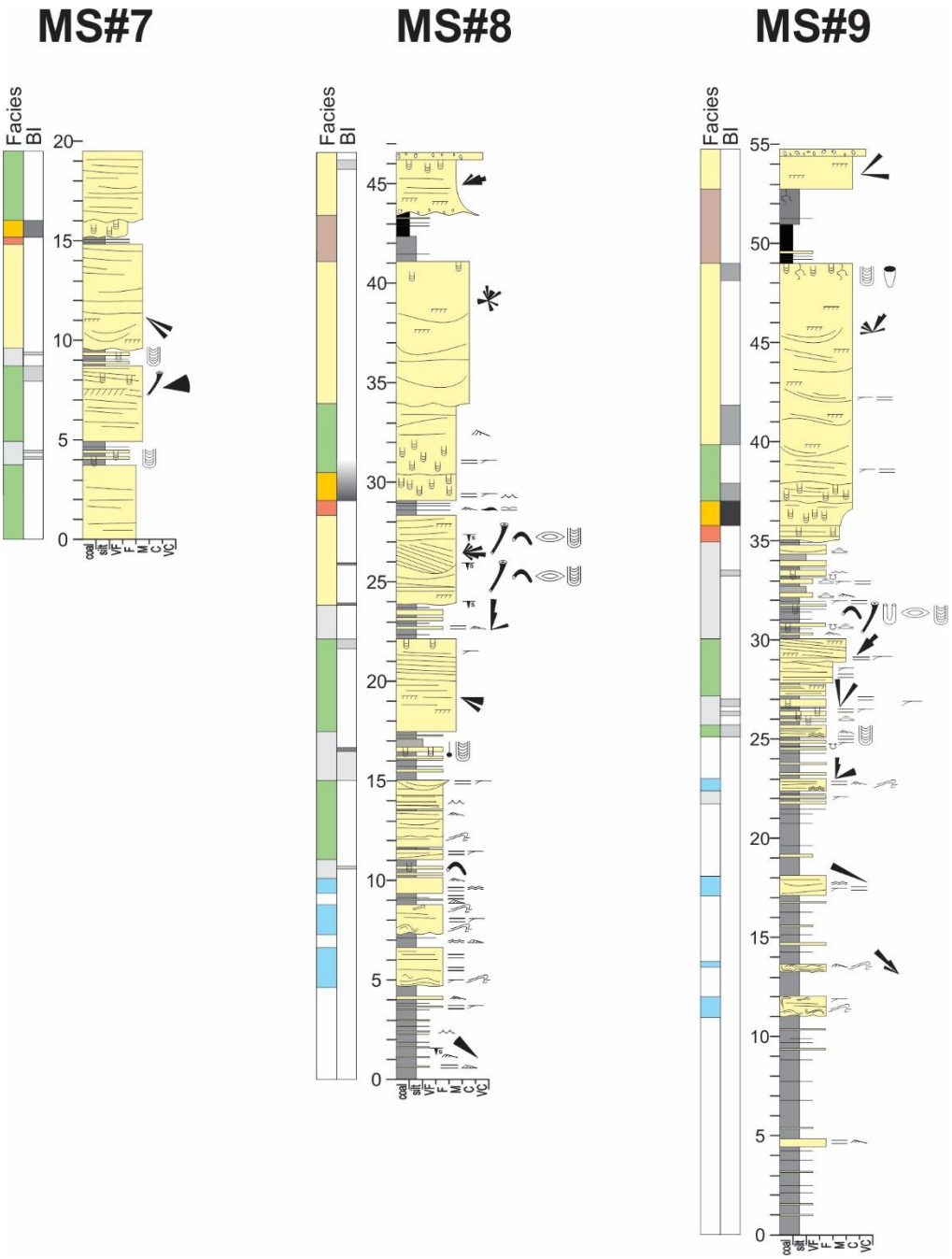

Appendices 1C – Measured Sections #10-15

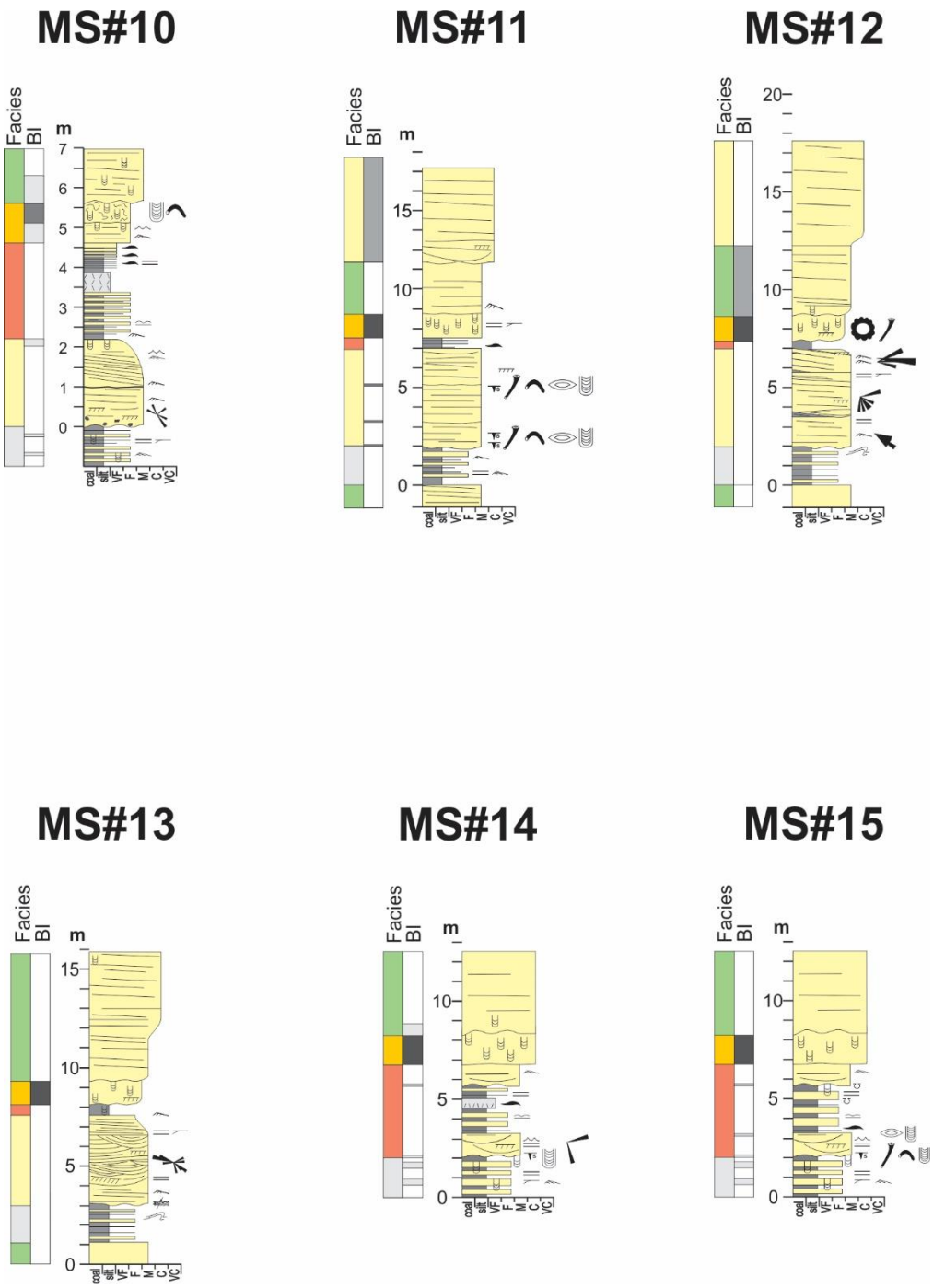

Appendices 1D – Paleocurrent Data organized by MS# and facies (color code in Figure 5B).

MS#1	MS#3	MS#5	MS#6	MS#7	MS#8	MS#9	MS#10	MS#12	MS#13	MS#14
002	198	069	276	076	307	295	056	103	067	348
003	211	071	261	084	316	312	114	116	090	072
006	206	194	270	091	003	312	299	125	121	
010	216	033	274	064	007	314	338	128	123	
042	272	044	279	095	008	318	056	140	136	
308	260	104	043	102	013	322	114	072	167	
352	270	112	045	122	080	299	118	077	263	
357	245	084	064		300	066	118	093	283	
	278	089	070		099	062	136	112	286	
	252	092	073		101	071	136	131	287	
	078	100	073		123	075	146	144	289	
		101	073		017	006	147	167	291	
			082		030	013	299	188	293	
			083		038	005	338	064		
			084		054	037	068	067		
			099		060	358	081	081		
			100		118	039		108		
			103		158	046				
			270		162	049				
			277		260	058				
			288		268	025				
			294		273	027				
			300		332	033				
					354	035				
					356	040				
					045	078				
					065	265				
					066	294				
					075	312				
					077	324				
					080	044				
					081	096				
					083					

Appendices 1E – Paleocurrent data for Figure 7

Fig. 7A – Ferron Sandstone Member

002	003	003	005	006	006	007	008	010	013	013	015
017	019	020	025	026	027	029	030	031	031	031	031
032	032	033	033	035	037	038	039	039	039	040	040
041	042	043	043	043	044	044	045	045	045	045	046
046	049	049	049	049	050	050	051	051	051	051	053
049	049	049	049	050	050	051	051	051	051	053	054
056	056	058	058	059	059	059	060	060	060	060	060
061	062	063	064	064	064	064	065	066	066	066	067
067	068	068	068	068	069	069	069	070	070	071	071
071	071	071	072	072	073	073	073	073	073	075	075
076	076	076	076	076	076	076	077	077	077	077	078
078	078	080	080	080	080	080	080	081	081	081	081
081	082	082	82	083	083	083	083	084	084	084	084
085	085	086	088	088	089	090	090	091	091	092	092
093	095	095	095	095	096	096	097	098	099	099	099
099	099	100	100	100	100	101	101	101	102	102	102
102	102	103	103	103	103	103	104	106	107	107	108
108	112	112	114	114	115	115	116	118	118	118	118
118	119	121	123	123	123	124	124	124	124	125	128
131	135	136	136	136	137	138	140	140	142	142	143
144	146	146	146	146	147	147	147	150	154	158	158
160	162	167	167	167	179	188	190	190	194	194	198
201	206	211	212	214	215	216	216	220	224	226	228
230	230	232	234	235	237	238	242	243	245	246	246
246	252	254	260	260	260	261	262	263	264	265	265
265	268	270	270	270	270	270	271	271	272	272	273
273	274	274	276	277	277	278	279	281	281	283	283
284	286	286	287	287	288	288	288	288	288	289	291
293	294	294	294	295	299	299	300	300	300	300	300
307	308	312	312	312	314	315	316	318	318	321	322
324	327	332	338	338	348	350	352	354	355	356	357
357	358										

Fig. 7B – Lower Ferron Sandstone Member

002	003	003	005	006	006	007	008	010	013	013	031
031	032	037	039	039	039	042	046	046	049	049	049
051	051	058	058	059	059	062	064	064	066	069	069
071	071	071	075	076	076	076	076	076	076	080	084
084	091	091	095	095	099	099	101	101	102	102	102
102	123	123	124	124	146	146	147	147	194	194	212
214	215	220	224	226	228	230	230	232	234	235	237
238	242	243	246	246	246	295	300	307	308	312	312
314	316	318	322	352	357	358					

Fig. 7C – Facies 1 – Combined

015	017	019	020	025	026	027	029	030	031	031	032
033	033	035	038	040	040	041	043	043	043	044	044
045	045	045	045	049	050	050	051	051	053	054	056
059	060	060	060	060	060	061	063	064	064	065	066
066	067	067	068	068	068	068	069	070	070	071	071
072	073	073	073	073	073	075	076	077	077	077	077
078	078	078	080	080	080	080	080	081	081	081	081
081	082	082	082	083	083	083	083	084	084	085	086
088	088	089	090	090	092	092	093	095	095	096	097
099	099	099	100	100	100	101	102	103	103	103	103
103	104	106	107	107	108	108	112	112	114	115	115
116	118	118	118	118	118	119	121	123	124	124	125
128	131	135	136	136	136	137	138	140	140	142	142
143	144	146	146	147	150	154	158	158	160	162	167
167	167	179	188	190	190	198	201	206	211	216	216
245	252	254	260	260	260	261	262	263	264	265	265
265	268	270	270	270	270	270	271	271	272	272	273
273	274	274	276	277	277	278	279	281	281	283	283
284	286	286	287	287	288	288	288	288	288	289	291
293	294	294	294	299	300	300	300	300	312	315	318
321	324	327	332	338	350	354	355	356	357		

Fig. 7D – Facies 1 – Variant 1

015	019	020	026	029	031	031	032	033	040	041	043
043	043	044	045	045	045	049	050	050	051	051	053
056	059	060	060	060	060	063	064	064	066	067	067
068	068	068	068	069	070	070	071	071	072	073	073
073	073	073	076	077	077	077	078	078	080	080	080
080	081	081	081	081	082	082	082	083	083	083	084
084	085	086	088	088	089	090	090	092	092	093	095
095	097	099	099	099	100	100	100	101	102	103	103
103	103	103	104	106	107	107	108	108	112	112	114
115	115	116	118	118	118	118	119	121	123	124	125
128	131	135	136	136	136	140	140	142	142	144	146
146	147	154	158	167	167	167	188	190	190	198	206
211	216	245	252	260	260	261	262	263	264	265	265
270	270	270	270	270	271	271	272	272	273	274	274
276	277	277	278	279	281	283	286	286	287	287	288
288	288	288	289	291	293	294	294	299	300	300	338

Fig. 7E – Facies 1 – Variant 2

017	025	027	030	033	035	038	040	044	045	054	060
061	065	066	075	077	078	080	081	083	096	118	124
137	138	143	150	158	160	162	179	201	216	254	260
265	268	273	281	283	284	288	294	300	300	312	315
318	321	324	332	350	354	356	357				

Fig. 7F – Facies 1 – Facies 3

056	072	085	096	098	100	114	299	338	348

Fig. 7G – Facies 1 – Facies 4

031	039	046	049	051	058	059	064	069	071	076	076
076	084	091	095	099	101	102	102	123	124	146	147
194											

Fig. 7H – Facies 1 – Facies 6

060	061	078	085	090	105	121	122	123	136	136	142
167	167	177	177	237	288	300					

Fig. 7I – Facies 1 – Facies 7

003	005	006	007	008	013	013	032	037	039	049	062
066	071	075	080	212	214	215	220	224	226	228	230
230	232	234	235	237	238	242	243	246	246	246	300
358											

Fig. 7J – Facies 1 – Facies 8

307	316

Appendices 1D – Paleocurrent data for Figure 16B

Channel 1

019	020	026	029	031	032	033	041	043	043	044	045
045	049	050	50	051	053	056	063	064	066	068	068
069	070	071	073	073	073	073	073	077	078	081	081
081	082	082	083	083	084	088	097	099	100	102	103
103	104	108	112	114	115	118	118	118	136	136	146
147	270	270	277	277	288	288	294	294	299	300	300
338											

Channel 2

031	040	043	045	051	059	060	060	060	060	064	067
067	068	068	070	071	072	076	077	077	078	080	080
080	80	81	082	083	084	085	086	088	089	090	090
092	092	093	095	095	099	099	100	100	101	103	103
103	106	107	107	108	112	115	116	118	119	121	123
124	125	128	131	135	136	140	140	142	142	144	146
154	158	167	167	167	188	190	190	260	261	262	263
264	265	265	270	270	271	271	272	273	274	274	276
279	281	283	286	286	287	287	288	288	289	291	293
327	355										